Thesis submitted in partial fulfillment of the requirements for the degree of Doctor of Philosophy

Cellular Tracking and Mitosis Detection in Dense *In-vitro* Cellular Data

By

Ketheesan Thirusittampalam

Supervisor: Professor Paul F. Whelan

Dublin City University
School of Electronic Engineering
April 2012

Declaration

I hereby certify that this material, which I now submit for assessment on the programme of study leading to the award of Doctor of Philosophy is entirely my own work, that I have exercised reasonable care to ensure that the work is original, and does not to the best of my knowledge breach any law of copyright, and has not been taken from the work of others save and to the extent that such work has been cited and acknowledged within the text of my work.

Signed: (Candidate) ID No.: 57123438

Date:

Title: Cellular Tracking and Mitosis Detection in Dense *In-vitro* Cellular Data

Author: Ketheesan Thirusittampalam

Abstract

Cell migration and cell division are two key processes that are associated with a wide range of biological phenomena including embryogenesis, inflammation, wound healing, tumour development etc. The study of these cellular processes has received a substantial interest from the cell and molecular scientists since the understanding of the mechanisms that stimulate and control these dynamic events has important practical implications. With the advent of modern microscopy imaging modalities the amount of information required to be analysed by the clinical experts has substantially increased and the development of computer-based automatic techniques that are able to robustly track cells in large image sequences is currently one of the most active topics of research. While cellular migration is the major source of information in describing biological processes, recent studies emphasised the growing importance of cell mitosis, as this information can be directly used in the estimation of the cell cycle and in the understanding of complex biological mechanisms.

Due to the increasing clinical interest in the automatic analysis of cellular data, a substantial number of studies have been recently reported in the field of cellular imaging and in the development of robust solutions that are able to identify the cell mitosis. Following a detailed analysis of published works in the field of cellular tracking, it can be concluded that the development of automated tracking strategies proved extremely challenging due to several factors such as changes in cell morphology over time, random motion, cell division, cell interaction and low signal to noise ratio. To answer these challenges in a robust manner, several approaches have been advanced where the key task was the cellular association. In this regard, the major directions of research explored cellular tracking techniques where the cellular association was implemented using either segmentation or model-driven strategies. The methods included in the former category attempt to identify the cells in each frame of the sequence and then they are later associated by employing rules that enforce the continuity of the tracking process in the spatio-temporal domain. For these approaches the cellular association process proved particularly challenging when the cells undergo shape deformation over time and their motility is generally described by random motion patterns. To adapt to these challenges, alternative approaches where parametric or non-parametric representations that sample the cells morphologies and their intensity patterns were employed to identify the corresponding cells in consecutive frames of the sequence. These methods offer the advantage that they do not entail the segmentation of the cells in each frame, but they were also problematic in the presence of cell mitosis and cell interaction - a situation when they are likely to be either trapped in local minima or to return incorrect cell associations. A distinct category of model-driven cellular tracking techniques applied motion prediction to guide the cellular association process, but practice has indicated that the simplistic inclusion of the motion estimators in the tracking process proved troublesome since the resulting tracking strategies are not able to sample in a coherent manner the modes of motion that encompass the cell migration. In the vast majority of the published works on cell tracking, the cellular division has been approached during cellular association and often their application was restricted to particular cellular data types.

The major objective of this thesis is to introduce a novel framework that is able to address the theoretical and practical challenges associated with the cell tracking and cell division (mitosis) detection in dense time-lapse image sequences. To this end, a multi-phase adaptive algorithm was developed where the cell association is carried out by evaluating the topology of the local cell structures in consecutive frames of the sequences. To allow for a detailed evaluation of the local cellular structures, the connectivity rules between the neighbouring cells are encoded using Delaunay triangulation. A particular challenge associated with phase-contrast cellular datasets is associated with the large intensity contrast variation and the relative high level of noise that is present in the image data, and the robust identification of the cells throughout the sequence proved problematic. To compensate for the inconsistent inter-frame cell segmentations, in the proposed framework, a novel approach based on the evaluation of the topology changes in the local cellular structures was developed, with substantial benefits in relation to overall tracking accuracy. The last component of the proposed algorithm addresses the mitosis detection using a backward tracking analysis that integrates the local cellular structures with a pattern matching algorithm for the identification of the mitotic cells that were missed in the forward tracking phase of the algorithm.

While the major contributions that emerge from this work are associated with the proposed computational framework that has been designed to address cellular tracking and mitosis detection, it would be useful to point out that another contribution resides in the detailed performance analysis of the algorithm. Thus, to comprehensively evaluate the performance of the proposed framework, several challenging time-lapse phase-contrast cell image sequences were used in the experimental study and the results returned by the proposed automatic cell tracking algorithms were compared against the manually annotated data. To further evaluate the performance of the developed method it has also been applied to public available cellular datasets and its performance is compared against those reported by the state-of-the-art cellular tracking and mitosis detection implementations. The experimental results indicate that the proposed method is able to successfully track phase-contrast cells in the presence of random migration and detect the mitosis events, and its performance proved superior to those attained by the state-of-the-art implementations.

Contents

List of Figures

List of Tables

Abbreviations

CA – Constant Acceleration

CCD – Charge Coupled Device

CT – Circular Turn

CV – Constant Velocity

EDCRF – Event Detection Conditional Random Field

GFP – Green Fluorescent Protein

HCRF – Hidden Conditional Random Field

HeLa – Henrietta Lacks – the donor of cervical cancer cells

HUVEC – Human Umbilical Vein Endothelial Cells

IMM – Interacting Multiple Model

JPDA – Joint Probabilistic Data Association

MDCK – Madin Darby Canine Kidney Epithelial Cells

MNP – Murine Neural Progenitor Cells

RW – Random Walk

SVM – Support Vector Machine

TL-HCRF – Two-Labelled Hidden Conditional Random Field

Acknowledgements

First of all, I would like to express my special thanks to Professor Paul F. Whelan for giving me the opportunity to work on this research programme and for his guidance and constant support throughout the course of this project.

I would also like to express my gratitude to Dr. Ovidiu Ghita and Dr. M. Julius Hossain for their constructive comments and for their help in relation to the understanding of the theoretical challenges associated with my project. In particular I would like to mention their unabated enthusiasm and their competent suggestions.

Special thanks go to Dr. András Czirók, Kansas University Medical Center, for providing most of the data used in the experimental study and for his valuable clinical input.

I would like to thank all members from the Center for Image Processing and Analysis (CIPA) for the helpful discussions and for their friendship during my research period. Also, I would like to extend my thanks to the CIPA administrator and to the technicians from the School of Electronic Engineering.

I would also like to express my gratitude to the NBIPI - National Biophotonics & Imaging Platform Ireland and to the Irish Government for funding my research programme.

Finally, I am most grateful to my parents, wife and my son for their permanent encouragements and their tremendous support. This project could not be successfully completed without them.

Publications resulting from this research

- K. Thirusittampalam, M. J. Hossain, O. Ghita, and P. F. Whelan, “A Novel Framework for Cellular Tracking and Mitosis Detection in Dense Phase Contrast Microscopy Images”, IEEE Transaction on Biomedical Engineering, 2011. (Under revision).

- K. Thirusittampalam, M. J. Hossain, O. Ghita, and P. F. Whelan, “A Novel Framework for Tracking In-vitro Cells in Time-lapse Phase Contrast Data”, in Proceedings of the British Machine Vision Conference, Aberystwyth, September 2010, pp. 69.1–69.11.

- K. Thirusittampalam, M. J. Hossain, O. Ghita, and P. F. Whelan, “Cellular Tracking in Time-lapse Phase Contrast Images”, in Proceedings of the 13th Irish Machine Vision and Image Processing Conference, Dublin, September 2009, pp. 77-82.

- K. Thirusittampalam, M. J. Hossain, O. Ghita, and P. F. Whelan, “Cell Segmentation in Time-lapse Phase Contrast Data”, in Proceedings of the 15th Irish Machine Vision and Image Processing Conference, Dublin, September 2011, pp. 120-121.

- K. Thirusittampalam, M. J. Hossain, O. Ghita, and P. F. Whelan, “Automatic Cellular Segmentation in Time-lapse Phase Contrast Images”, Bioengineering, University of Oxford, September 2009.

Chapter 1:

Introduction

This thesis describes the development of a novel automatic tracking framework that has been specifically designed for cell tracking and mitosis detection in phase-contrast time-lapse image sequences. Cellular tracking is an important research area in the field of molecular biology, since the tracking results can be directly used by clinical experts to estimate motility and proliferation indicators (please refer to Appendix A for additional details). These cellular indicators are often used in the process of interpreting a wide spectrum of biological phenomena including embryogenesis, inflammation, wound healing, tumour development, etc [7, 68, 69, 70]. Typically, cell migration and cellular division (proliferation) are evaluated in time-lapse image sequences where the image data is captured by a CCD camera that is fitted to a digital microscope [71]. Subject to various image protocols that are adjusted for each type of in-vitro cell line, the CCD camera captures cellular structures at specific time intervals over a long observation period (in some studies the acquisition time may span several days). While the acquisition of dense time-lapse image sequences is beneficial as it allows a precise estimation of cellular indicators, on the other hand it generates a vast amount of image data that has to be analysed by the clinical experts. The manual analysis of such large cellular datasets has become (in many situations) impractical, and as a consequence, the development of computer-based techniques that are able to robustly attain cellular tracking results represents one of the most active contemporary topics of research in this field. While cellular migration is the prime source of information when applied to the description/modelling of in-vitro biological processes, recent studies emphasised the importance of cellular division, as the frequency of the mitosis events defines a key indicator that can be used in the assessment of the efficiency of newly developed therapeutic agents. To this end, the major objective of this thesis is to advance a fully automatic framework that can accurately estimate the migration patterns and detect mitosis events in challenging time-lapse phase-contrast image sequences.

1.1 Motivation

Cellular motility and proliferation (mitosis or cell division) are two key indicators that are assessed in the study of artificially induced physiological and pathological processes that lead to the development of new drugs and therapies. The traditional approach that is applied to identify motility patterns and the frequency of mitosis events involves a user-driven procedure where the cells and the association rules in the image stack are established based on the decisions made by a clinical expert (molecular biologist). In general, the manual interpretation of cellular data returns satisfactory results, but it is important to note that due to the advent of new microscopy imaging modalities, the amount of data that needs to be interpreted by the biologists is constantly increasing. There is no doubt that the availability of cellular data with high spatial and temporal resolutions is welcome as it allows a detailed analysis of biological processes. At the same time the vast amount of data renders impractical in many clinical studies the procedure associated with the manual cell annotation. In addition, manual annotation procedures are prone to intra- and inter-observer variability, and the accuracy of the user-driven data interpretation is highly influenced by the experience of the molecular biologist [67]. This is one of the major reasons that motivated the development of automatic cellular tracking solutions, which currently represents one of the most important areas of research in this field.

During the development of automated cell tracking algorithms, the accurate association of cells in large image sequences represents the major challenging task. This is caused by several factors such as the high similarities between the intensity of the cells present in each frame of the sequence and the predominately random nature of the cellular migration process. In addition, since the image acquisition process involves the application of specific protocols that are adjusted for each type of *in-vitro* cell (for instance, one protocol entails the administration of fluorescent agents to increase the image contrast between the cells and the background), computer vision-based tracking solutions have to be designed to accommodate the imaging characteristics of the data to be analysed. There were substantial studies centred on the optimisation of the imaging and the specimen preparation protocols, but these studies were in particular concerned with issues related to extraneous effects on the

biological process that are caused by staining agents (fluorescent dyes) or the illumination set-up. From an image analysis standpoint, the major objective is to design an optimised protocol that is able to generate cellular data with sufficient image contrast, which allows the application of computer vision-based solutions for the estimation of the relevant biological indicators. To this end, a wide variety of cell tracking algorithms have been published in the specialised literature where they attempted to address a specific application domain in the field of molecular biology. To answer this application driven scenario, the proposed algorithms were custom designed to serve the segmentation and tracking of specific cellular data. This strict application context of the published works motivated the research work detailed in this thesis, whose main goal is to develop a more generic framework that can be successfully applied to cellular datasets that consist of image sequences that are captured for diverse cell types. Among the cellular data types that are currently used in clinical studies, the time-lapse phase-contrast image sequences define a very complex and challenging tracking scenario that is the main focus of the work detailed in this thesis. Thus, the proposed framework has been carefully developed to be able to address several issues related to faint image contrast, intra and inter-frame intensity variations, large deformations in the shape of the corresponding cells in consecutive frames of the sequence, random migration and various rates of cellular division. All these challenges form a difficult research problem and in this thesis, novel solutions have been advanced to achieve a robust and distinct cell tracking framework.

Another area of interest was focused on the robust identification of cell division events. During cell division or mitosis, the parent cells divide into two child cells (or daughter cells) and the identification of these biological events is particularly relevant in the estimation of the cell cycle and other related biological parameters. In some distinct types of cellular datasets, mitosis events are preceded by apparent changes in the intensity profile of the parent cell and this information can be used for the robust identification of parent-child cells links. However, other types of cellular data (such as MDCK datasets) do not exhibit such prominent intensity transitions, and as a consequence, the precise detection of cellular mitosis requires the development of more complex solutions that rely on the application of backward tracking strategies.

1.2 Objectives of the research

The final goal of this research work is the development of a fully automated framework that adaptively employs the topological information associated with local cellular structures in the tracking process and in the detection of the cellular division events. Since the incidence of cell segmentation errors has undesirable effects on the accuracy of the tracking process, another major aim of this work was the development of targeted algorithmic solutions that evaluate the consistency of the cellular association decisions in consecutive frames of the time-lapse image sequence.

Since the cells in phase–contrast data exhibit similar intensity and shape characteristics, the process associated with the identification of the corresponding cells over the entire image cannot be robustly carried out using standard pattern matching techniques. In addition, the motility of the cells is defined by random migration and this fact restricts the use of motion prediction in the implementation of robust cell tracking strategies. To address this challenging cell matching scenario, the main concept behind the cell tracking approach proposed in this thesis resides in the construction of a graph-based representation that is able to encode the local relationships (or topological structure) between the cells that are present in each frame of the image sequence. By using this representation, the cellular tracking process can be elegantly formulated as a graph matching process in pairs of consecutive frames in the image sequence. One important problem, as indicated earlier, is caused by the cell segmentation errors that occur due to the low contrast between the cells and the background. Under-segmentation inserts local disturbances in the graphs that are constructed in each frame, and as a result, artificially reduces the efficiency of the cell tracking process. To compensate for this issue, a novel approach to identify and correct these segmentation errors has been developed in this research work.

The next objective of this research work consists of developing a robust cellular division detection strategy that is sufficiently flexible to adapt to situations where the division events are not signalled by conspicuous transitions in the intensity profile of the parent cells. To achieve this research objective, a novel backward

tracking strategy has been developed that is able to return accurate results in the presence of segmentation errors. The last major objective associated with this research work is to perform a comprehensive evaluation of the developed cell tracking and mitosis detection framework when applied to various cellular datasets and to compare its performance with respect to those obtained by the state-of-the-art implementations.

1.3 Contributions of this research

As indicated in the previous section, the process associated with the precise tracking of cellular structures in phase-contrast time-lapse image data is very challenging. This is caused by a wide variety of imaging and biological factors including the low image contrast, intra and inter-frame intensity variations, unpredictable changes in the shape of the cells in consecutive frames of the sequence, cellular division, random migration patterns, etc. All these adverse factors prevent the direct application of common feature-based tracking strategies to address the cell tracking in long phase-contrast image sequences. In addition, the incidence of cellular mitosis cannot be robustly predicted/modelled *a priori*, and this further complicates the methodologies that have to be devised to achieve robust inter-frame cellular association.

According to the research objectives stated in Section 1.2, the most visible contribution associated with this research work consists of the overall cell tracking and mitosis detection framework. The proposed framework has been developed in a modular manner and in this work substantial efforts have been devoted to provide a flexible implementation that allows the inclusion/testing of various computational components of the proposed cellular tracking and mitosis algorithm using a plug-in approach.

The second major contribution resulting from this research work is associated with the theoretical aspects related to the development of the cellular association process. Thus, in this thesis, a novel graph-based cell association technique has been introduced, where the spatial relationships between the cells are encoded in a hierarchical manner by the use of Delaunay triangulation. This approach proved

particularly robust when tracking dense cellular structures in the presence of random (Brownian) motion and one major aspect that is useful to mention is the fact that the tracking scheme discussed in this thesis is well adapted to deal with situations caused by cellular division, which explains its high accuracy when applied to challenging cell tracking scenarios.

The methodology devised for cell division detection represents another major contribution resulting from this work. In the proposed approach, the normal tracking (forward tracking) results are analysed using a backward tracking strategy, which entails the application of a hybrid algorithm to identify and redress the errors inserted by the segmentation process.

The last major contribution is located in the detailed experimental validation of the proposed method on various cellular datasets and in its comparison against relevant state-of-the-art cell tacking and mitosis detection methods.

Another contribution resulting from the investigation detailed in this dissertation resides in the algorithmic solution proposed to redress the segmentation errors (under-segmentation) during the normal (forward) and backward tracking stages of the algorithm. In the proposed work under-segmentation is addressed by applying an intensity based pattern matching technique that is combined with a process that evaluates the consistency of the local cellular structures in adjacent frames of the image sequence.

1.4 Overview of the proposed cell tracking framework

This section provides a brief description of the structure of the proposed cell tracking framework that has been developed during this research programme. The main computational components of the cell tracking and mitosis detection scheme are shown in Figure 1.1. The proposed tracking framework consists of three major modules including cell segmentation, forward tracking and backward tracking modules. The developed framework initially detects the cells' centroid points in each frame of the image sequence by applying a morphology-based segmentation approach. Once the cell segmentation process is complete, the next component, the

forward tracking module, is applied to associate the corresponding cells in the time-lapse sequence. To accomplish this goal, a graph based cell association process has been applied where the local cellular relationships are sampled using a Delaunay representation. One issue that required special attention was to counteract the negative influence of the segmentation errors on the tracking results. The segmentation errors are mainly caused by the improper image contrast present in the image, which generates situations when cells are not detected by the segmentation algorithm. The occurrence of under-segmentation has adverse effects when the cells are associated in consecutive frames of the sequence with respect to the local cellular relationships. To reduce the level of uncompleted cell lineages, a hybrid algorithm has been applied to identify the locations of the undetected cells that minimise the disturbances in the local Delaunay meshes.

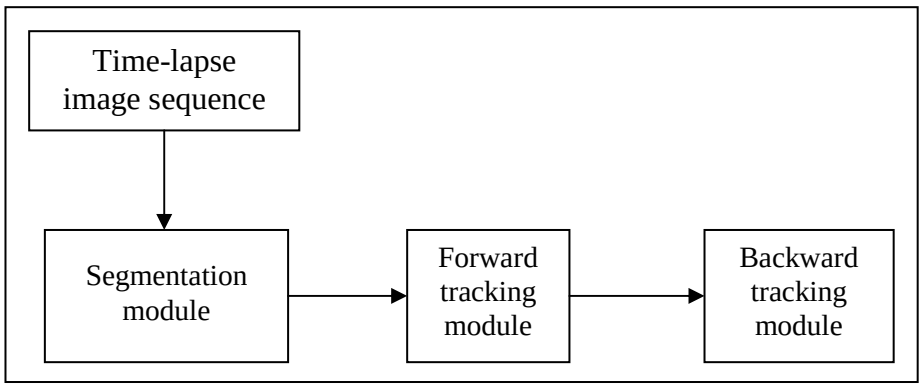

Figure 1.1. Main computational components of the proposed cell tracking and mitosis detection framework.

The last component of the proposed framework entails the application of the backward tracking module to identify cell division (mitosis) events. The major objective of this computational module was to link the parent and child cells and to provide detailed information that complements the statistics that describe the migration indicators that are extracted from the forward tracking results. Similar to the forward tracking module, an approach that is able to identify segmentation errors has been implemented during the backward tracking process to eliminate as much as possible the incorrect cell associations that are caused by under-segmentation. All computational components illustrated in Figure 1.1 are discussed in detail in the third chapter of this thesis.

1.5 Thesis organisation

Chapter 2 provides an in-depth analysis of past research works on automatic cell segmentation, tracking and mitosis detection that are published in the specialised literature. In this chapter the most relevant techniques are discussed and categorised based on their algorithmic content, and a comprehensive discussion is provided to emphasise the connections between the theoretical contributions and the clinical application context.

Chapter 3 presents in detail the development of the cell tracking and mitosis detection framework, where ample discussions are included to motivate and emphasise the theoretical advances associated with each component of the proposed framework.

Chapter 4 details the experimental results that emerged from a comprehensive validation of the proposed cell tracking framework on various types of cellular data. The reported results are compared with the manual ground truth annotations to illustrate the efficiency achieved by the automatic cell tracking framework with respect to tracking and mitosis detection accuracy. To provide a wider assessment of the proposed cellular tracking framework, its performance was quantitatively evaluated on publicly available datasets and compared to those achieved by state-of-the-art cell tracking and mitosis detection algorithms.

Chapter 5 summarises the main conclusions and contributions resulting from this research work and discusses the main future directions of research.

Chapter 2:

Literature Review

The study of cell migration entails a three-step process: live cell microscopy, application of computer vision-driven cell tracking techniques, and evaluation of the tracking results to understand/model the biological implications associated with the cell migration. Generally, the cell images are captured by a digital camera that is fitted to a microscope in order to record the cellular migration/proliferation over a long period of time. During the data acquisition phase, the camera captures images at a specific interval of time (usually in the range of minutes) which is generally set in agreement with the cell type, migration patterns, therapeutic agents, cell environment interactions, etc. Existing microscopic imaging modalities [90, 110] that are typically employed to capture sequences of time-lapse images include bright-field/dark-field [89], phase-contrast [91, 109], differential interference contrast [109], Hoffman modulation contrast [109] and fluorescence microscopy [89] – a detailed discussion about most common cellular time-lapse imaging modalities is provided in Appendix B. The time-lapse images obtained in this process are analysed using computer vision and image processing techniques that are able to track the cell migration, detect automatically the mitosis events and generate statistical indicators that describe the cellular motility such as speed, distance travelled, directionality, cell cycle, etc. These results are analysed by the molecular scientists to determine/model the biological processes associated with cellular migration and cellular division. While the biological implications associated with the interpretation of time-lapse cellular data represent a very specific and active area of research, it is important to note that this dissertation mainly addresses the development of automated computer vision algorithms for cellular tracking and mitosis detection. Thus, the major objective of this chapter is to provide a comprehensive review of past research work that was focused on the development of algorithmic solutions that addressed the automatic tracking of multiple cells and the detection of cell division in time-lapse microscopic image sequences.

When analysing cellular activity from a biological perspective, the identification of cellular migration and the detection of cell division are two separate problems. Along with cellular migration, which is the major source of information in describing/modelling biological processes, several recent studies emphasised the growing importance of the cell mitosis (as this information can be directly used in the estimation of the cell cycle and in the understanding of complex biological mechanisms). Although cellular migration and mitosis are distinct biological processes, when they are evaluated from a computer vision standpoint, they cannot be considered in isolation, since the tracking information that quantifies the cell migration plays an important role in the identification of the cell division events. By extending this observation, we can note that the occurrence of cell mitosis has adverse implications on the robust identification of the corresponding cells in consecutive frames of the sequence, as the new cells may generate incorrect tracking decisions. The optimal approach to identify the mitosis events opened a difficult research problem. Consequently, a distinct category of approaches detailed in the literature dealt with cellular division in coordination with cellular tracking, while another category of methods analysed the cell tracking and cell division as independent problems. For clarity reasons, in this chapter the state-of-the-art cellular tracking and cell division detection algorithms are discussed in two different sub-sections.

2.1 Cell tracking

Generally, live cell imaging is targeted to particular biological applications that have their own specific requirements. Hence, the strong application characteristic of the cellular data has a direct impact on the image features that has to be evaluated by the automatic tracking algorithm. Also, as indicated in the previous section, a wide variety of microscopy imaging modalities are applied in current studies and the main properties of the image data captured by a particular method are fairly distinct when compared to those captured by a different image acquisition method. Moreover, some image acquisition techniques (due to constraints related to the specimen (living cells) being observed and in particular due to the imaging problems induced by the illumination set-up) generate poor quality image data which effects the performance of the automated cell tracking. For instance, phase-contrast

microscopy is very popular when applied to live cell imaging because it requires standard imaging equipment and does not involve cytotoxic effects generated by spotting proteins (SPs) used in fluorescent microscopy. As a downside, phase-contrast microscopy has certain disadvantages such as poor photomicrography, halo and shade-off effects [1, 2, 3, 85]. One solution to increase the contrast between the specimen and the surrounding cell environment involves the use of fluorescent dyes. However, these dyes have cytotoxic effects that induce artificial changes to the cells' health and this issue is particularly important when cells have to be monitored for long periods. To limit the cytotoxicity induced by the fluorescent agents, scientists have designed complex image acquisition protocols that allow the use of low concentrations of fluorescent dyes for which the microscope is still able to generate image data with an appropriate signal to noise ratio [4]. Nonetheless, the large variety of imaging protocols corroborated with the wide-range of cell types generate a complex scenario that has to be addressed by automated cell tracking solutions.

Cellular image sequences typically contain a large number of cells with similar characteristics and this substantially increases the difficulty of the cell matching process. As time-lapse microscopy records cells over a long period of time, there are large frame-to-frame variations in the image contrast with respect to the imaged cellular structures. Cells are non-rigid biological structures, i.e. their size and shape vary frequently throughout the image sequence, and they are guided by self-propelled motility which makes the task to predict their future states difficult. In addition, cells undergo division and interact each other (forming cellular clusters), which turn the identification/segmentation/tracking process into a difficult problem. The challenges associated with automated tracking vary substantially depending on the characteristics of the imaging systems or on the nature of the cell types being analysed. Hence, numerous semi-automatic [1, 5, 6] and fully automatic [7, 8, 74] algorithms have been proposed in the literature to solve the cellular association task for different cell lines.

The cell tracking algorithms reported in the literature can roughly be divided into four broad categories as follows: detection-based, model-based, filter-based and hybrid methods. Each broad category can be further sub-divided and Figure 2.1 provides a graphical organisation of categories and sub-categories of methods that

have been developed in the context of cellular tracking. In this diagram, processes or modules are marked with oval shapes, whereas categories and sub-categories of cellular tracking approaches are marked with rectangles. Details in regard to each category and sub-category of methods are provided in the remainder of this chapter.

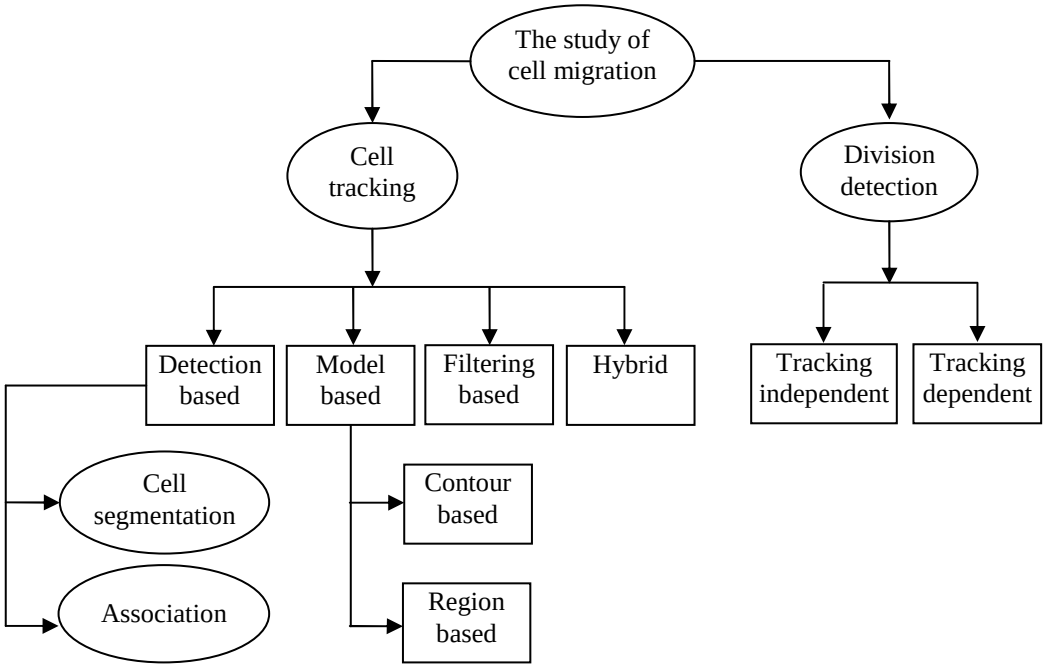

Figure 2.1. Categorisation of the processes and approaches in the field of cellular tracking and mitosis detection.

2.1.1 Detection-based cell tracking methods

In this category of methods, the cells are initially segmented in each frame of the sequence and then the segmented cells are associated across adjacent frames. This process is relatively straightforward when the segmentation of individual cells in each frame is accurate and cells can be unambiguously associated in the subsequent frames. In general these approaches entail a two-step tracking process, namely the segmentation/detection phase and the cell association phase. The segmented cells are typically associated by means of feature matching, a process that proved particularly challenging when tracking multiple cells that exhibit different intensity or shape characteristics. Consequently, several techniques have been proposed to address cellular association, whose main objective was to maximise the

use of the image features during the cellular matching process. However, segmentation errors such as under/over segmentation are unavoidable [9] when dealing with challenging data, and in this scenario, false matching or incomplete tracking results may often occur. The occurrence of segmentation errors is the major problem for the detection-based cell tracking strategies and the vast majority of the algorithms developed have included the implementation of additional post-processing steps to reduce as much as possible the rate of incorrect tracking decisions [10]. While cellular segmentation is one component that has a substantial effect on the overall performance of the cell tracking process, in the next section I discuss in detail the most relevant techniques that have been published in the specialised literature.

2.1.1.1 Segmentation

As cellular segmentation has a key role in the cellular tracking process, some published papers analysed the cell segmentation as an independent problem [7, 11, 73, 78]. At this stage it is useful to mention that due to the large variety of cell types, imaging protocols and the frequency of mitosis events, a large palette of approaches has been proposed. While the analysed cellular data is often characterised by distinct characteristics such as variation in cell morphology, intensity profile, illumination set-up and different degrees of cellular agglomeration, the proposed methods were, in general, custom designed. In this regard, some segmentation algorithms apply simple detection/thresholding technique, others explored more sophisticated segmentation approaches to accommodate the poor image contrast and high level of noise [12, 13], while another category based on active contours or level sets addressed the segmentation problem in close coordination with the tracking process [14].

However, as the application context was the key element in the development of cellular segmentation strategies, this makes their precise categorisation extremely difficult. The published cellular segmentation methods employ a wide range of techniques such as thresholding, watershed, mean shift, deformable models and wavelet transform to achieve accurate results. In this regard, the thresholding-based

cell segmentation methods are based on the assumption that the intensity of the background is uniform and it can be robustly separated from the intensity signal associated with the cell regions [15, 83]. Thus, these methods initially binarise all images that compose the time-lapse sequence using adaptive thresholding techniques [16] followed by some morphological operations that are applied to merge and split the detected regions in order to deal with under-segmentation and over-segmentation, respectively. These methods proved successful when applied to data that can be precisely approximated with a bi-modal distribution, but they have shown substantial limitations when applied to more challenging cellular data that exhibit substantial intensity variation within each frame or across consecutive frames in the image sequence. Watershed algorithms were also used for cell segmentation. These methods are generally marker-controlled, where the seed points are selected by applying either adaptive thresholding or the *h*-maxima operation. For instance, in [17], the *h*-maxima transform has been used to detect the seeds in the gradient image and the image regions resulting from the watershed process are subsequently merged to avoid over-segmentation. In [7], cell segmentation is carried out using a multi-step algorithm that initially binarises the input image using an adaptive thresholding technique [77]. To limit the level of under-segmentation, the authors applied a distance transformation [76] to accommodate the situations generated by the cellular interaction (cell clustering). The last step applies a watershed-based algorithm to merge the cell nuclei in order to eliminate false cell detection. A different cell segmentation method based on the morphological top-hat and the *h*-maxima transform is reported in [12]. In this method the segmentation errors are redressed during the tracking process by analysing the initial tracking results in the temporal domain.

Mean shift is another method that proved popular in the context of cellular segmentation and in general these methods involve a multi-step analysis that is usually designed for a particular data type [19]. In [20], the authors presented a wavelet transform-based method that was employed to identify the bright spots in fluorescence images. In this approach, the authors used the multi-scale correlation of the filtered wavelet coefficients to enhance the peaks of the spots and to reduce the level of noise present in the image. This method has been further developed in [21] to detect apparent spots in 3D image stacks. However, it is important to point out

that the application of this method to cell segmentation in phase-contrast imaging is not appropriate, as the intensity of the cell region is not substantially higher than that of its immediate neighbourhood.

As indicated in the introductory part of this section, a distinct category of methods attempted to integrate the cell segmentation in the tracking process. In this sense, the cell segmentation methods based on active contours [22] and level sets [14] make use of the information relating to the shape of the cells and image contrast. In this process the results obtained in the current frame are utilised as the initial solution for the next frame, where the final segmentation is achieved by evolving the contours based on the gradient information and some parameters that constrain the geometric properties of the contour. These methods proved highly successful when applied to sparse cellular data, but they have shown substantial drawbacks such as erroneous contour merging and convergence to high contrast non-cellular regions when applied to data characterised by low image contrast and high cellular density. In addition, they have an inherent inability to adapt to situations caused by large cellular movements (migration) in consecutive frames of the sequence.

The analysis of the main directions of research in cellular segmentation that has been carried out in this section allowed us to draw some useful conclusions. The most apparent is that the vast majority of the developed methods have been developed to serve a particular application domain (cell type, image conditions and protocols, cell density, etc.) – for additional details refer to Table 2.1. However, in spite of the strong application context that was the prevailing factor in the development of cellular segmentation strategies, this section attempts to identify the advantages and limitations associated with existing segmentation algorithms. An important conclusion resulting from this study is that precise cell detection/segmentation using standard segmentation approaches is impractical due to the wide range of morphology and intensity variations that are present in cellular data. This issue proved particularly visible when the algorithms are applied to challenging cellular datasets and the limitations associated with the imperfect cell segmentation generate a difficult research problem that will receive full attention in this thesis. The conclusions that emerged from this survey prompted the

development of the framework presented in this dissertation that treats the segmentation and tracking problem in an integrated manner to limit as much as possible the impact of the segmentation errors on the overall tracking accuracy.

Table 2.1: An overview of cell segmentation methods that were proposed for the analysis of different cell lines.

Reference	Cell line	Modality	Segmentation approach
1	Murine neural progenitor cells	Phase-contrast	Uneven illumination removal + adaptive thresholding + marker-based watershed
8	Human osteosarcoma & amnion epithelial cells	Phase-contrast	Region based (gray scale morphology + level set)
78	Histopathology images	Fluorescence	Graph cut binarization
92	Drosophila cells	Fluorescence	Active contour & H-minima & marker-based watershed
94	Melanoma cells	Phase-contrast	Optical flow & level set
93	Breast cancer tissue	Fluorescence	Multiple filters & watershed-region growing & dilation
95	Breast cancer cell MDA-MB2 31	Phase-contrast	Flow-guided active contours
96	HeLa	Fluorescence	Adaptive threshold & Watershed & Region merging
97	H4 neuroglioma cells	Fluorescence	Background correction & Gaussian filtering & watershed & statistical region splitting

2.1.1.2 Cellular association

Each image of the cellular sequence contains cells with similar intensity profiles, a fact that complicates their matching/association in consecutive frames. Cells also undergo random motion, deformation and division, and these factors further enhance the difficulty of the cellular tracking process. Several matching (cellular association) techniques have been reported in the literature that are principally based on image features [1, 23, 24], motion estimation [21, 25, 26], spatial relationship [7, 27, 82] and hybrid implementations (image and motion features) [12, 28, 84].

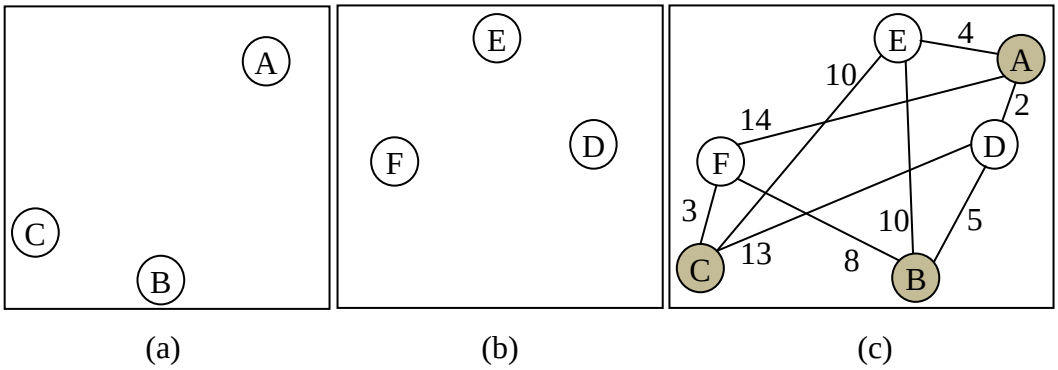

Figure 2.2. Illustration of the cell association process that tries to minimise a global objective function. Nodes marked by grey-filled circles denote cells in the current frame. Nodes marked with white circles depict the cells in the next frame. (a) Current frame. (b) Next frame. (c) Principles of the cellular association process.

The most straightforward cell association process is based on the estimation of a similarity metric that evaluates the disparity between sets of features associated with the segmented cells in adjacent images. Although different features can be theoretically employed in the context of cell association, the objective is to minimise the overall disparity in matching which translates to maximising the overall matching confidence. This is illustrated in Figure 2.2 where the cells in the current frame and the next frame are shown in Figure 2.2(a) and Figure 2.2(b), respectively. Figure 2.2(c) shows the relative position of these cells in a single frame where the cells from the current frame are marked with grey-filled circles. In this diagram, the number associated with an edge represents the Euclidean distance between the cells that are connected by the respective edge. Now, if association is carried out using a

simple greedy approach [98], A, C and B will be associated with D, F and E, respectively, generating a matching cost of 2, 3 and 10, respectively. Thus the total cost will be 15. However, the cellular association A-E, B-D and C-F will result in an overall matching cost equal to 12, which illustrates the inability of this approach to generate reliable matching decisions.

If the cells in adjacent frames of the sequence do not show large migration patterns (such as depicted in Figure 2.2), the distance between the cell centroids can be used as a cell association metric. In this regard, the methods proposed in [10, 29, 30] implemented cell matching based on the distance between the centroids of the segmented cells and the amount of overlap in the cell regions in consecutive frames. Apgar *et al* [29] validated their method using micro-sphere particles fluorescent image sequences and the inter-frame particle association was carried out with respect to nearest neighbour rules. The experimental results indicate that this association process produces satisfactory results, but it is useful to mention that the distribution of the micro-spheres is sparse and the displacements between corresponding particles in consecutive frames are very small. A similar approach was reported in [31] where the size of the cells was used to complement the Euclidean distance between the cells' centroids in the association process. Related association principles were applied by Jaeger *et al* [30], where they initially segmented Dictyostelium cells in each image and then associated them based on the distance between their contours. Since the association process is implemented by minimising an overall cost function, the problems generated by the segmentation errors proved particularly cumbersome to address. This issue has received a substantial level of attention in [10] where the authors developed an elaborated segmentation process to identify Escherichia coli cells in fluorescence images.

A distinct characteristic of cell tracking methods based on the simple evaluation of the minimum distance between cells is that they return an appropriate level of performance when applied to track spatially sparse cells only in situations where the segmentation errors are not significant. Indeed, incorrect cell association decisions are determined by several factors, including unexpected shape changes that are encountered during the cell growth, high cell density and more importantly by the random migration of cells. For instance, to accommodate different cell motility

patterns, multiple features need to be concurrently analysed in the cell association process [23, 32]. Nath *et al* [23] employed three discrete distances (the overlapping area of the bounding boxes that enclose the segmented cell regions, the distance between cell contours and the amount of overlap between the cell regions) to track cells in time-lapse phase-contrast epithelial cell image sequences. This tracking solution proved efficient when applied to image sequences captured with a small time lapse interval, but since the algorithm strongly relies on the area of overlap between cells in consecutive frames, it is not applicable to tracking scenarios where cells undergo large migration. A related approach is presented in [32] that incorporates two distinct measurements, namely the overlap area and the distance between cell centroids, measures that were normalised with respect to the maximum size of the cells under analysis. The experiments were conducted on fluorescence image data containing cancer cells (HeLa cells) and the authors reported that more than 90% of cells were correctly tracked. However, it is important to point out that this high tracking accuracy is achieved under the condition that accurate cell segmentation is available (>98%). This condition was satisfied in their study, as the identification of the nuclei of the HeLa cells requires a fairly straightforward segmentation process. There is no doubt that this favourable scenario cannot be applied when dealing with challenging phase-contrast data that is often characterised by low image contrast and a high level of noise. In this situation the segmentation errors have to be accommodated during the cell tracking process, and some algorithmic solutions have been reported in [9, 33].

When all challenges associated with complex time-lapse phase-contrast data are taken into consideration, simple measurements that record the displacements between cells in consecutive frames are inadequate to obtain robust cellular association. To provide more confidence in the tracking process, multiple measurements have been included to generate more detailed features that can substantially increase the overall tracking accuracy. As an example, the method presented in [1] evaluated the likelihood for all possible pairs of cells in two adjacent frames using the following set of features: centroid, area, eccentricity, major axis length and orientation. To achieve a global minimisation in this high dimensional feature space, the authors employed linear programming. However, the association process based on large feature sets is computationally expensive as it generates a

large matrix whose size is proportional to the number of cells present in the image. In their experiments, the authors evaluated phase-contrast data containing murine progenitor cells, and in their study they showed that the incidence of segmentation errors artificially increases the number of broken tracks. To overcome this problem, the authors proposed to approximate the position and the shape of the undetected cell in the next frame with that of the unmatched cell in the current frame. This process is repeated over a number of consecutive frames and if no matching cell is found, the tracking for the cell in the current frame is terminated. While this approach to address the under-segmentation errors is intuitive, it is applicable only in situations where the inter-frame migration is very small. Moreover, the approach applied to estimate the location of the missed cell is inappropriate when dealing with cell data characterised by random migration patterns. A similar idea was applied in [34], where the authors employed a sliding temporal window to redress the errors caused by under-segmentation. To alleviate the problems associated with the approach detailed in [1], additional constraints were enforced in [34] to handle the situations when the cells are entering and exiting from the region of interest that is imaged by the microscope.

Another important issue associated with detection-based tracking methods is the identification of the optimal computational architecture for robust cell association. In this sense, in [4] the authors introduced a graph-based framework that formulated the cell association problem as a flow network that can be efficiently solved using the minimum-cost flow algorithm. In this framework, a weighted bi-partite graph is used where one set of nodes represents the cells in the current frame and the other set represents the cells in the next frame. The weight/cost of an edge is defined by the absolute difference between feature vectors associated with the nodes that are connected by that edge. Using this data structure, the cell association is given by the minimum weighted bipartite matching. The approach based on bipartite graphs proved well adapted for cellular association and it has been extended to cover more complex situations including cell division. In [4], the authors evaluated their algorithm using fluorescence HeLa cell sequences and the reported results proved very promising. A related cell tracking framework based on the bipartite graph formulation has also been reported in [12].

As indicated above, the cellular tracking approaches based on feature matching proved inefficient when applied to cellular data characterised by low contrast or/and random migration. To answer such a challenging tracking scenario, some of the existing methods attempted to use structural information associated with neighbouring cells. Such an implementation has been reported in [27] where the structural (spatial) relationship between the neighbouring cells was encoded into a graph representation. The use of structural information proved critical in increasing tracking accuracy especially in complex situations that are generated by random migration. However, the main problem associated with this approach is the methodology applied to encode the spatial relationships between closely located cells. For instance, even small changes in the topology of the cells in the consecutive frames can have a significant impact on the graph representation [27], and this substantially complicates the cellular association process. However, the advantages of using the spatial information for cellular tracking outweigh the limitations, and many efforts have been devoted to improve the manner in which the spatial information is included in the tracking process. In this regard, Delaunay triangulation [35] has been actively used in the context of cell tracking [7, 13, 36, 37]. This representation has several advantages, such as it generates a unique planar graph that is independent of the topology of the nodes [35], and at the same time maximises the minimum angles of the triangles that compose the mesh. Moreover, in the Delaunay mesh the triangles tend towards equiangularity and the insertion or the removal of a node affects the mesh representation only at the local level. These properties are particularly well adapted to encode the neighbouring relationship between the cells in the image, as the insertion and the removal of nodes can be caused either by cellular division or by under-segmentation.

In [7] the authors reported a tracking algorithm where the spatial distribution of the cells in each frame is encoded using Delaunay triangulation and the cell association decisions were obtained by employing a linear programming algorithm. The algorithm detailed in [7] has been evaluated on fluorescent data containing HeLa cells and the reported results clearly demonstrate that the use of spatial information proved to be the key factor in obtaining high cellular tracking accuracy. As a disadvantage, the tracking process detailed in [7] consists of a rigid architecture, and it proved inefficient in accommodating the errors that occur during the segmentation

process. This problem formed one of the main research issues that received special attention in the development of the cellular tracking method discussed in this thesis. The problem caused by improper segmentation is most apparent when dealing with phase-contrast cellular image sequences, as they are typically characterised by large intensity variations within the same image and a relatively high level of noise. Due to this challenging segmentation process, under-segmentation frequently occurs, and this significantly reduces the tracking accuracy by generating incomplete cell lineages (trajectories). To address this problem, recently, a flexible cell tracking algorithm was reported in [12] that includes a computational module that was designed to link the broken tracks generated by segmentation errors. In this approach, five features including motion information are adaptively combined to measure the similarity between cells in consecutive frames and a post-processing step has been applied to bridge the broken cell tracks throughout the sequence. The major drawback associated with this approach is that it cannot handle the situations where the under-segmentation occurs in the presence of cellular division. This is another research problem that has been fully addressed in the cellular tracking framework presented in this thesis. The errors induced by the segmentation process form the main challenge associated with the detection-based cellular tracking approaches. To alleviate this issue, computer vision researchers have approached the cellular association from a more supervised perspective, which implies the accurate identification of prior models that describe the shape variation and/or the migration patterns. These methods are reviewed in the next section of the thesis.

2.1.2 Model driven cell tracking methods

As pointed out in the concluding remarks of the previous section, since cells are difficult to segment in each frame of the image sequence, substantial research efforts have been concentrated on the development of model-driven techniques. In these methods, a model is constructed for each cell to be tracked. The model generally encodes information relating to the shape or/and the intensity profile of the cell. The constructed model is propagated to the next frame(s) and is evolved to identify the most probable target in that (those) frame(s). Model propagation and target identification using this approach simultaneously solves both the cell detection and tracking problems. The model-based techniques developed in the context of

cellular tracking can be classified into two sub-categories: contour-based and region-based. Snake/active contours [38] and level sets [39] are the predominant methods employed in the development of contour based cell tracking methods, whereas normalised cross-correlation [40] and mean-shift [41] approaches were used in the implementation of region-based cell tracking methods.

2.1.2.1 Contour-based methods

The snake/active contour methods [38] are well known techniques that are popular in the development of cellular tracking techniques. An active contour represents a deformable model where its deformation is controlled by user-defined parameters and image information (usually gradient data). When this approach is applied to analyse the cell migration, the contour for each cell in the current frame is propagated to the next frame (i.e. the contour in the current frame is used as an initial condition for the contour in the next frame). The propagated contour is evolved with respect to the image information and subject to the internal parameters that impose *a priori* constraints on the smoothness of the evolved contour. From a biological perspective, this model is especially suitable for describing the shape variation during the cell migration. However, active contours do not generally handle cellular division which needs to be addressed using additional post-processing steps.

In [42], an active contour method is applied for single cell tracking, where the contour initialised in the first image is passed to the next frame and evolved until convergence. In this work the authors applied a multi-scale filtering process to remove noise, to smooth the original image data and to emphasize image features such as edges or contours. Goobic *et al* [43] also proposed a cell tracking method based on active contours and experimentally compared the performance of their method with that achieved by the centroid and correlation-based tracking methods. The authors conducted the experimental validation using 33 sequences, and concluded that tracking with active contours returns better results. While the use of active contours may be beneficial when applied to well-imaged cellular data that is characterised by small cellular migration, the active contour framework has several limitations when applied to more challenging scenarios. These include convergence problems when dealing with poor contrast data, inability to accommodate cell

division, incorrect propagation into the contours of nearby cells and errors caused by large cellular migration. To address these issues, algorithmic solutions have been proposed to improve the suitability of the active contour methodology when applied to challenging data.

To overcome the difficulties associated with the ambiguities between the cells' boundaries, an edge map based on the average intensity dispersion is applied in [44] to take advantage of the relatively homogenous background. The same problem was also addressed in [45] by employing a modified/texture constrained active contour formulation that is able to grow across isolated strong edges and stop at weak boundaries. To avoid contour merging and at the same time allowing cell division, in [46] repulsive forces and topological constraints were applied, whereas in [47] the authors modified the standard active contour framework to be able to accommodate large cell migrations. However, the inclusion of the additional constraints to control the active contour evolution significantly increased the "custom-designed" characteristic of the devised methods. In [22], size and shape constraints are integrated within the energy functional to precisely track leukocytes (white blood cells) in time-lapse data. In this work, the authors coupled active contours with Kalman filters to infer the location of the leukocyte cells when they are occluded or undetected. The application of the Kalman filter proved successful, as the migration of the leukocytes can be well approximated with a linear model. Ray and Acton [47] reported another extension of this work by including the motion gradient vector flow to track large cell movements.

The geometric active contours, which are widely referred to as level sets, were also used for cell tracking because they are able to handle topological changes such as contour splitting, a property that is extremely useful when dealing with cell division. As an example, the application of the level sets in the development of cell segmentation and tracking has been reported in [14, 48]. However, in its standard form, the level sets methods do not prevent two boundaries from merging and thus it is prone to erroneously joining multiple cells that are close to each other into a single cell. To address this issue, different implementations were developed to prevent the cell merging when the cells are spatially close [49]. This approach was further extended to track cells in 3D data and it has been reported in [18, 79]. However, it is

useful to note that this approach shows limitations when applied to dense cellular structures (the occurrence of cell agglomeration proved particularly problematic).

2.1.2.2 Region-based methods

In distinction to the contour propagation-based cell tracking techniques, in region-based approaches the shape of the cell is not explicitly used in the tracking process. Instead, the intensity profile of the cell region is utilised in the process of inferring the cell association decisions. In this approach, the mass centre for each cell is first identified, which provides information relating to the position of the cell within frame. Then, a template/pattern surrounding the mass centre is created and the cell is tracked by identifying a template/pattern in the next frame that minimises a cost-matching functional. This process is sequentially carried out to track the corresponding cells in the subsequent frames of sequence. The normalised cross correlation [40] was generally employed to identify the corresponding (associated) cells in the image sequence and several methods that followed this approach were reported in [43, 50, 51]. In [51], the intensity pattern of the cell under analysis is selected in the first frame of the sequence and the point that maximises the normalised cross-correlation matching criteria is selected as the location of the corresponding cell in the next image. The tracking path for each cell is obtained by connecting the best locations in the temporal domain. While this approach is simple and intuitive, it is likely to generate matching errors as the cells frequently change their shapes and intensity profiles in consecutive frames of the image sequence. Therefore, simplistic template matching is not sufficiently robust to identify the corresponding cells over long periods of time especially in challenging time-lapse phase-contrast data. In [43], the authors also applied a correlation-based method to track *in vitro* leukocytes in a flow chamber environment. This approach proved successful, but it is useful to note that the leukocyte cells do not exhibit large migration patterns and the image data show only minor inter-frame intensity changes. There is no doubt that this favourable scenario is not usually encountered in time-lapse cellular data, and in the context of large migration and inter-frame intensity changes, the template matching process returns erroneous decisions [50]. Thus, the researchers included further features in the matching process to provide more robust information when deciding if the candidate cell location is correctly

identified [26]. This issue has received special attention in this dissertation and in the proposed cellular tracking framework the limitations associated with the standard correlation-based template-matching approach have been addressed by incorporating additional information that describes the spatial distribution of the cells in each frame of the sequence.

To further improve the accuracy of the cellular association process, other region-based tracking methods employed the mean-shift strategy to identify the corresponding cells in the image data [5, 52]. The mean-shift implements an iterative process that locates the mode of the intensity pattern within the search space for the given intensity pattern. The mean-shift-based cell tracking method proposed in [5] is semi-automatic and defines an octagon kernel to encompass the area covered by each cell in the phase-contrast image. Thus, based on the cell intensity profile, which is defined by a dark cell nucleus that is surrounded by a bright region, two intensity-based kernels are coupled which are completed with a third kernel that models the cell division. While the user is allowed to select only a restricted set of cells in the first image, this approach has difficulties in tracking new cells that enter or exit the region of interest that is imaged by the microscope. Consequently, the performance of this approach is downgraded by the occurrence of false matching. The application of the mean-shift for cellular tracking proved very problematic due to the following limitations: (a) the mean-shift tracking is likely to generate incorrect association when the cells present similar pixel-intensity characteristics, (b) after a few frames the tracking process usually diverges from the actual cell location and it is often trapped by local minima, and (c) it does not naturally handle cell division.

2.1.3 Stochastic filter-based methods

Stochastic filter-based tracking methods involve a probabilistic/Bayesian approach and they usually rely on *a priori* knowledge about cell motion characteristics and/or deformation patterns. These methods are extremely powerful if the cell motion and the deformation patterns can be accurately modelled [4], and the application of Bayesian frameworks to cellular tracking has been extensively studied in recent years. The major advantage of this approach consists of its ability to estimate the future states of the target (cell) in terms of its position, size, intensity,

etc, by making use of prior assumptions. When dealing with complex cell tracking data this estimation is very useful, especially in situations where the cell segmentation is extremely challenging. Thus, such model-based estimation can be used to identify the target cell [53] or it can be combined with additional cost functions to increase the matching confidence of the cell association process [54, 80]. Within the Bayesian framework, the posterior probability density function is derived from the state transition model, which can be linear in the case of Kalman filter [55] and non-linear in the case of particle filtering [56]. Methods that use the Kalman filter for tracking are based on the hypothesis that the noise distributions are Gaussian and the system dynamics are linear [56]. However, in the case of cellular tracking, the Gaussian and linear assumptions are sub-optimal. In this context, particle filtering-based schemes are more appropriate because they are able to accommodate the nonlinear cell migration and the non-Gaussian distributed noise. As a downside, these methods require accurate *a priori* knowledge about the motion patterns associated with the cells to be tracked.

The methods presented in [21, 25, 26, 54, 57] involve the application of Kalman filtering to track spot-like particles/cells in fluorescence images. The application of the Kalman filter to track the cells in time-lapse image sequences is appealing as it provides a recursive solution to estimate the state of the tracking process by minimising the mean of the squared error. In these approaches the transition model that describes the cellular motion plays a very important role. As cell migration does not follow a particular motion pattern, it is difficult to describe them using only a single motion model. Thus, a number of motion models (random walk, first order linear extrapolation (constant velocity), and second-order linear extrapolation (constant acceleration)) that describe different migration patterns are integrated with the aim of implementing an interacting multiple model (IMM) algorithm [21]. In this approach, the switching between different models is controlled by a finite state Markov chain. Genovesio *et al* [21] evaluated their IMM tracking technique on synthetically generated image data and attempted to characterise the 3-D movements of the endocytic vesicles containing quantum dots. Although the experimental results proved accurate, the synthetic generated data does not fully encompass all challenges associated with complex cell migration.

To improve the robustness of the probabilistic tracking process, non-linear single-model particle filters [26, 45, 53, 54] and multi-model particle filters [25] have been applied to track spot-like biological targets. In these implementations the particle filters were implemented as a set of random samples/particles and their associated weights are used to compute the posterior density function. Then, the samples and their weights are propagated to give an approximation of the particle distributions in subsequent frames. During this operation, re-sampling of the particles is often necessary to avoid the degeneracy problem [56] (i.e. when the weights associated with the vast majority of the particles attain very low values compared to the remaining ones). In spite of these limitations, the particle filtering-based methods provide a better integration of the spatial and temporal information than approaches based on Kalman filtering, and in addition, they offer the possibility of incorporating more detailed prior knowledge that samples more accurately the cell migration and image dynamics. Similar to Kalman filtering based strategies, the particle filtering methods are generally application dependent and they are designed to model specific migration patterns

A different tracking approach involves the application of joint probabilistic data association (JPDA), which considers for the cell under analysis in the current frame more than one candidate as a potential target in the next frames of the sequence [33, 58]. Kirubarajan *et al* [33] reported a JPDA based method for the tracking of fibroblast (tissue) cells in phase-contrast image sequences. This framework proved able to accommodate difficult situations that are caused by under-segmentation and cell division. However, the efficiency of this method is highly influenced by a large number of *a priori* assumptions, a requirement that is difficult to fulfil when dealing with random migration. This issue has been fully addressed in [58] where the authors developed a JPDA tracking method that evaluates a large set of *a priori* conditions. To attain a computational tractable approach, the authors applied the Hungarian method [58] that entails a linear programming optimisation process.

2.1.4 Hybrid methods

Considering the large spectrum of challenges associated with the cellular tracking problem, some published techniques integrate multiple algorithms into a single framework to obtain better performance. In this dissertation, these approaches are referred to as hybrid methods. For instance, a method included in this category has been reported in [8], where a topologically constrained geometric active contour algorithm was combined with edge-based segmentation and an interactive multiple motion models approach to robustly track cells in phase-contrast images. As post-processing, the authors applied a track compiler to validate the identified cell tracks and a track linking module to connect the broken tracks. In this way, this method incorporates the advantages associated with both filter-based and contour-based approaches, but one obvious disadvantage resides in the substantial level of supervision required to identify the optimal values for a large set of parameters.

In [60], the individual cells in each frame were segmented first by applying a level sets method that is extended with a customized pruning procedure to identify the individual cells in the presence of cell clustering (agglomeration). Then, the final cell tracking process was implemented using a stochastic filtering approach. In this tracking method, the authors assume that the migration for each cell can be approximated with only two models: random diffusion and goal-directed movement. Thus, a two-state Hidden Markov Model was applied, where the cell migration was modelled as a random walk with Gaussian distributed displacements. It is important to note that this particular cell migration modelling was suggested by the motility characteristics of the adult neural stem/progenitor cells and may not be suitable for accurately approximating the migration of other types of cells.

In [70], the authors detailed a framework that is able to track cells in growing plant roots. This method involves the application of the Network Snakes technique [72] (which is a variant of parametric active contours) that allows the optimisation of arbitrary graphs that encode both the geometry and the boundaries between adjacent cells. To allow the tracking of fast-moving cells, the Network Snakes method is combined with a Markov Chain Monte Carlo algorithm [75], and to obtain a precise

initialisation for each cell contour, the authors applied a semi-automatic algorithm based on the watershed transform.

In [59] the authors combined the optical flow and region-based active contours methods by implementing a unified energy formulation to track neuronal cell data. A similar approach was proposed in [61] where a standard detection-based method was combined with an active contour method. In line with all methods included in this category, these approaches were also designed to serve well-defined cellular application domains.

2.2 Cellular division (mitosis) detection

A characteristic of modern cell culturing and imaging equipment is that they facilitate the monitoring of cell behaviours over long periods of time. Thus, the time-lapse image sequences encompass a large number of cell division events. While cell migration remains the main field of research, in recent years the automatic detection of cellular division started to capture the attention of molecular scientists. This research interest was motivated by the role of cellular mitosis in biological studies, as this information is crucial in the process of quantifying the cell cycle and the growth rate of the cell population [48, 62, 63]. To answer this research interest, similar to cellular tracking, computer-vision algorithms have been developed to identify mitotic events in cellular data with no user interaction. The methods published in the literature attempt to detect mitosis events either during the cellular association process, or they approached the cell division as a post-processing step that relies on the availability of cellular tracking results. Thus, the existing cell division detection algorithms can be broadly classified into tracking-independent [7, 62, 64, 65] and tracking-based [5, 8, 12, 37] cell division approaches. In the first sub-category, intensity-based features are usually extracted to detect the cell divisions, while in the second sub-category the tracking results are utilised to identify the mitosis events.

2.2.1 Tracking independent cell division detection

Mitosis detection methods included in this category exploit the distinctive intensity features that are associated with cells prior to the cellular division event. More exactly, these methods use the knowledge that mitotic cells undergo distinct phase changes during the cell cycle [48, 86] that are reflected in significant intensity and shape variations. In some cellular images, during cell division the shape of the cells becomes very regular (circular) and their outlines show a very bright intensity halo. Thus, these apparent visual features have been often employed to identify cell division events.

The method presented in [7] first identifies the child cells (anaphase) in the next frame that follows the division event using a Support Vector Machine (SVM) classifier. Thus, if both child cells are identified based on their shape and intensity similarity, then they are associated with the closest parent (metaphase) cell in frame that precedes mitosis. The results returned by this method were promising when applied to fluorescence HeLa cell data, as the phase changes associated with the mitotic events are apparent. As a limitation, this approach is highly dependent on the results returned by the segmentation process, since each cell needs to be evaluated in order to measure its suitability to be assigned as a child cell. Thus, accurate cell division detection can be obtained only in situations where both child and parent cells are available as input for the cell division process. Also, the application of this method to dense cell phase-contrast image data is not straightforward due to the substantial challenges associated with the cell segmentation procedure.

A different classification-based cell division detection method has been proposed in [65] that has been specifically designed to detect mitotic cells in phase-contrast image data. This method first identifies the image sub-regions where the potential cell division may have occurred. Then, a trained Hidden Conditional Random Field (HCRF) [66] was applied to the selected sub-regions to determine whether each potential candidate contains a mitotic event. This work has been further extended in [63, 64] to enhance the accuracy of the mitosis detection. In [64] the HCRF was replaced with the Event Detection Conditional Random Field (EDCRF), which is a probabilistic approach that is able to model the dynamic

changes before and after the cell division event. The detection accuracy of this method proved excellent when applied to low to medium density cellular data, but it has shown problems when applied to dense phase-contrast data. In [63], a Two-Labelled Hidden Conditional Random Field (TL-HCRF) was used, an approach that complements the changes in the intensity profile of the mitotic cells with the information that samples the timing associated with the cell division process.

As a common property of the mitosis detection methods analysed in this section, they are based on the assumptions that the cellular division is signalled by conspicuous changes in the shape and the brightness of the parent cell. These assumptions are not always present in all types of cellular phase-contrast data [1, 7]. Another limitation is associated with their dependency on the accuracy of the segmentation results, and, in addition, the mitosis detection implies a computationally intensive search process.

2.2.2 Tracking dependent cell division detection

When dealing with cellular data where the mitosis events are not signalled by distinct shape and intensity changes, more sophisticated procedures have to be developed by analysing the spatio-temporal information encompassed in the tracking results [1, 5, 12, 32]. The use of the tracking results in the context of mitosis detection leads to increased accuracy, and at the same time permits the implementation of computationally efficient algorithms.

The cell division detection method proposed in [32] applied the one-to-many matching constraint during the cell association process. In other words, two child cells in frame (at time T+1) that follows mitosis correspond to only one cell in the current frame (at time T). However, multiple cell divisions may occur at the same time and they may generate ambiguities in the cell division detection. This problem has been partially addressed in [32] by using geometric information that is calculated for all cells situated in the neighbourhood of the mitotic cells. The major limitation associated with this method lies in the assumption that all child cells are detected after the cell division, which may not be the case when dealing with low contrast image data.

A similar approach for cell division detection has been reported in [1] where the likelihood that a cell is divided is estimated based on the absolute differences between the feature vectors associated with the parent and the child cells. To do this, the pairs of candidate child cells are merged, and the prior estimates of the mean and covariance of the difference vectors (calculated for each parent cell) are employed to increase the confidence of the parent-child matching process. Thus, a successful detection can be obtained when the parent and the child cells are correctly segmented, a condition that may be difficult to fulfil when the algorithm is applied to low contrast cell data.

Cellular tracking results are affected by segmentation and cell association errors. Hence, often during segmentation one or both child cells may be undetected in several frames after the mitosis event. There is no doubt that these errors have a negative effect on the accuracy of the mitosis detection, and to reduce their occurrence, backward tracking analysis has been applied to identify the child cells that are missed by the segmentation process. More precisely, the goal of the backward tracking process is to identify the location of the cells that are missed by the forward (normal) tracking in frame or frames that follow mitosis. To solve this task, pattern recognition methods based on normalised cross-correlation [12] and mean-shift [5] have been reported. For example, in [5] an integrated multiple mean-shift kernel-based backward tracking procedure was employed to detect the cell division. To alleviate the problems caused by the sudden intensity shifts, the proposed kernels were tuned to accommodate the intensity variation during the mitotic event. The method presented in [12] also employed the reverse tracking process for mitosis detection in phase-contrast cell data. In [12], a normalised cross-correlation based method was incorporated to detect the missing cell locations in frames where the segmentation results are not available, and backward tracking was applied to identify the parent-child cells links.

2.3. Conclusions

The goal of the literature survey presented in this chapter was to analyse the main directions of research in the area of cellular tracking and mitosis detection. The evaluation of the state-of-the-art algorithms mainly addressed the technical aspects relating to the implementation of computer vision-based automatic cell tracking solutions and details about the application context were also provided whenever such information was made available in the analysed papers. Since the cellular tracking and mitosis detection play a central role in the process of understanding/modelling diverse biological processes, a substantial number of approaches have been published in this field of research. One distinct conclusion that emerged from the literature survey is that the complexity of the cellular tracking and mitosis detection algorithms was dictated by the innate characteristics of the analysed cellular data. This conclusion is not unexpected, since the biological patterns that are captured in sequences of cellular images exhibit strong particularities that are related to the type of cells being analysed. Nonetheless, this conclusion is extremely important as it elevated one main direction of research that was followed in this thesis, namely the need of developing more flexible cell-tracking and mitosis-detection algorithms that are able to better accommodate the problems relating to improper image conditions such as low contrast and image noise, and the issues associated with the random nature of the cell migration.

Another important objective of this chapter was to analyse from a technical standpoint the most important algorithms published in the literature and to identify their advantages and limitations. To facilitate this discussion the algorithms analysed in this section have been grouped in distinct categories based on the approach applied to solve the inter-frame cellular association. In this regard, four major categories have been identified: detection-based, model-based, filtering-based and hybrid cellular tracking strategies. As indicated in Section 2.1.1, a dominant characteristic associated with the detection-based techniques is their dependence on the accuracy of the segmentation process. Since segmentation errors are unavoidable when dealing with dense time-lapse phase-contrast data, these methods have shown substantial limitations in the presence of cellular interaction and random migration, and these limitations motivated the researchers to investigate more sophisticated

cellular tracking strategies. Indeed, in an effort to reduce the undesirable effects induced by the segmentation errors, the researchers have investigated alternative solutions based on the inclusion of intensity and geometric models in the cellular association process.

The major advantage associated with model-based cellular tracking approaches is that they do not require the explicit identification of cells in each frame of the image sequence, but they have several inherent limitations. Among these limitations two are most apparent.

Firstly, the model-based cellular tracking methods are not able to achieve accurate results when applied to datasets that are characterised by large migration patterns. Secondly, they are not suitable for handling the topological changes in the cellular structures that are caused by cellular division events. To overcome the major limitations of the model-based approaches, the cellular tracking process has been addressed by constructing *a priori* motion models that describe cellular migration.

The cellular tracking methods based on Kalman and particle filters use the assumption that the future states (locations) of the cells in consecutive frames of the sequence can be efficiently predicted using well-defined state transition models that are often integrated in a Bayesian framework. While the Kalman and particle filtering schemes are theoretically attractive when analysed in the context of cellular tracking (as they are not dependent on the accuracy of the segmentation process) they proved problematic when applied to data that is characterised by random cellular migration. The random migration cannot be accurately modelled using particular motion models, and as a consequence, more complex schemes based on the interaction of multiple motion models were proposed. The application of multiple motion models to solve the cellular association is opportune, but substantial practical problems emerged in relation to the identification of the optimal motion model that best approximates the image dynamics and the substantial level of supervision that is required in the training process. In an effort to generate more flexible and accurate cell tracking strategies (that can better adapt to the large spectrum of challenges that are present in dense time-lapse cellular datasets), hybrid techniques that integrate multiple tracking algorithms have been recently investigated. Indeed, the hybrid

cellular tracking implementations proved more robust when compared to the detection, model or filtering-based tracking strategies, but one apparent problem is associated with the optimisation of large sets of parameters.

Thus, in conclusion, the critical analysis described in this chapter was particularly useful as it highlighted the major theoretical areas in the field of cellular tracking that require additional research. In this work, substantial efforts have been devoted towards the development of a robust cellular tracking framework that is able to minimise the tracking errors that are caused by the incidence of segmentation errors.

Another area of interest focused on was the robust identification of cellular division events. As indicated in Section 2.2, two categories of mitosis detection algorithms have been identified. In this regard, the algorithms included in the first category approached the mitosis detection by exploiting the apparent intensity changes that are associated with the parent cells prior to cellular division. These algorithms proved robust in the identification of the patent-child cells links, but they are not feasible for application in the absence of such conspicuous intensity changes that signal the mitosis events. Thus, the second category of algorithms approached the problem of mitosis detection from a more generic standpoint by analysing the cell tracking results in a backward manner. One prominent limitation associated with these algorithms is the negative impact of segmentation errors, which generates incorrect parent-child cells links. This problem has received special attention in this thesis, where a novel backward tracking scheme that is able to redress the under-segmentation problems has been proposed and comprehensively evaluated.

The proposed theoretical framework provides an integrated solution for cell tracking and mitosis detection. In this research work a novel cellular association algorithm has been developed that evaluates the topological information between the cells in each frame of the sequence. To alleviate the negative influence of segmentation errors on the accuracy of cell tracking and mitosis detection, a distinct module has been designed to identify and redress the segmentation errors during the forward and backward tracking processes. The theoretical and practical problems

relating to the development of the proposed cell tracking and mitosis detection framework are extensively discussed in the next chapter of this thesis.

Chapter 3:

Cellular Tracking and Mitosis Detection

As indicated in the previous chapter, the topic of cellular tracking and mitosis detection has received substantial interest from computer vision researchers. This interest has been largely motivated by the wide spectrum of molecular application domains that can be targeted by the development of fully automatic cellular tracking solutions. The aim of this chapter is to detail a novel image processing framework that has been designed to robustly identify the migration patterns and mitosis events in time-lapse phase-contrast image sequences.

As mentioned above, the main objective of this chapter is to present the technical details associated with the proposed cellular tracking and mitosis detection algorithm and to emphasise how the major limitations identified in the previous chapter are addressed in the solution advanced in this dissertation. The main issues that hamper the development of robust cellular tracking algorithms are as follows:

- Under-segmentation
- Random motion
- Cell division
- Cellular agglomeration
- Cells that enter/Exit the ROI imaged by the microscope

In order to provide a flexible and efficient solution for automatic cell tracking and mitosis detection, in this work a multi-stage approach has been developed that involves a computational framework that consists of three main components: segmentation, forward-tracking and backward-tracking modules. Figure 3.1 illustrates the block diagram of the full system where the sub-modules of the three main components of the developed algorithm are also shown.

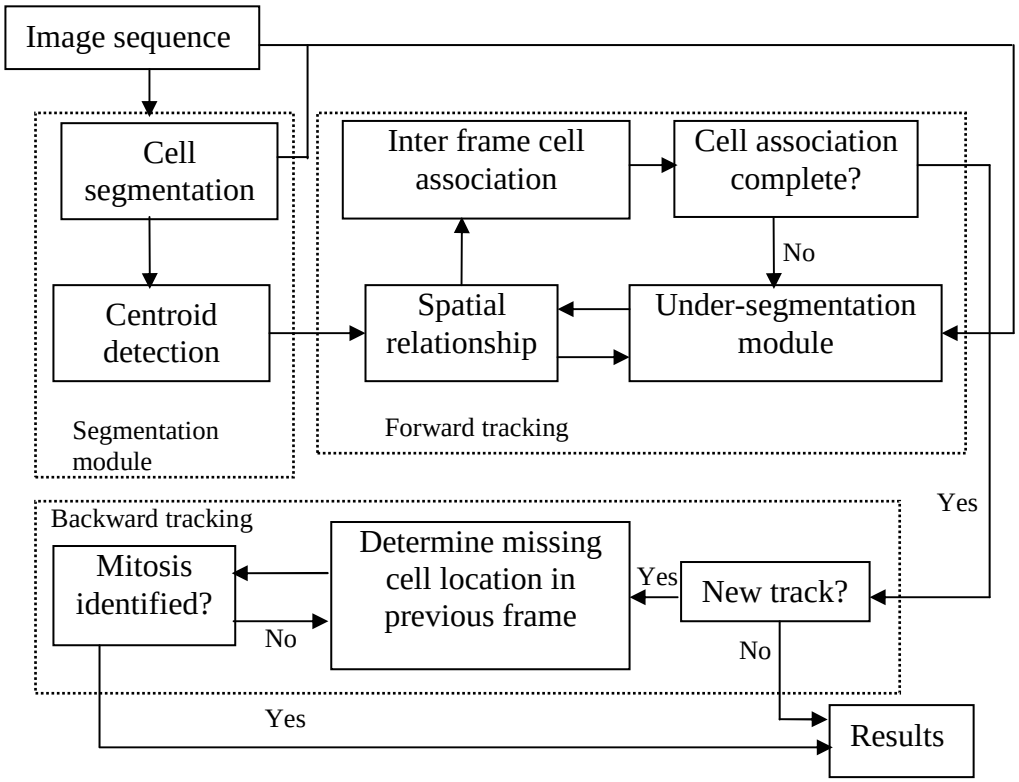

Figure 3.1. The block diagram of the proposed cellular tracking and mitosis detection framework.

The first computational component of the proposed framework is represented by the *Segmentation module*. The main goal of this module is to identify the cells in each frame of the phase-contrast image sequence and to determine their centroid points. The identified centroid points (that describe the location of the cells in each frame) are passed to the forward tracking module to determine the cell lineages (migration patterns) in all frames that compose the image sequence. In the proposed cell segmentation approach, to maximise the contrast between the cells and background a morphological process has been applied to precisely localise the intensity peaks that represent the nuclei of the cells in phase-contrast images.

The next component of the proposed framework is the *Forward tracking module* whose aim is to implement the cell tracking process. Since in phase-contrast data the cells exhibit similar intensity characteristics and random motion, the cellular association (particularly when dealing with dense cellular data) is very challenging. Thus, to generate an efficient solution a novel graph-matching-based cellular association is proposed in this thesis. Here the cellular association process evaluates

the local distribution (topological structure) of the cells that is encoded using a graph-based representation for each frame of the sequence. In this work, the graph that describes the relationships between neighbouring cells is constructed using Delaunay triangulation that encodes the spatial position of the cells within frame. The proposed cellular association is formulated as a graph matching process where the cell trajectories (or cell tracks) are obtained by identifying the corresponding centroid points in consecutive frames of the image sequence. One problem that had to be addressed in the proposed graph-based cell association process was to tackle the errors that are caused by under-segmentation. In this regard, a pattern matching approach (under-segmentation module in the block diagram shown in Figure 3.1) has been devised that is able to signal the occurrence of under-segmentation and to identify the location of the cells that have been missed by the segmentation process. More exactly, if the cell tracking identifies an unmatched cell during cellular association, the under-segmentation module is activated to find the cell location in the next image using a pattern matching algorithm that minimises the local distortion in the Delaunay mesh. The under-segmentation module forms one contribution that enhanced the performance of the proposed graph-based cell tracking algorithm.

The last module is designed to deal with cell division (mitosis) detection that performs the cell tracking in a reverse manner to identify the links between the parent and child cells. Cellular division is a biological process where a parent cell divides into two identical child cells. In this situation, the Forward tracking module associates the parent cell with one child cell, while the other child cell is considered as a new cell that will erroneously initiate a new track. The cellular division cannot be handled during the forward association process, so to link the un-associated child cell with the correct parent cell, in this thesis a reverse tracking strategy has been implemented that makes use of the cellular association results provided by the Forward tracking module. In this way, if an unmatched cell (due to cell division) is identified, a searching process is initiated using pattern matching and local cellular structure to identify the parent cell in the previous frame. In the following sections of this chapter each component (module) of the proposed framework are explained in detail.

3.1 The segmentation module

The segmentation module is the first component of the proposed cell tracking framework whose aim is to segment the cells in each frame of the image sequence. As discussed in Chapter 2, the segmentation process is hampered by limitations in the image acquisition process such as the low contrast and image noise, and it is useful to note that this scenario is particularly present when dealing with phase-contrast image data. To alleviate these adverse image conditions, researchers have developed image protocols that require the use of staining fluorescence agents to increase the contrast between the cells' nuclei and the background. However, the administration of fluorescent agents is not feasible for all cell lines as they negatively affect the cell cycle and may compromise the analysed molecular indicators. In this scenario, phase-contrast image modalities are often applied but the generated image sequences are characterised by low contrast and high intra-frame intensity variation. These adverse imaging conditions substantially complicate the segmentation process, and the main objective of the proposed cellular segmentation solution consists of the development of a robust morphological-based technique that is able to accommodate the intra- and inter-frame intensity variations and adapt to the low intensity contrast that is common for Madin Darby Canine Kidney Epithelial Cells (MDCK) and Human Umbilical Vein Endothelial Cells (HUVEC) cellular datasets.

3.1.1 The proposed cell segmentation method

In phase-contrast data, the image areas covered by cells have generally a darker interior (nucleus) which is surrounded by a peripheral bright halo. Following this intensity profile model, the cells can be theoretically extracted using threshold-based segmentation techniques. However, in practice the application of simplistic thresholding schemes proved ineffective, as the phase-contrast data cannot be precisely approximated with a bimodal distribution. The segmentation method described in this thesis entails a greyscale morphological process that is applied to increase the contrast between the cells' nuclei and the background. A block diagram that outlines the proposed cell segmentation technique is illustrated in Figure 3.2.

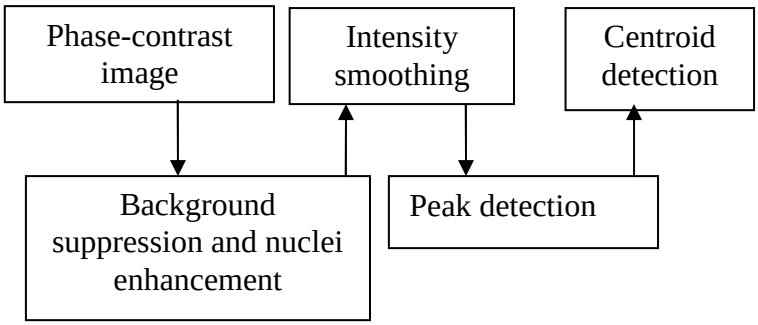

Figure 3.2. The overview of the cell segmentation module.

The main objective of the proposed cell segmentation method is to find the intensity peaks that are associated with the cells' nuclei, which facilitates the separation of the cells from the background. Since the intensity profiles of the cells are non-uniform, the first step requires the enhancement of the intensity profile of the cells' nuclei with respect to the surrounding background regions. To achieve this goal, a top-hat filter has been applied to the inverted image (the image has been inverted as the cells' nuclei are defined by low intensity signals when compared to the background). These morphological operations are indicated in equation 3.1, where the top-hat filter retains the bright intensities within the structuring element (SE) while eliminating those situated outside the SE. The application of the top-hat filter eliminates the uneven illumination and the small artefacts that are caused by the image noise.

$$I_{top} = tophat(I_{inv}) = I_{inv} - \left(I_{inv} \circ s\left(r\right)\right) \tag{3.1}$$

where I_{inv} is the inverted image, $(\circ)$ is the greyscale morphological opening operation and $s(r)$ denotes a circular structuring element with a radius *r*. The radius *r* is a user-defined parameter and should be selected in relation to the average size of the cells. The automatic identification of this parameter may be problematic in the absence of *a priori* knowledge regarding the cell data, and in this study the parameter *r* is set to a value greater than the average cell size (the parameter *r* is used to identify the cells in all frames of the image sequence).

Although the application of the top-hat transform increases the contrast between the cells' nuclei and the background, this process is not able to remove the extraneous peaks that are generated for a single cell region. This issue is illustrated in Figure 3.3.2(a). To compensate for this problem, the image data resulting from the application of the top hat transform is smoothed using a Gaussian filter where the scale parameter is adjusted to implement an $r \times r$ kernel. Next, to detect the cells' nuclei the extended maxima transform has been applied, which is the regional maxima of the *h*-maxima, and the final segmentation results are shown in Figures 3.3.2(e) and 3.3.2(f). Figures 3.3.1 and 3.3.2 details all computational steps associated with the proposed cell segmentation process and additional segmentation results are provided in Figure 3.4.

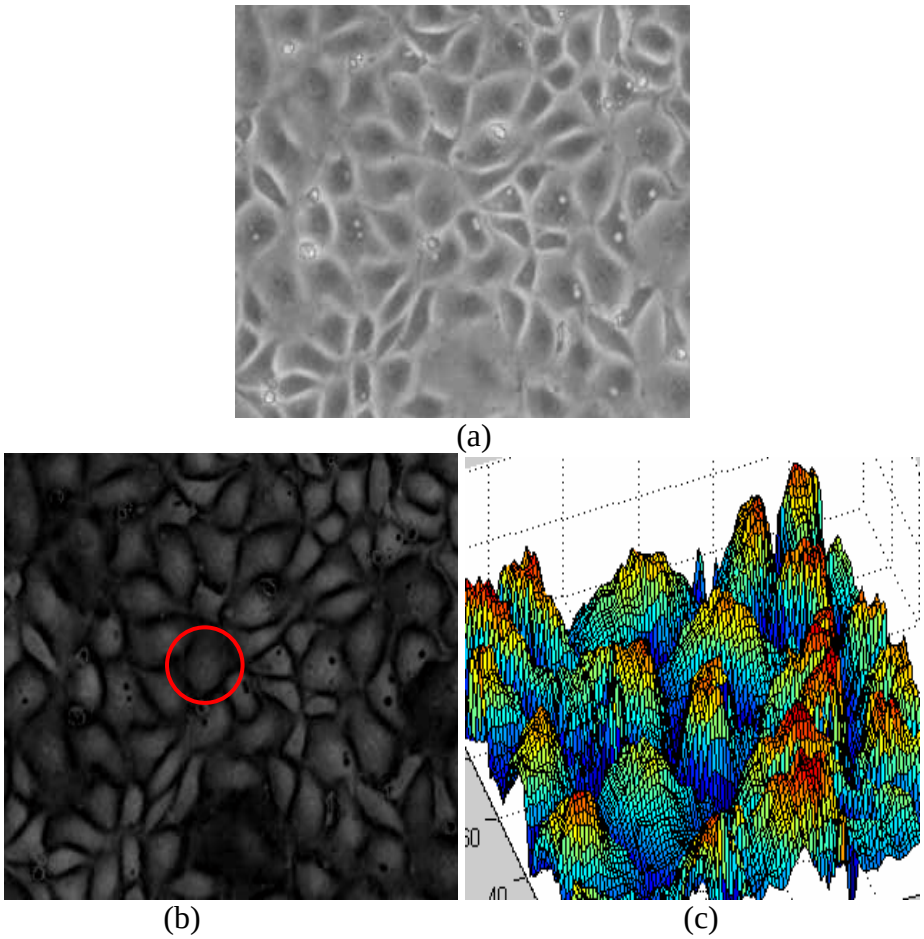

(a)

(b) (c)

Figure 3.3.1. Cell segmentation process. (a) The original phase-contrast image (Madin Darby Canine Kidney Epithelial Cells - MDCK). (b) The top-hat transformed version of the inverted image. The circular structuring element with radius *r* is marked with a red circle (c) 3D view of the image shown in (b) (further cropped to illustrate the occurrence of the multiple peaks).

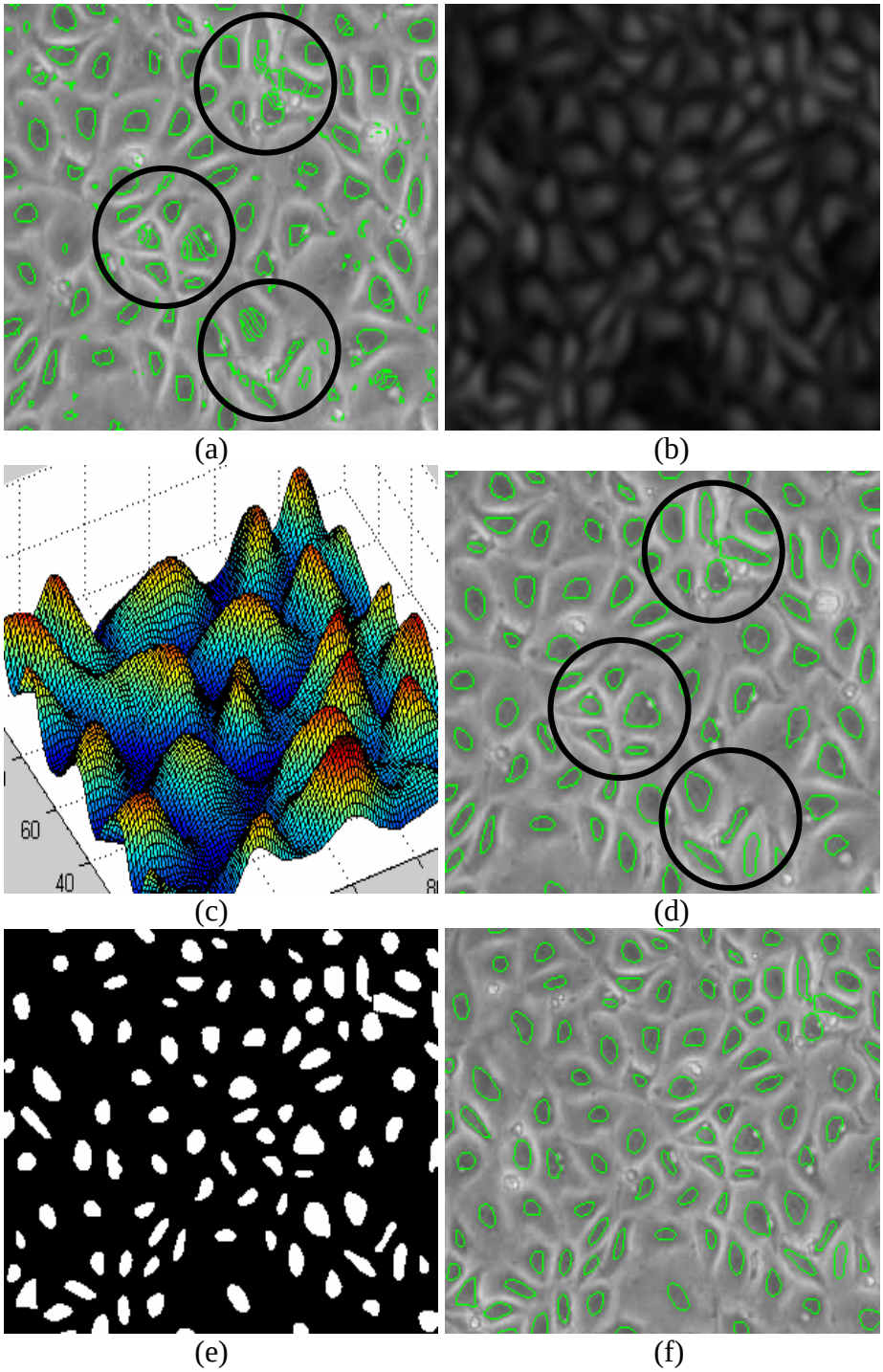

Figure 3.3.2. Cell segmentation process. (a) The segmentation result from image (c) in Figure 3.3.1 using the *h*-maxima transform – note the issues caused by the multiple peaks which generate multiple responses for a cell region – marked with black circles. (b) The image resulting after filtering the image (b) in Figure 3.3.1 with a Gaussian filter. (c) 3D view of the Gaussian smoothed result shown in (b). (d) The segmentation results from the image (b), where a single peak defines a single cell region. (e) and (f) depict the final segmentation results, where the identified cells borders are super-imposed on the original image.

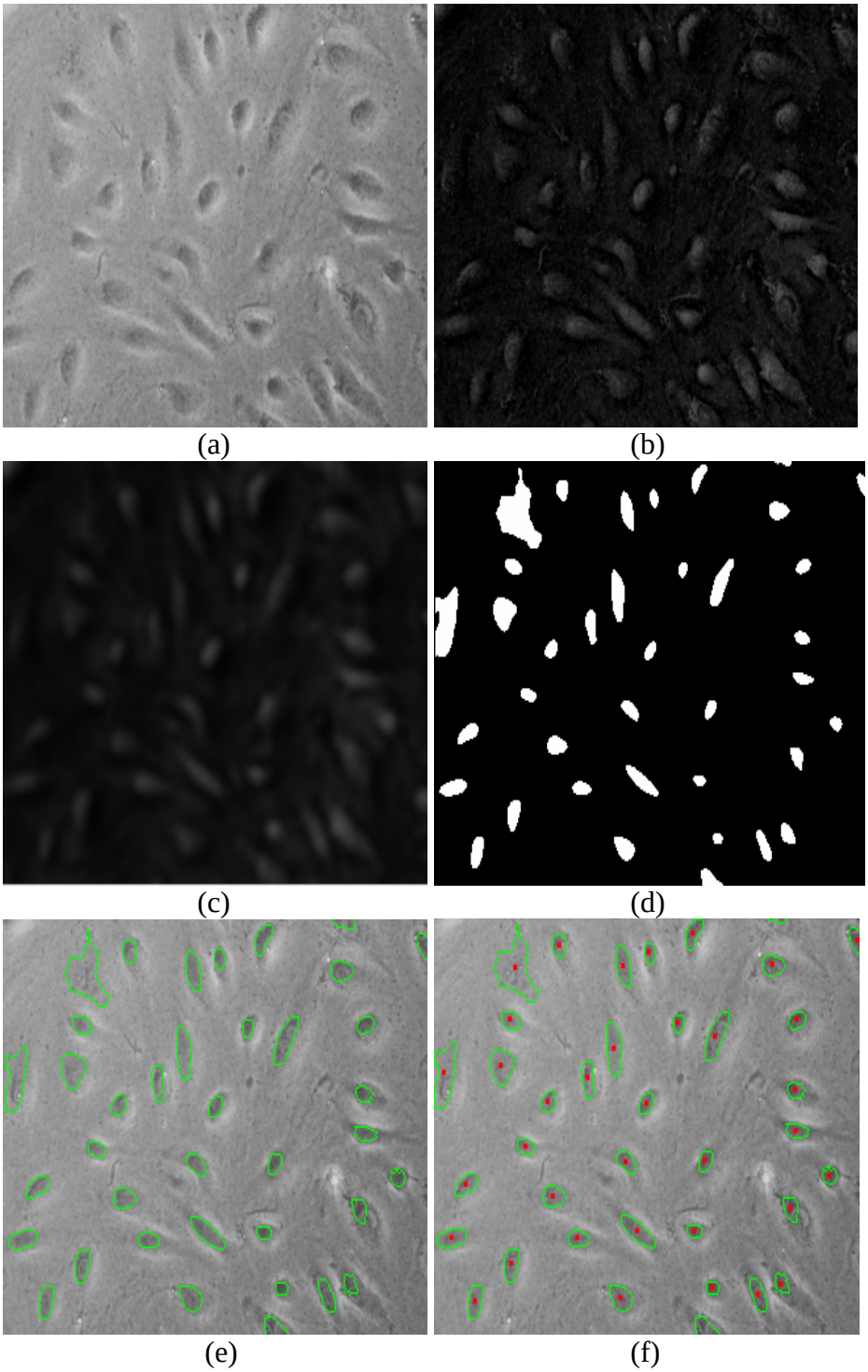

Figure 3.4. Additional segmentation results for Human Umbilical Vein Endothelial Cells (HUVEC) phase-contrast data. (a) Original image. (b) Top-hat filtered image. (c) The image resulting after filtering the image shown in (b) with a Gaussian filter. (d) Segmentation result where each blob represents a cell. (e) - (f) Segmentation results where the cells borders and their centroids (red dots) are overlaid on the original image shown in (a).

The proposed cell segmentation technique returns promising results when applied to challenging MDCK and HUVEC datasets. However, due to the extremely low contrast between the cells and the background there are situations when cells are undetected by the algorithm (under-segmentation). Such examples are illustrated in Figures 3.5.1 and 3.5.2 and the locations where under-segmentation occurs are marked with yellow and blue circles. For clarity purposes, the detection failures caused by large morphological changes are marked with yellow circles, while the blue circles denote the failures generated by the faint image contrast. The incidence of under-segmentation has negative effects on the performance of the cell tracking process and in this thesis an approach that combines a pattern matching technique with the topological information that samples the local relationships between cells has been integrated in the proposed tracking framework. The developed cell tracking approach will be detailed in the next section of this chapter.

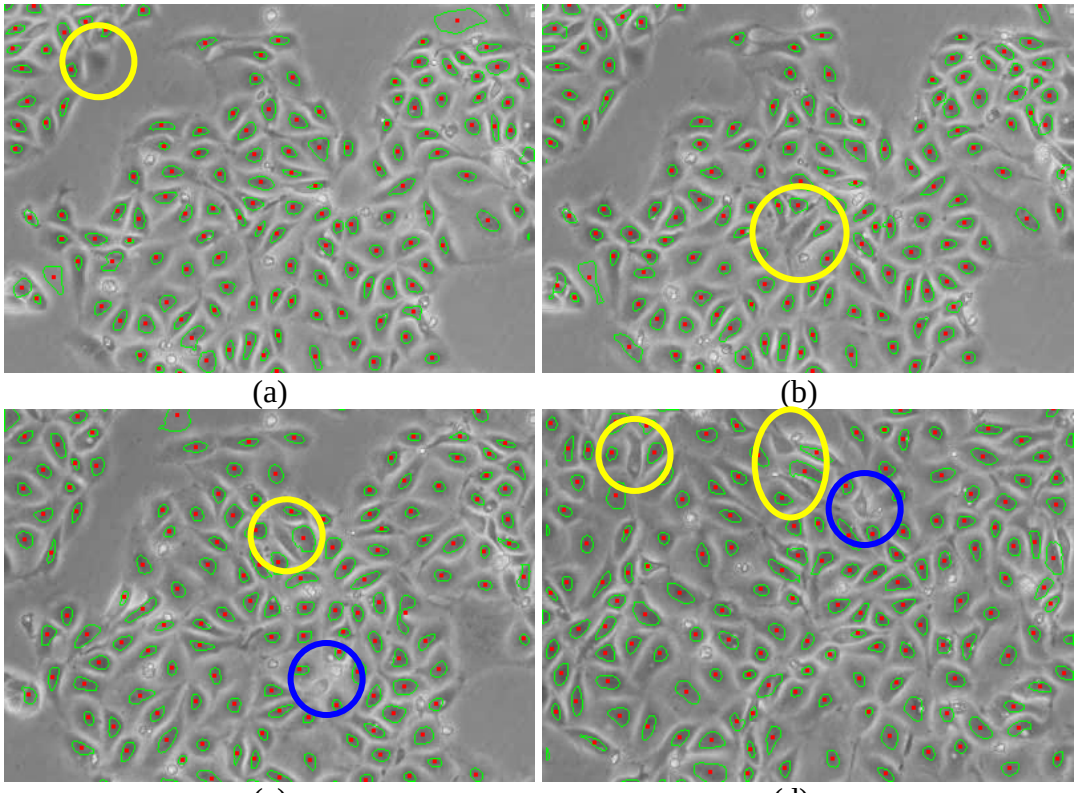

Figure 3.5.1. Examples that illustrate under-segmentation errors (MDCK data). The segmentation failures that are caused by large morphological changes are marked with yellow circles while the segmentation failures due to the faint image contrast are marked with blue circles.

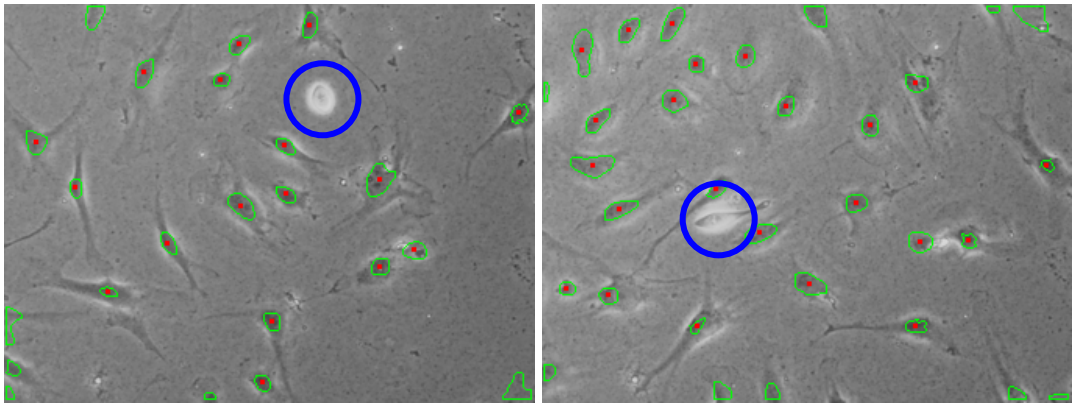

(a) (b)

Figure 3.5.2. Examples that illustrate under-segmentation errors (HUVEC data). The segmentation failures due to the faint image contrast are marked with blue circles.

3.2 The forward tracking module

The forward tracking module represents the main component of the proposed cell tracking framework. As emphasised in the literature survey provided in Chapter 2, the cellular association in time-lapse dense cellular data is the most complex process since cells have similar intensity and shape characteristics and cell migration is dominated by random motility patterns. To circumvent the issues relating to feature ambiguity or inconsistent motion estimation, the proposed cell tracking framework evaluates the structural (topological) relationships among neighbouring cells with the aim of identifying the corresponding cells in adjacent frames of the image sequence. The spatial neighbourhood relationship of a finite set of nodes (cells) can be encoded using global and local representations. Global representations construct complete graphs where each cell is linked to all other cells in frame as shown in Figure 3.6.1(a). This representation is defined by an exhaustive graph where all links between cells are considered. One disadvantage associated with this global mesh representation is that any changes in the structure of the mesh at local level (that can be caused by under-segmentation, cellular division or situations when the cells enter or exit the area visualised by the microscope) will distort the entire mesh structure. An alternative global representation considers only the links that are directly connected to the cell under observation. This simplified global representation is shown in Figure 3.6.1(b) where only the links associated with cell u are considered in matching process. Since this new global representation alleviates

several issues that are associated with the more complex exhaustive topological representations, still is not well adapted to deal with problems that are generated by local disturbances in the mesh structure. To further reduce the impact of the problems generated by local disturbances, the graph associated with a cell *u* can be constructed by considering only its neighbours situated inside a circular region R_C around it, as shown in Figure 3.6.1(c). While this approach substantially reduces the number of links required to encode the local relationships between a cell and its neighbouring cells, the structure of the resulting mesh largely depends on the selection of the radius R_C. Due to variations in cell density and different cell motility patterns in consecutive frames, the optimal selection of the parameter R_C is critical. In this sense, a small R_C value will result in disconnected graphs, while a large value will generate a graph representation as shown in Figure 3.6.1(b). Due to changes in cellular motility, an inappropriate selection for the parameter R_C will insert unpredictable changes in the structures associated with corresponding cells in consecutive frames of the image sequence and this fact may compromise the accuracy of the cell tracking process. Figure 3.6.1(d) illustrates such a situation where a small migration of one cell will result in a very different structure that is sampled within the radius R_C. In this figure the red dots denote the position of the cells in the previous frame (Figure 3.6.1(c)), while the black dots denote the position of the cells in the current frame.

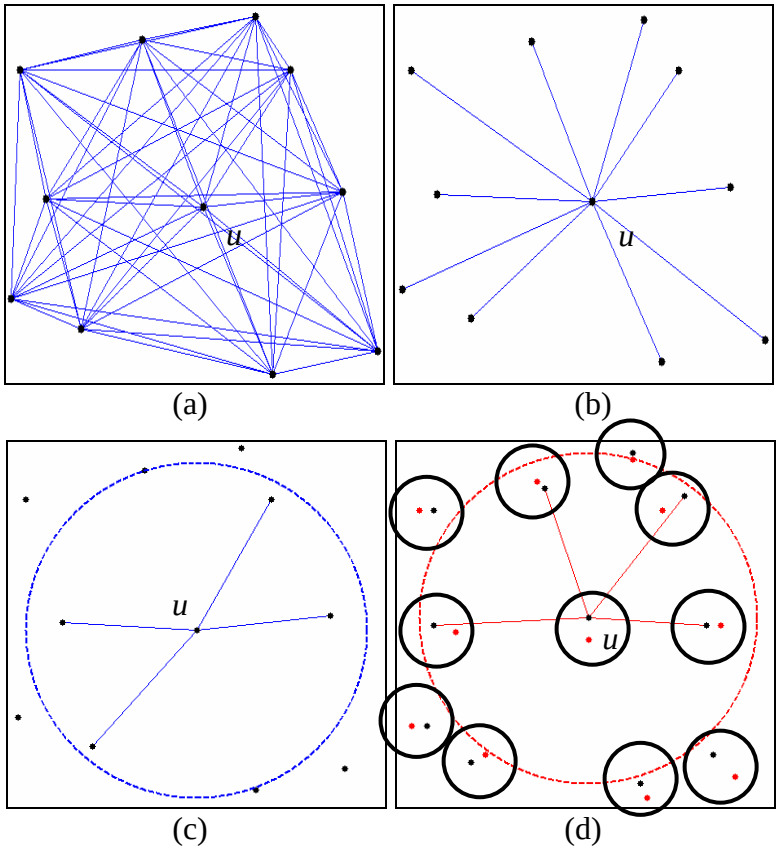

Figure 3.6.1. The use of global and local cellular relationships for cell association. (a) Exhaustive global representation where the links between all cells in the image are considered. (b) Global representation where only the links between the cell *u* and its neighboring cells are considered. (c) Local representation that is constructed using the nodes sampled around the node *u* within a circular region R_C. (d) Inconsistencies in the local structure that are caused by cellular migration.

In order to perform cell association, the spatial structure associated with a particular cell in the current frame is matched with the structures associated with other cells in the next frame. To implement an efficient cell association algorithm a compact graph representation is required. Such representation should be able to encode the spatial arrangement between cells without any user-defined parameters, be able to maintain the mesh structure in the presence of cell migration, and more importantly, the insertion and deletion of nodes that may arise due to cell division and under-segmentation should induce only local disturbances. Several methods such as relative neighbourhood graph [107], Gabriel graph [108], and β-skeletons [108] have been reported in the literature as efficient approaches for encoding the neighbouring relationships between the nodes contained in a set. These techniques are able to accommodate the issues related to the insertion/removal of nodes in the local structure, but they are either dependent on explicit parameters or they are not

able to preserve the structure when the initial positions of the nodes are altered. Thus, these methods have not been considered in the proposed implementation since the location of the cells in consecutive frames is disturbed due to cellular migration.

To achieve all properties mentioned earlier, in this work the intra-frame cellular relationship (or spatial structure) is encoded using Delaunay triangulation [35]. Delaunay triangulation generates a planar graph where each node in the mesh is optimal linked to its neighbours [102, 106]. Figure 3.6.2(a) illustrates an example where the Delaunay mesh has been constructed using the cells' centroid points and the relationships between neighbouring cells are represented by the edges that connect the nodes in the graph. This representation is suitable for cell association since the spatial structure encoded by Delaunay triangulation is minimally affected by cell migration in consecutive frames. Figures 3.6.2(b) and 3.6.2(c) show the construction of the Delaunay mesh for the cell *u* in two cases: before and after the local structure has been disturbed by random migration. In Figure 3.6.2(c) it can be observed that although the initial positions of the cells around the node *u* have been distorted, the resulting mesh is still similar to that depicted in Figure 3.6.2(b).

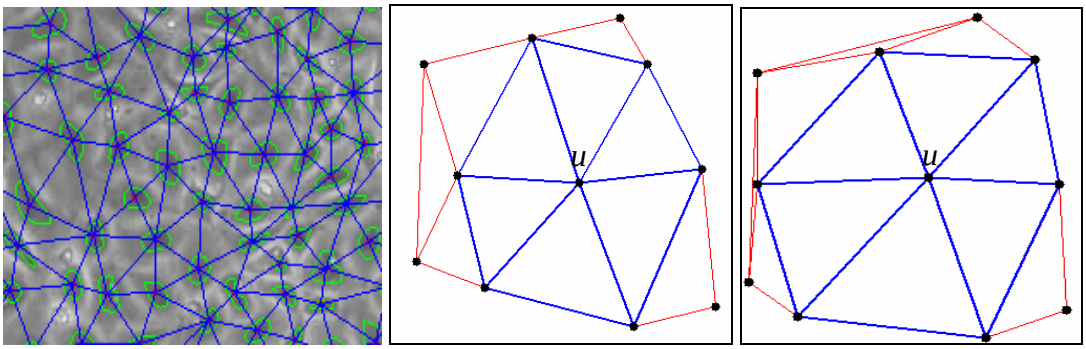

(a) (b) (c)

Figure 3.6.2. Delaunay triangulation and its advantages in cell association. (a) Delaunay mesh that is constructed using the centroids of the cells that are detected in one frame of the sequence. (b) Delaunay mesh constructed for the points sets in Figure 3.6.1(a). (c) Delaunay mesh constructed for the same set of points where a random migration is incorporated with each of the points.

In the structure encoded by the Delaunay mesh, the triangles tend towards equiangularity and the insertion or removal of a node affects the mesh representation only at the local level [81, 106]. This property is particularly well-adapted to encode the neighbouring relationship between the cells in the image, as the insertion and the

removal of nodes can be caused by cellular division or under-segmentation. This is illustrated in Figure 3.6.3. Figures 3.6.3(b) and 3.6.3(c) shows the effect of deletion and insertion of a node in the mesh in the original graph shown in Figure 3.6.3(a) and it can be observed that the insertion/deletion of nodes disturbs the original mesh only at local level.

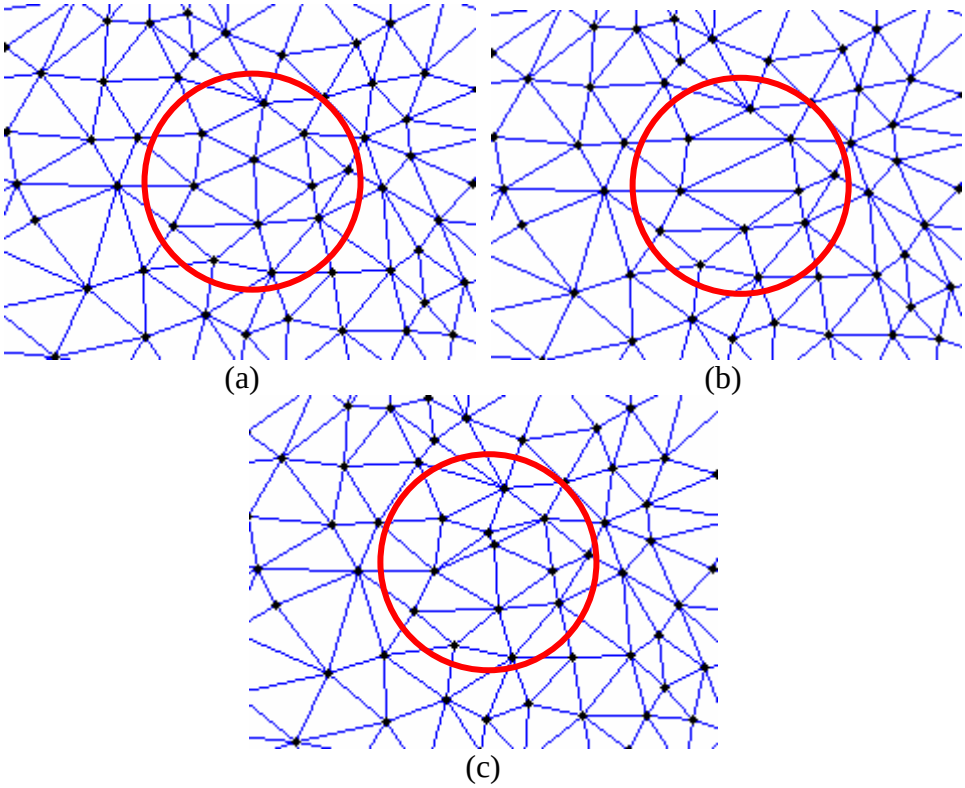

Figure 3.6.3. Examples that illustrate that the removal (under-segmentation) and the insertion (cell division) of nodes (cells) affect the structure encoded by the Delaunay mesh only at local level. (a) Initial Delaunay mesh. (b) Mesh after node deletion. (c) Mesh after node insertion.

Once the Delaunay meshes are constructed in two consecutive frames, the cellular association process can be formulated as a graph-matching problem. Since the cell relationships are accurately modelled using this graph-based formulation, the similarities between the local structures in two consecutive frames can be efficiently estimated based on the assumption that the cells are accurately detected in each frame and the similarity measurements can be evaluated for the cellular association. As the identification of the corresponding cells in consecutive frames of the sequence entails a sequential process based on the evaluation of the local structure, missing cells in one frame will have a detrimental effect on the accuracy of the

tracking process (i.e. it will generate discontinuities in the cell lineages that are determined for each individual cell). To overcome this problem, a procedure referred to as under-segmentation module has been incorporated in the proposed cell tracking strategy, which aims to redress the undesired effects generated by under-segmentation. This computational step will be detailed in the Section 3.2.2 of this chapter.

3.2.1 The cellular association process

The aim of the cell association process is to identify corresponding cells in consecutive frames of the image sequence. In the proposed approach, the correspondence between the cells in frames T and T+1 is determined, as indicated in the previous section, based on the similarities in the local structures that are encompassed in the Delaunay graphs D^T and D^{T+1}. (The Delaunay graphs D^T and D^{T+1} are constructed using the centroid points resulting after the application of the cell segmentation process). More precisely, the cellular association (node matching) process evaluates the level of similarity in the local structure for all nodes in the graphs D^T and D^{T+1}. Key to this matching process is the mesh (or graph links) that encompasses the local structure contained in the Delaunay representation for each node in the image. An example that illustrates this concept is shown in Figure 3.7.1

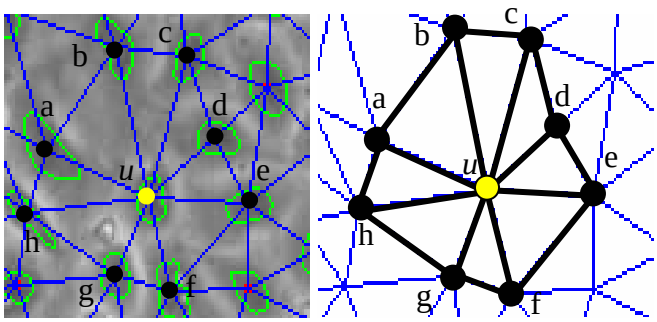

(a) (b)

Figure 3.7.1. The local structure S_u^T associated with the cell u in the Delaunay mesh D^T, frame T. (a) Delaunay mesh D^T. (b) The local structure associated with the node u in the mesh D^T.

When translated into a mathematical formulation, the local structure S_u^T associated with the node u in the Delaunay D^T mesh in image T is defined as follows,

$$S_u^T = \{\Delta upq\} \;\; u, p, q \in D^T, u \perp p, u \perp q, p \perp q \tag{3.2}$$

where Δupq is the triangle connecting the nodes *u*, *p*, and *q*, $u \perp p$ denotes that the nodes u and p are linked by the edge $\overline{up}$ and {.} is the mathematical set operator. To evaluate the level of similarity between the local structures associated with two nodes $u \in D^T$ and $v \in D^{T+1}$ it is necessary to define a metric that is able to evaluate the distortion level in the mesh in the D^T and D^{T+1} graphs.

Since the local structure associated with a node in the Delaunay mesh is represented by a number of triangles that are directly incident to the node, the cellular association process is carried out by measuring the similarities of these triangles in two consecutive frames. To achieve this goal, the Hausdorff distance [103, 102] has been employed to determine the triangular dissimilarity. The Hausdorff distance provides a robust measure to quantify the mutual proximity for all vertices that generate the triangles in the two Delaunay meshes, by considering the maximal Euclidean distance between any vertex of one triangle with respect to the vertices that form the other triangle. The Hausdorff distance for two triangles Δ_1 and Δ_2 is defined in equation (3.3).

$$H(\Delta_1, \Delta_2) = \max\left(\varphi(\Delta_1, \Delta_2), \varphi(\Delta_2, \Delta_1)\right) \tag{3.3}$$

$$\varphi(\Delta_1, \Delta_2) = \max_{p \in \Delta_1} \left\{ \min_{q \in \Delta_2} \{d(p, q)\} \right\} \tag{3.4}$$

where $d(p,q)$ is the Euclidean distance between two nodes with indexes *p* and *q*.

The Hausdorff distance has been extensively used for shape matching [80, 99-105] since it is a more precise dissimilarity measure than the shortest Euclidean distance. The shortest Euclidean distance does not provide satisfactory results since it is shape independent metric and in addition is not able to sample the changes in the vertex locations. Figure 3.7.2 illustrates this limitation when the shortest Euclidean distance is applied to evaluate the dissimilarity between two triangular shapes. As

indicated in Figure 3.7.2, the shortest Euclidean distance (marked with a red line) is the same in both cases shown in Figures 3.7.2 (a) and (b) although the positions between the two triangular shapes in these two scenarios are quite different. Since, the Hausdorff distance is computed based on the mutual proximity of all vertices that compose these two triangular shapes, the dissimilarity measure is affected by the distortion of triangular shapes or by changes in vertex locations. Using the same judgement, it can be easily observed that the Hausdorff distance is more precise in sampling the shape dissimilarity than the metric provided by the distance between the centroid points of the two triangular shapes. The favourable properties associated with the Hausdorff distance motivated its use in the proposed cellular association algorithm to measure the dissimilarities between the triangular shapes encoded in two consecutive Delaunay meshes.

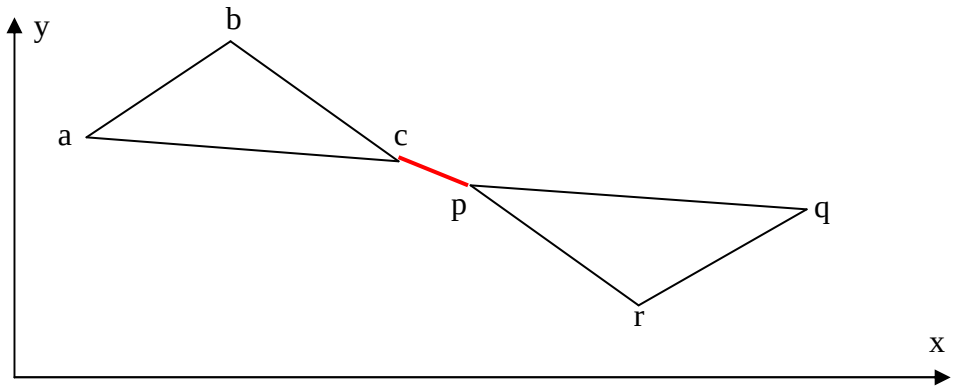

(a)

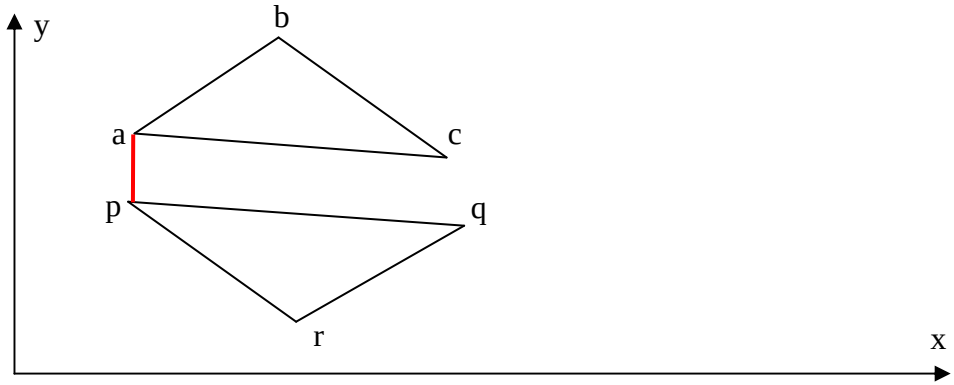

(b)

Figure 3.7.2. Example that illustrates the problem associated with the use of the shortest Euclidean distance when applied to measure the dissimilarity between two triangular shapes.

During the cell association process, all triangles associated with a node in the current frame are matched based on the Hausdorff distance measure. With respect to equation (3.3), the triangles Δ_1 and Δ_2 are assumed to be similar only if their Hausdorff distance is smaller than a predefined threshold α as indicated in equation (3.5). This predefined threshold restricts a triangle associated with the node *u* in the current frame to be matched with triangles that are associated with non-corresponding nodes in next frame. In the implementation detailed in this thesis, α is set to the maximum instantaneous cell movement in two consecutive frames to accommodate the inherent distortion that is caused by cell migration.

$$MT\left(\Delta_1,\Delta_2\right)=\begin{cases}1 & H\left(\Delta_1,\Delta_2\right)<\alpha\\ 0 & otherwise\end{cases} \tag{3.5}$$

Since the local structure associated with each node consists of a set of triangles that are generated by the node of interest and the adjacent nodes in the Delaunay mesh, to completely evaluate the similarity between the nodes $u\in D^T$ and $v\in D^{T+1}$ a matching confidence function *M*(.) that evaluates the similarity between two local structures S_u^T and S_v^{T+1} has been defined as indicated in equation (3.6).

$$M\left(u,v\right)=\frac{\sum_{\Delta_1\in S_u^T,\Delta_2\in S_v^T} MT\left(\Delta_1,\Delta_2\right)}{\max\left(\left\|S_u^T\right\|,\left\|S_v^{T+1}\right\|\right)} \tag{3.6}$$

where $\left\|S_u^T\right\|$ represents the number of triangles contained in the set S_u^T. The term that defines the denominator in equation (3.6) has been applied to normalise the matching confidence *M*(.) in the range [0,1].

Based on the value returned by equation (3.6) for each pair of cells (nodes) in frames *T* and *T*+1, the cells are associated in multiple stages. In the first stage, the nodes (cells) in frames *T* and *T*+1 that have their local structure completely matched (i.e. *MT*(.) =1 for all triangles in the local structures S_u^T and S_v^{T+1}) are associated. An example where two nodes *u* and *v* in frames *T* and *T*+1 have their local structures

completely matched is shown in Figure 3.8, where the corresponding triangles in meshes D^T and D^{T+1} are shaded and indexed in agreement to the Hausdorff distance. It is important to note that the nodes that are matched in the first stage of the cellular association process are matched with the highest level of confidence and they are included in a reference list R (refer to equation 3.7) that will be used to guide the following steps that attempt to identify the corresponding nodes for which the local structure was only partially matched.

$$R = \left\{ (p,q) \mid p \in D^T, q \in D^{T+1} \right\} \tag{3.7}$$

where p and q form a pair of corresponding nodes in frames T and T+1, respectively that are matched in the first stage of the cellular association process.

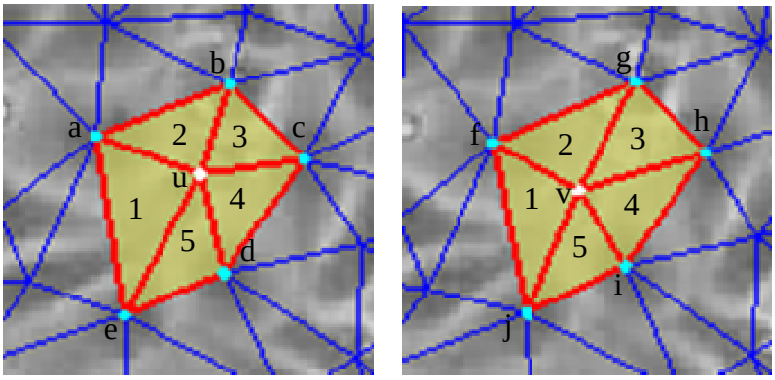

(a) (b)

Figure 3.8. An example that illustrates a case where the local structures for two nodes u and v in frames (a) T and (b) T+1 are completely matched with respect to equation (3.6).

A graphical example that illustrates the cells that are matched in the first stage of the cellular association is presented in Figure 3.9. In this diagram, for clarity purposes, the cells that have their local structures fully matched are marked with white dots in the images corresponding to frames T and T+1, whereas the un-associated cells are marked with small red dots. (To further emphasize the un-associated nodes in Figure 3.9, the edges in the Delaunay graphs D^T and D^{T+1} corresponding to un-associated local structures are marked with red lines).

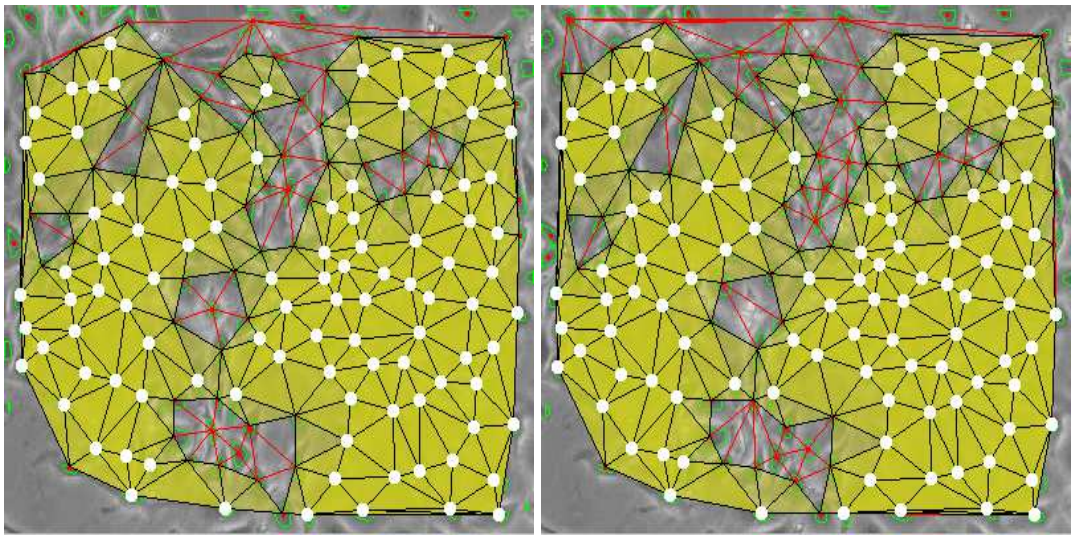

(a) (b)

Figure 3.9. The first stage of the cell association process. (a) Frame *T*. (b) Frame *T*+1. The cells associated in the first stage are marked with white dots. The remaining cells for which their local structures were only partially matched in frames *T* and *T*+1 are marked in this diagram with small red dots.

Due to cellular division, under-segmentation and degeneracy problems in the construction of the Delaunay mesh, the local structure for the node u (S_u^T) in the first Delaunay mesh (frame T) could be distorted when compared to structure of the corresponding node v (S_v^{T+1}) in the next frame. As a result, some of the triangles in the local structures S_u^T and S_v^{T+1} may not be matched with respect to (3.5). Figure 3.10 illustrates two examples for which the local structures of corresponding nodes u and v in frames T and T+1 are only partially matched.

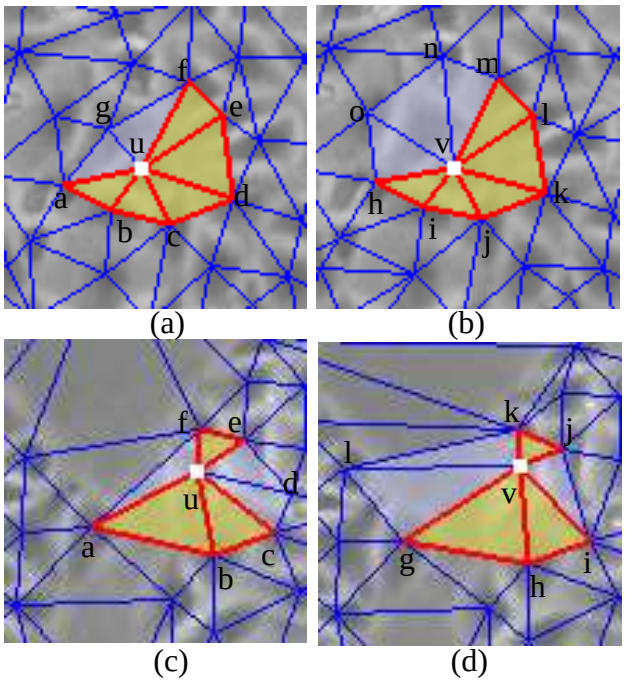

Figure 3.10. Examples that illustrate two cases of corresponding nodes for which their local structure has been partially matched. (a) and (b) illustrate the distortion in the local structure that is caused by under-segmentation. (c) and (d) show the distortion in the local structure that is caused by large migration. (a, c) frame *T*. (b, d) frame *T*+1.

The second stage of the cell association process deals with the cells that were not matched in the first stage (i.e. they have their structures only partially matched). To provide more confidence in the second stage of the cell matching process, a partial matching confidence *PMC*(.) is measured using equation (3.8) that evaluates both the similarity for triangles and mesh edges with respect to the reference nodes contained in the list *R*. In this node association stage, edge matching is also evaluated (see the second term in equation 3.8) to maximise the use of the local structure when matching the nodes with *M*(.) < 1. This avoids the incorrect matching decisions that may be caused by cellular migration and under-segmentation. The last term in equation (3.8) is introduced to penalise the displacement between the nodes *u* and *v* in frames *T* and *T*+1, respectively.

$$PMC(u,v) = M(u,v) + \frac{ME\left(E_u^T, E_v^{T+1}\right)}{\max\left(\left\|E_u^T\right\|, \left\|E_v^{T+1}\right\|\right)} + \left(1 - \frac{d(u,v)}{\alpha}\right) \qquad (3.8)$$

where $E_u^T = \{\overline{up}\} \mid p \in R$, $E_v^{T+1} = \{\overline{vq}\} \mid q \in R$, $ME\left(E_u^T, E_v^{T+1}\right)$ denotes the number of matched edges between E_u^T and E_v^{T+1}, $\left\|E_u^T\right\|$ is the number of edges in the set $\{E_u^T\}$, $d(.)$ is the Euclidean distance and α is the maximum cell's displacement in two consecutive frames. The distance constraint term is added to maintain a high level of matching accuracy when dealing with large migration patterns that may occur during cellular division and to prevent incorrect matches that are caused by larger than α instantaneous cellular motilities that are generated by under-segmentation.

The nodes that were unmatched in the first stage and that maximise the value of *PMC*(.), are associated and are included in the list *R*. This process is shown in Figure 3.11 where the nodes associated in the second stage are marked with large blue dots.

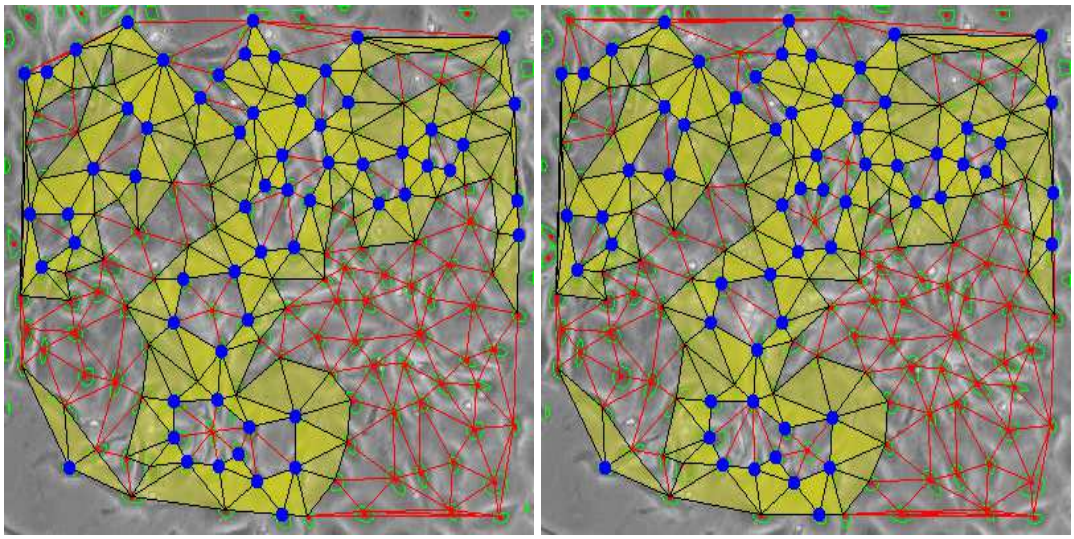

(a) (b)

Figure 3.11. The cell association using partial structure matching. (a) Frame *T*. (b) Frame *T*+1. The nodes matched in the second stage of cellular association are marked with blue dots and the corresponding matching structures are shaded in yellow.

Due to under-segmentation, cellular division and cells that enter/exit the area imaged by the microscope, there are still cells in frames *T* and *T*+1 that are left un-associated. This is illustrated in Figure 3.12 where the results returned after the application of the two-stage cellular association procedure are shown. In this diagram, the cells matched in the first stage are marked with white dots, the cells

associated in the second stage are marked with blue dots, while the cells left un-associated are marked with solid black circles.

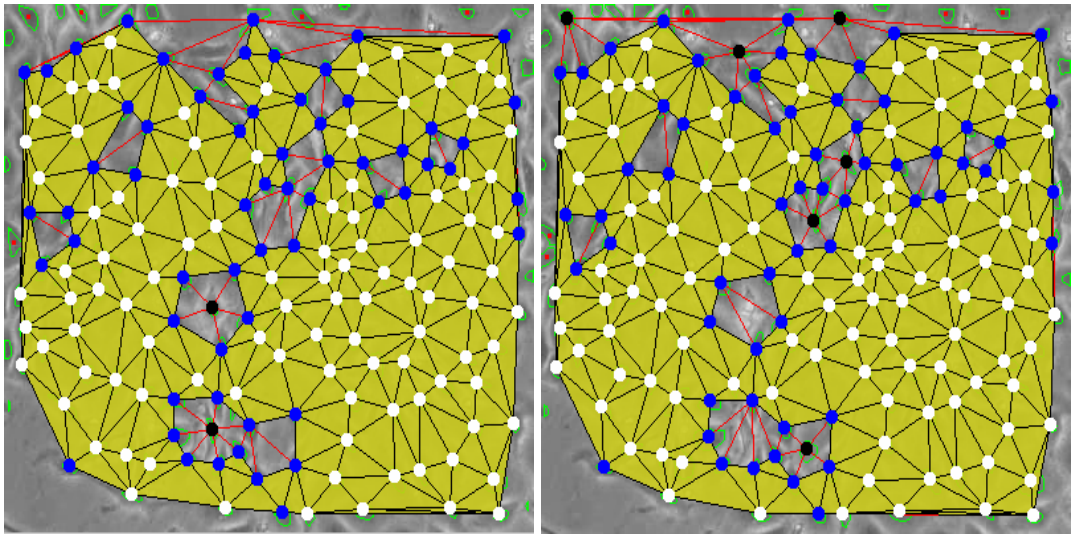

(a) (b)

Figure 3.12. Matching results at the end of the two-stage cellular association process. The white dots denote the cells associated in the first stage. The blue dots illustrate the cells matched in the second phase of the association process. The remaining cells marked with black dots in image (a) are left un-associated due to under-segmentation. The cells marked with black dots in (b) are cells that entered the region of interest imaged by the microscope in frame *T*+1 and they do not have corresponding cells in frame *T*.

From the un-associated nodes shown in Figure 3.12, the nodes in frame *T*, for which the corresponding nodes in frame *T*+1 left the region of interest, were correctly left un-associated. Similarly, the same observation applies for nodes that enter the region of interest only in frame *T*+1. As these nodes do not have corresponding cells in frame *T*, they were correctly left un-associated. Thus, in the last stage of the cell association process we focus on the un-matched nodes (in frame *T*) that were not associated due to under-segmentation. This situation occurs when nodes in frame *T*+1 were missed by the segmentation process. In the next section, a proposed solution to redress the errors caused by under-segmentation is detailed.

3.2.2 Redressing under-segmentation errors

There are situations when cells are not detected by the proposed *h*-maxima-based segmentation algorithm due to the very low contrast in the image. As explained in Section 3.2.1, the occurrence of segmentation errors disturbs the local structure in the Delaunay mesh in the *T*+1 frame. Therefore, the local structure for the cell in frame *T* will not be matched in frame *T*+1 if its corresponding cell is left undetected by the segmentation process. If such a situation occurs, the trajectory (cell lineage) for the cell in frame *T* will be terminated, and another track will be initialised when the unmatched cell in frame *T*+1 is detected in the subsequent frames. Practically, the incidence of under-segmentation will generate gaps in the identified cell lineages (or cell tracks) as illustrated in Figure 3.13. (In this diagram the 2D+time cell tracks are plotted for 100 frames.)

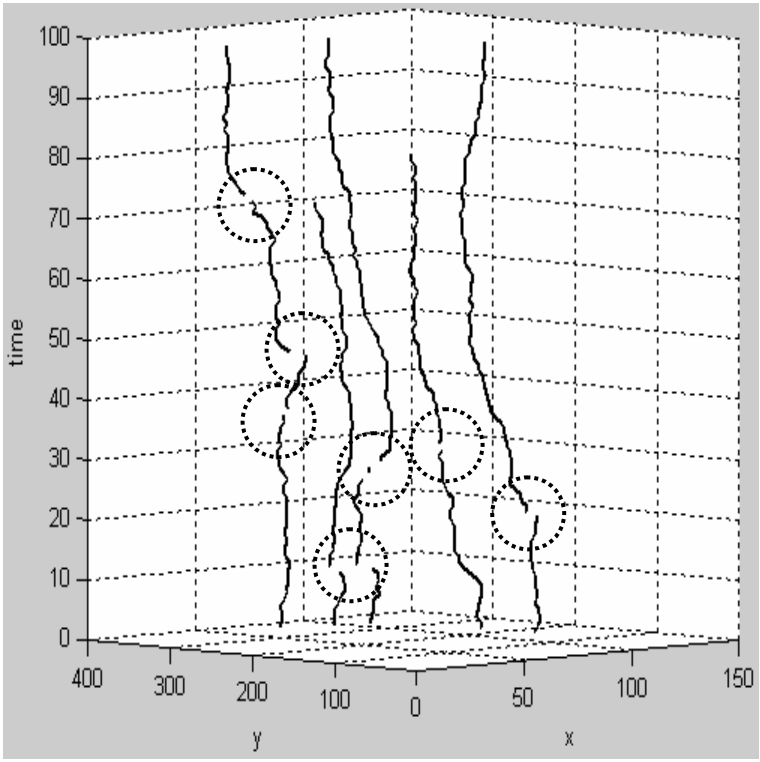

Figure 3.13. 2D+time plot detailing the cell tracks for 100 frames. The under-segmentation errors generate gaps (indicted by dashed circles) in the cell tracks that were obtained after the application of the two-stage cell association process.

If cells are left un-associated in frame *T*, this triggers the activation of the procedure that is applied to redress the problems caused by under-segmentation. To

accomplish this goal, the proposed algorithm initiates a search process to identify a suitable cell location in frame T+1 using the normalised cross-correlation and the local structure encompassed in the Delaunay mesh. In this sense, the algorithm attempts to identify an image location in frame T+1 that approximates the intensity profile of the unmatched cell in frame T (the intensity profile of the cell in frame T is sampled within a rectangular mask). To avoid the potential identification of cell locations that are too far with respect to the position of the un-associated cell and the previously matched local structures (i.e. nodes included in the list R) in frame T, the search region in frame T+1 is restricted within a $(2\alpha+1)\times(2\alpha+1)$ area whose center is the coordinate of the centroid of the un-associated cell in the frame T. The application of the normalised cross correlation procedure will generate multiple peak points within the image area enclosed within the $(2\alpha+1)\times(2\alpha+1)$ mask. To select the best location among the multiple peaks, the local structures associated with the un-matched cell in the frame T and the local structures constructed for each peak point are evaluated next, and the peak point that minimises the equation (3.9) is selected as the best location in frame T+1 for the un-associated cell in frame T. To maximise the level of confidence when the expression in (3.9) is assessed, the local structure for each peak in frame T+1 is constructed by linking the peak point and the reference nodes (cells) contained in the list R.

$$DL(u,v_i)=\frac{\sum_{a,b\in R}\left(l(\overline{ua})-l(\overline{v_ib})\right)}{\max\left(l(\overline{ua})-l(\overline{v_ib})\right)}+\frac{\sum_{a,b\in R}\left(\theta(\overline{ua})-\theta(\overline{v_ib})\right)}{\max\left(\theta(\overline{ua})-\theta(\overline{v_ib})\right)} \qquad (3.9)$$

where u is the unmatched cell in frame T, $\overline{ua}\in D^T$, $\overline{v_ib}\in D^{T+1}$, v_i is the i^{th} peak point, $l(e)$ returns the length of the edge e and $\theta(e)$ returns the angle of the edge e with respect to the horizontal axis. As mentioned earlier, the location v that approximates the unmatched cell in frame T+1 is the peak point v_i that minimises the DL as follows,

$$v=\arg\min_{v_i|i\in[1..m]}\left(DL(u,v_i)\right) \qquad (3.10)$$

where m is the number peaks returned by the normalised cross correlation process in frame T+1. Equations (3.9) and (3.10) evaluate the similarity between the length and angles associated with edges for each potential peak points v_i in frame T+1 and those calculated for the un-matched node u. These new measurements provide additional information that is able to sample the subtle differences between the structures constructed for each candidate point with positive effects in the identification of the best peak point within the search window.

The step-by-step operations that are applied to redress the problems caused by under-segmentation are detailed in Figure 3.14. The cell labelled with u in frame T (Figure 3.14a) could not find a corresponding cell in frame T+1 due to a segmentation error (Figure 3.14b) (to illustrate the corresponding cells in frames T and T+1, in Figures 3.14(c, d) the track indexes are provided for each cell). The activation of the under-segmentation module identifies the local maxima points (peaks) with respect to the normalised cross correlation and the identified peak points (v_1, v_2 and v_3) are marked with solid black circles in Figure 3.14(f). The edge structures constructed for each peak point are shown in Figure 3.14(g-i) and the peak location that minimises the expression shown in (3.9) is marked with a red circle in Figure 3.14(j).

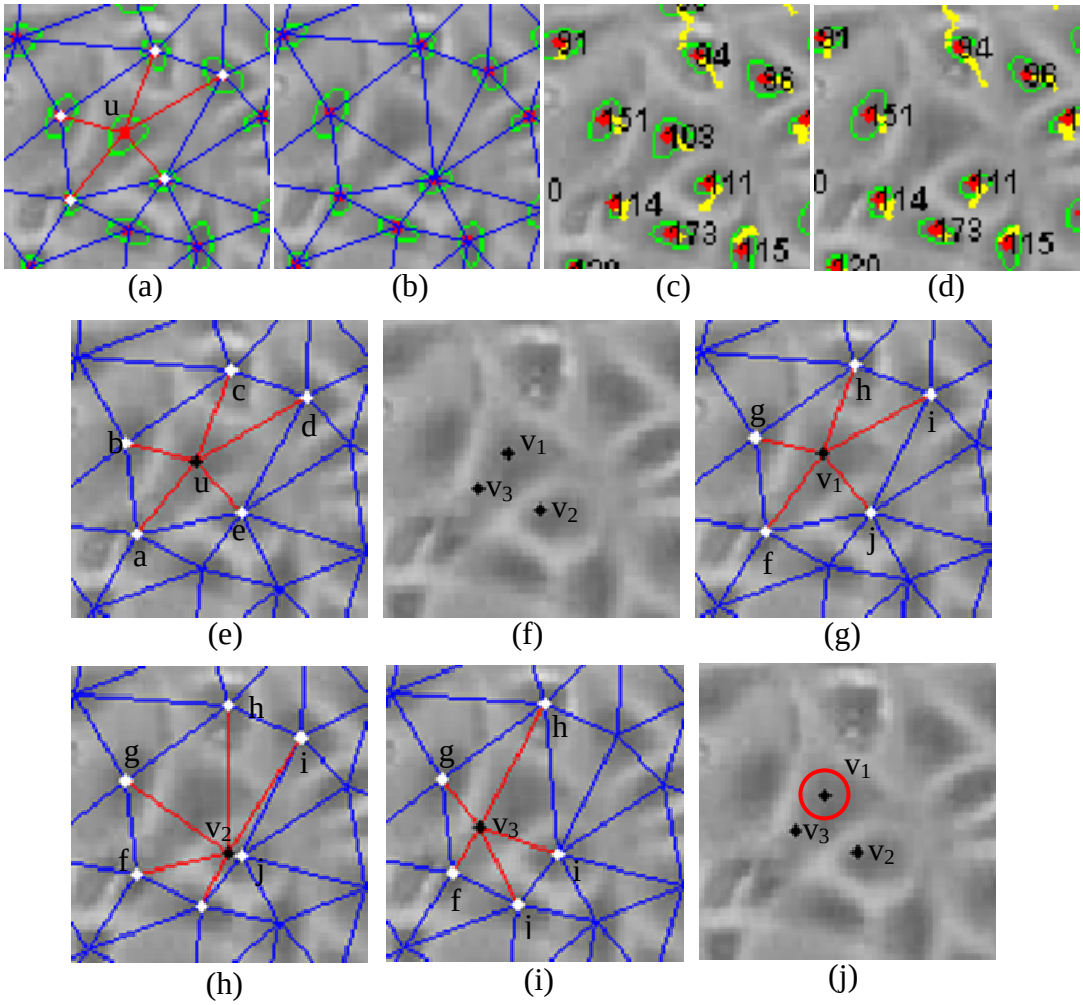

Figure 3.14. An example that illustrates the step by step operations associated with the under-segmentation module. (a, b) Frames *T* and *T*+1, respectively, where is illustrated a case where a cell *u* in frame *T* is left un-associated due to under-segmentation. (c, d) Track indexes for each cell in frames *T* and *T*+1. (e) Same as (a), the edge structure associated with the cell *u* in frame *T*. (f) The peak points identified by the normalised cross correlation. (g-i) The edge structures constructed for each peak points illustrated in (f). (j) The peak point that minimises the expression shown in (3.9). The algorithm assigns this point as the corresponding node for the unmatched cell *u* in frame *T*.

To visually illustrate the improvement in cell tracking accuracy that is achieved by the application of the proposed under-segmentation module, Figure 3.15 shows the 2D+time tracking results obtained on the same set of cells as illustrated in Figure 3.13. As illustrated in this diagram, the gaps in the tracks that were caused by under-segmentation were successfully eliminated by the application of the proposed module (see the points marked in red in Figure 3.15).

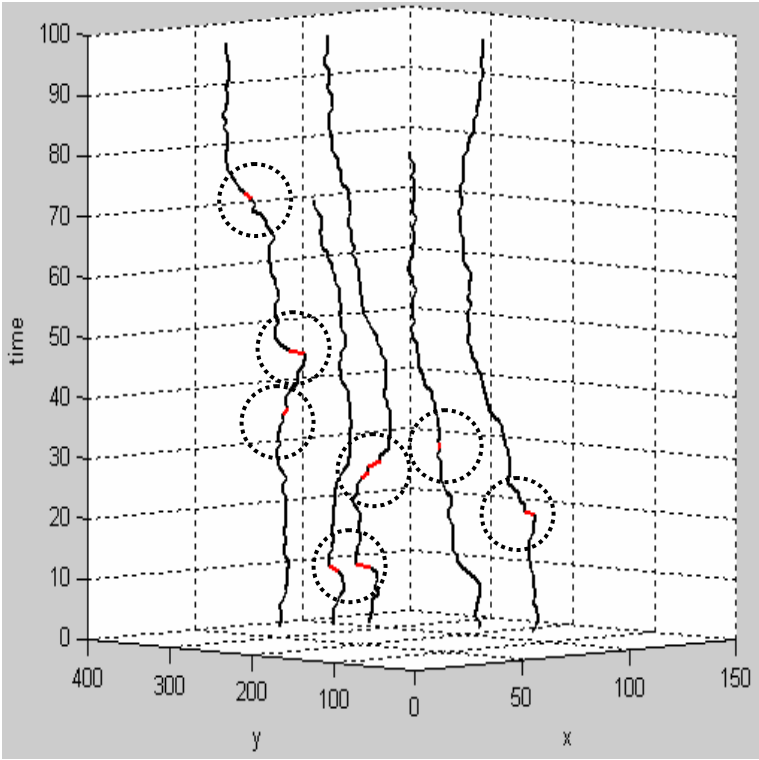

Figure 3.15. 2D+time plot that illustrates the tracking results when the under-segmentation module has been applied to redress the segmentation errors.

As indicated in Figure 3.15 the proposed under-segmentation module successfully identifies the locations of the cells missed by the segmentation process. To numerically evaluate the improvement in performance caused by the application of the proposed under-segmentation module, Table 3.1 shows the percentage of cell tracks that were correctly identified by the forward tracking process in two situations: (a) when the under-segmentation module is de-activated and (b) when the under-segmentation module is integrated in the development of the cellular association process. Full details in regard to the process applied to generate the ground truth data are provided in Section 4.1, whereas the metrics employed to quantify the accuracy of the segmentation and tracking process are indicated in equations 4.1 and 4.3.

Table 3.1. Tracking and segmentation accuracy with and without the activation of the under-segmentation module.

Cell type	No. of frames	Under-segmentation module de-activated		Under-segmentation module activated	
		Segmentation	Tracking	Segmentation	Tracking
MDCK-1	100	97.41%	62.25%	98.15%	89.47%
MDCK-2	100	97.28%	60.95%	98.91%	87.50%
MDCK-3	100	96.96%	60.27%	98.11%	82.18%

3.3 The backward tracking module

Cellular division is a self-occurring process that cannot be accurately predicted during the standard forward tracking procedure, unless the parent cells exhibit apparent intensity transitions in frame (or frames) that precede cellular division. Unfortunately, this favourable situation is not present when dealing with standard phase-contrast cellular data, and this fact can be observed in Figure 3.16.1, row-1 and row-3, where consecutive images from a MDCK sequence are depicted to illustrate a cell division (marked with circles) event in two distinct cases. These two cases illustrate the problems created by under-segmentation during the cell division process. The first row in Figure 3.16.1 depicts a practical scenario where the parent cell and one of the child cells are not detected (case 1), while the third row (case 2) presents a situation when one child cell is missed by the segmentation process. Thus, cell division detection during forward tracking is not practical, as the cellular association entails a one-to-one matching constraint. As a consequence, one of the child cells resulting from mitosis is associated with the parent cell, while for the other child cell, a new track will be initialised with a new index. This is illustrated in Figure 3.16.1, row-2 and row-4, where the parent cell (index 110 in row-2, 45 in row-4) is matched to one of the child cells, whereas for the other child cell a new track index (342 in row-2 and 328 in row-4) is generated. To help visualise the problems caused by cellular mitosis during the forward tracking process, in Figure 3.16.2, the 2D+time cell tracks that are identified by the forward tracking module are shown. In this diagram the unconnected branches (marked by circles) that are generated by the cell division events can be observed. Thus, the last problem that has to be addressed prior to the estimation of the migration patterns and cellular cycle is

to link, in a robust manner, the parent and child cells resulting from mitosis events. To achieve this objective, in this thesis a multi-stage backward tracking process has been developed.

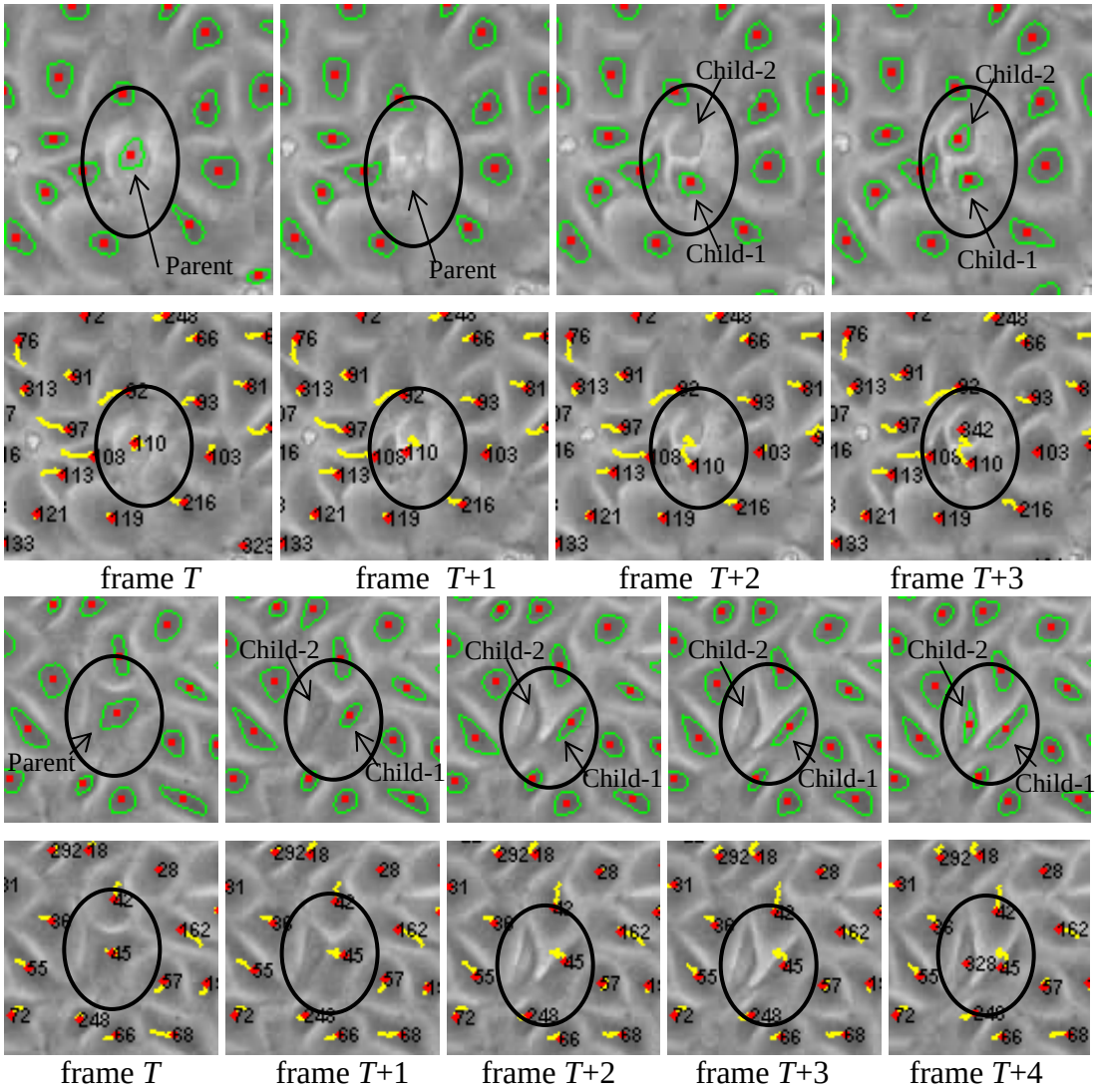

Figure 3.16.1. Two examples that illustrate the problems generated by under-segmentation during the cell division event. First row: the parent and one child cell have been missed by the segmentation process. Third row: one child cell has been missed by the segmentation process. Second and fourth rows: corresponding forward tracking results.

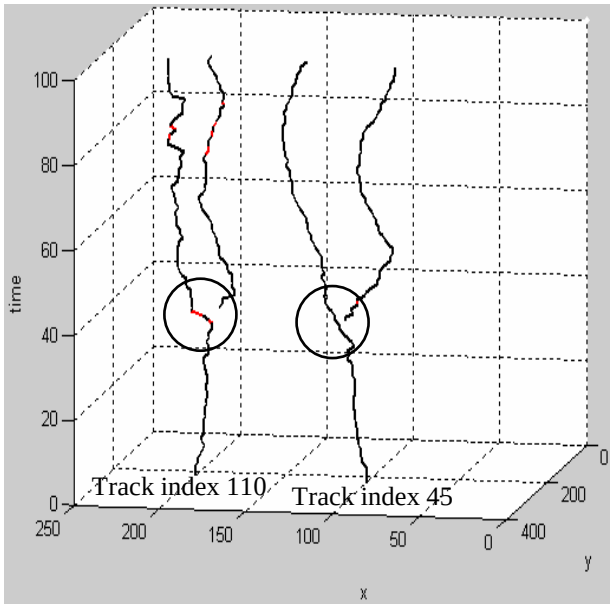

Figure 3.16.2. 2D+time plot that illustrates the forward tracking results in the presence of cellular division. Full explanations in regard to this diagram are provided in the text.

The application of backward tracking is successful in detecting the mitosis events only if all cells (parent and child cells) are correctly detected by the segmentation process. Unfortunately, due to the low intensity contrast that is a characteristic of phase-contrast images, there are situations when some child cells resulting from cellular division events are missed by the segmentation algorithm. This situation can be observed in the third row of Figure 3.16.1 where it is indicated that the child cell-2 has not been identified by the proposed segmentation scheme. Since the child cell-2 was not identified by the segmentation algorithm, this fact did not trigger the activation of the under-segmentation procedure and the parent cell has been associated with the child cell-1. The child cell-2 is detected by the algorithm only in frame T+4 (see third row- Figure 3.16.1) and it will be further detected with a new track index. Thus, this type of under-segmentation problems needs to be addressed during backward tracking using a hybrid procedure that combines the intensity model of the missed cell with the local structural information contained in the Delaunay meshes.

In the proposed backward tracking scheme, for each cell track identified by the forward tracking module, the backward tracking process is carried out from the

end of the track towards the first cell of the track. In this way, the backward tracking can be successfully applied (from frame *T* towards frame *T*-1), only in situations when all child cells are identified. If under-segmentation occurs (see the third row in Figure 3.16.1) the tracking is initiated from frame where the child cell is detected first (frame *T*+4) and the algorithm will attempt to identify the suitable locations for the corresponding cells in frames *T*+3, *T*+2 and *T*+1 using a process similar to that applied to redress the under-segmentation problems. This process is applied until the child cell-2 is linked to its parent cell in frame *T*. To provide more details, when attempting to identify the missing cell in frame *T*+3, the algorithm initiates a search operation within a $(2\alpha+1)\times(2\alpha+1)$ neighbourhood (for details please refer to Section 3.2.2) to identify the locations in frame *T*+3 that approximate the intensity profile associated with the cell detected in frame *T*+4. The candidate locations are determined using normalised cross-correlation. The selection of the best candidate location is carried out by minimising the expression as indicated in equation (3.9).

An example that illustrates all steps associated with the backward tracking process is shown in Figures 3.17.1 and 3.17.2. As shown in Figure 3.17.1, the cell division occurs in frame *T*+1, but one of the child cells (c2) is detected only in frame *T*+3 and tracked with the index 171. In this situation the backward tracking module could not find a suitable corresponding cell in frame *T*+2 using the local structure provided in the Delaunay meshes. In order to determine a suitable location for the missing cell in frame *T*+2, a normalised cross-correlation search process is activated to identify the candidate locations in frame *T*+2 that approximate the intensity profile of the child cell in frame *T*+3. From these multiple peaks, the one that minimises the expression in (3.9) is selected. This process is sequentially applied until the child cell is linked to a parent cell. To avoid the incidence of false positives that may be created by cells that enter the area imaged by the microscope, trajectories initialised near the borders of the image are eliminated. Furthermore, the backward tracking process is applied for maximum of five consecutive frames. Figure 3.17.2 depicts the backward tracking results when the selection of the best candidate location is performed using the proposed strategy that combines normalised cross-correlation with the information sampled in the local structure of the Delaunay meshes. As can be observed in these diagrams, the track associated with the child cell identified in

frame *T*+3 is correctly linked to the parent cell in frame *T*. To illustrate the benefits of using the structural information in the backward tracking process, in the last row (j-l) of Figure 3.17.2 are illustrated the results where the identification of the missed cell location is carried out using only intensity information (i.e. the location of the best candidate is decided based on the result returned by the normalised cross correlation only). As indicated in these diagrams, the estimation of the missed cells in frames *T*-2 and *T*-1 is erroneous, and as a result the detected locations drift from the position of the parent cell in frame *T* (track index 111). To visually emphasize the performance of the proposed backward tracking in the detection of cellular division events, diagrams that illustrate the tracking process in 2D+time are shown in Figures 3.18 and 3.19. To complement these visual results, the proposed backward tracking strategy has been numerically evaluated and results are provided in Table 3.2.

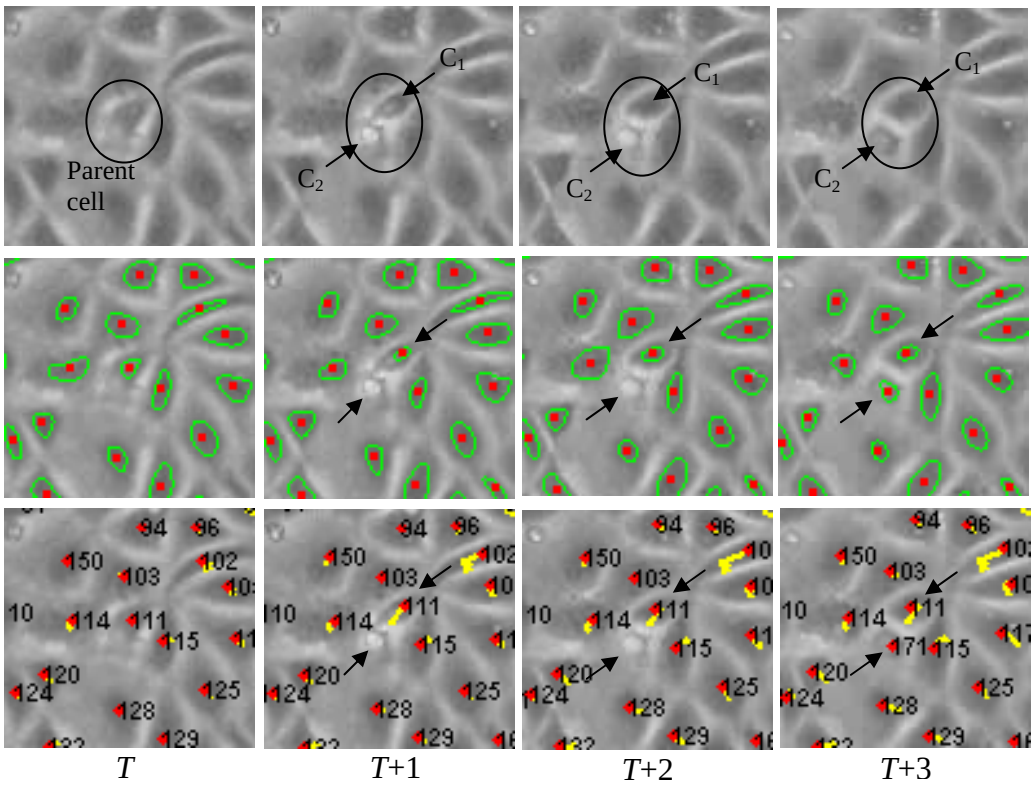

Figure 3.17.1. An example that illustrates four consecutive frames that depict a cell division event. First row: Original frames. Second row: Cell segmentation results. Third row: Forward tracking results. This example is used in Figure 3.17.2 to show how the under-segmentation error has been redressed during the backward tracking process.

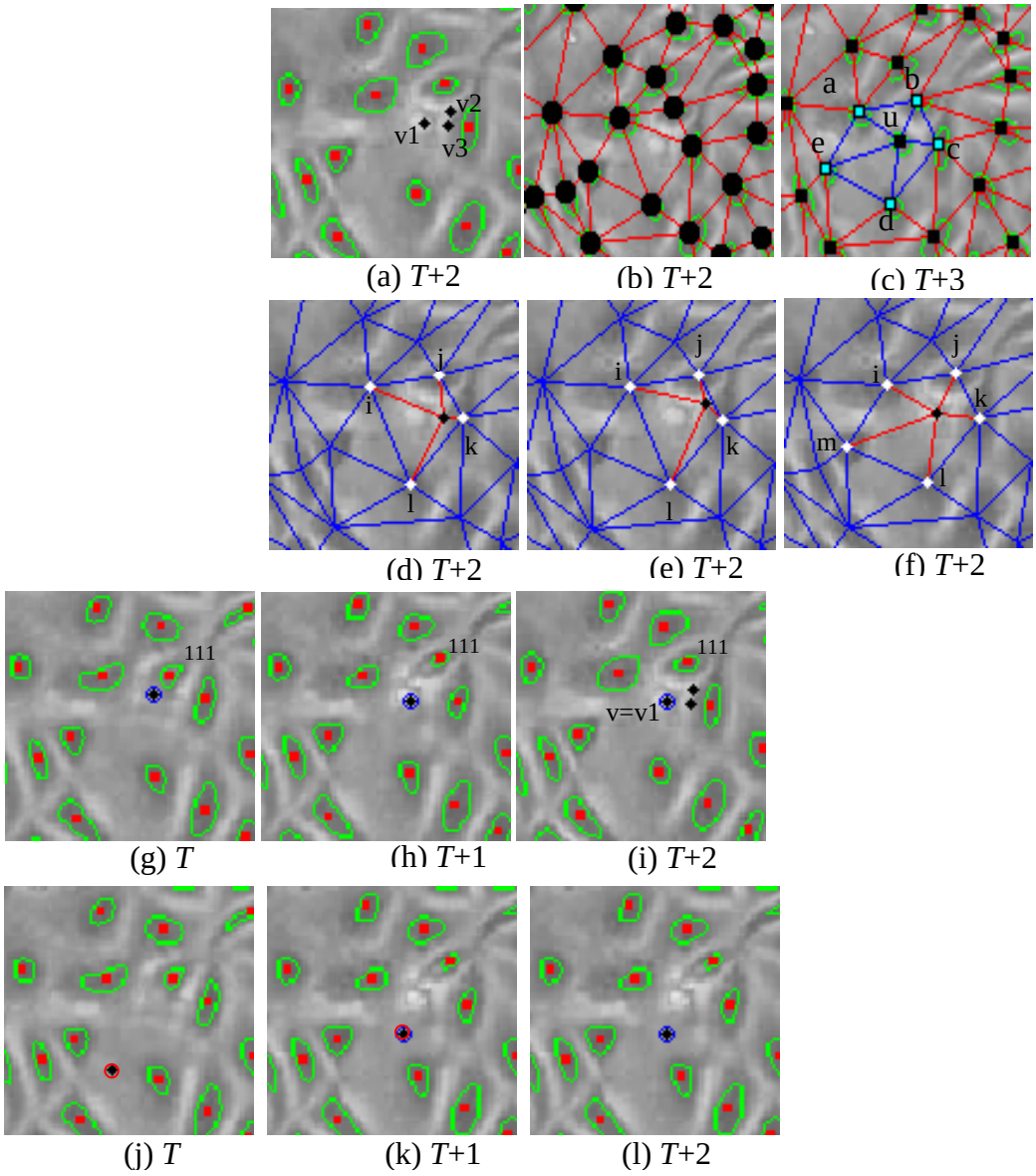

Figure 3.17.2. The backward tracking process in the presence of under-segmentation. (a) Candidate cell locations that are detected using normalised cross-correlation in frame T+2. (b) The spatial relationship in T+2 when the child cell C_2 (see Figure 3.17.1) is not segmented. (c) Local structure associated with the child cell u in image T+3. (d-f) Local structures that are constructed for each candidate point v_i. (g-i) Shows the detected cell locations in frames T+2, T+1, and T where it can be observed that the child cell is correctly tracked to the parent cell in frame T. (j-l) Shows the divergence of the backward tracking when the cell detection process in frames T+3, T+2, T+1 and T is carried out using only normalised cross-correlation.

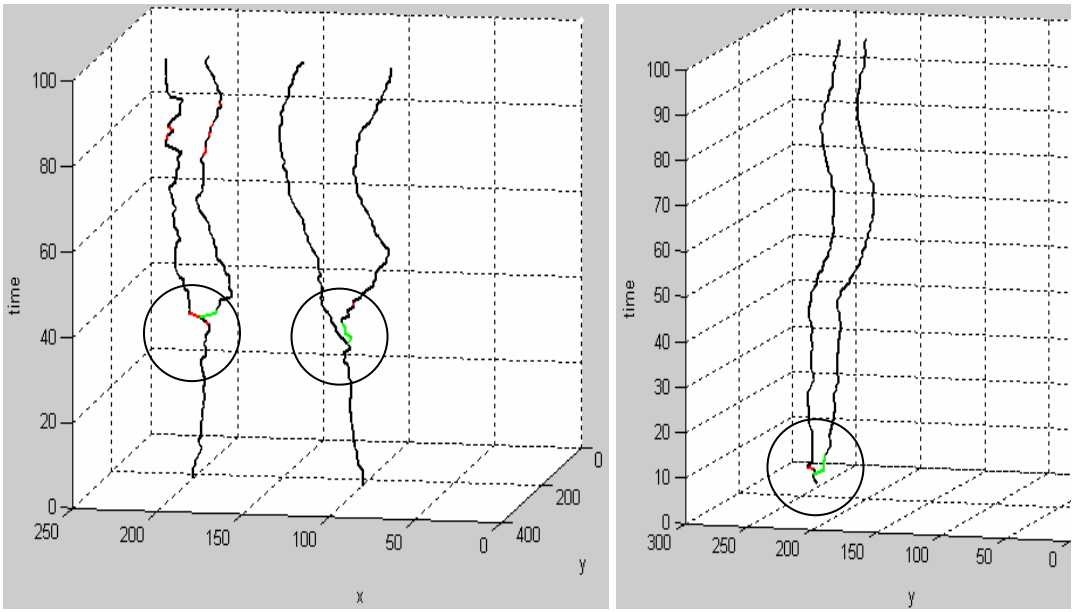

Figure 3.18. Tracking results displayed in 2D+time plots. In these graphs the black points indicate forward tracking results. The backward tracking results are shown in green, while the red points indicate the identified tracks when the under-segmentation module is activated for both forward and backward tracking modules.

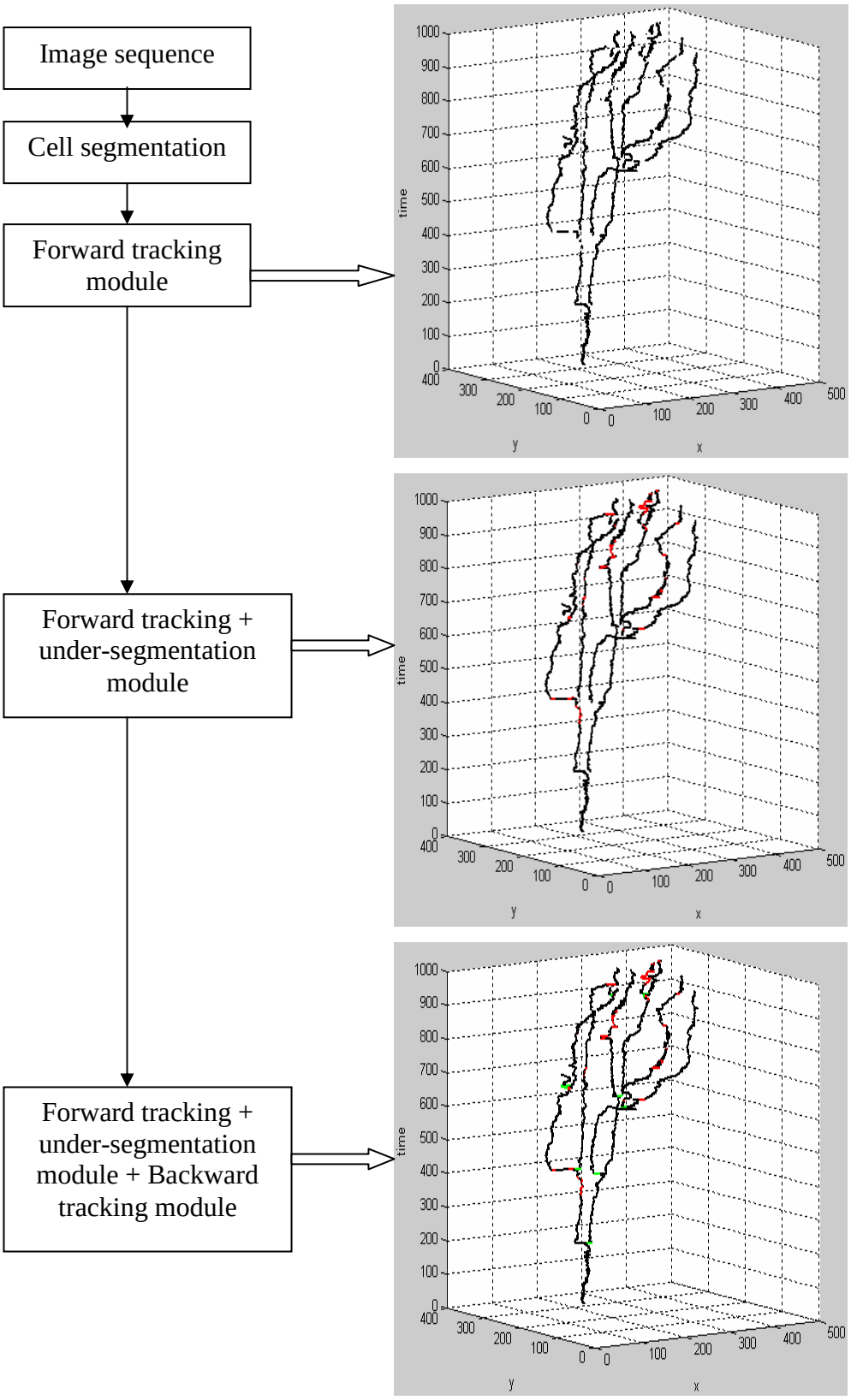

Figure 3.19. 2D+time plots that outline the results obtained by the proposed cellular tracking and mitosis detection algorithm. For clarity reasons, tracking results for only one cell are illustrated.

Table 3.2. Cell tracking accuracy after the application of the forward and backward tracking.

		Cell detection accuracy	
Cell type	No. of frames	Forward tracking	Forward-tracking + Under-segmentation module + backward tracking
MDCK-1	100	97.41%	98.21%
MDCK-2	100	97.28%	99.09%
MDCK-3	100	96.96%	98.28%

Chapter 4:

Experimental Results

This chapter provides an extensive evaluation of the proposed framework, analyses the experimental results and compares the performances obtained by the proposed cell tracking and mitosis detection algorithm to state-of-the-art implementations. To allow for a comprehensive evaluation of the performance attained by the proposed scheme, experimental results are reported to sample the accuracy levels for both areas of interest: cellular tracking and identification of the cellular division events. To facilitate the calculation of the performance indicators that are able to numerically sample the accuracy of the proposed and state-of-the-art cell tracking and mitosis detection algorithms, seven time-lapse video sequences (three sequences of Madin Darby Canine Kidney Epithelial Cells - MDCK and four sequences of Human Umbilical Vein Endothelial Cells - HUVEC cell data) were employed in this study. The spatial resolution of these datasets varies from 0.87 to 1.3 μm/pixel and the temporal resolution is in the range 5 to 9 min/frame. These seven video sequences were captured using phase-contrast microscopy image acquisition modalities (for additional details refer to appendix B) and, as indicated in Chapter 2, they are characterised by substantial intensity variations and a high level of noise. The MDCK cell datasets contain dense cellular structures that undergo frequent cell division, and these characteristics raised substantial challenges for all computational components of the proposed algorithm, cellular segmentation, forward tracking and mitosis detection. In addition, since the region of interest imaged by the microscope is limited, there are frequent situations when the cells situated near the border of the ROI exit and re-enter the area encompassed by the field of view. As opposed to MDCK data, the cellular structures sampled in HUVEC image sequences are relatively sparse and a distinct characteristic is the high level of mitosis events. Since the number of cells contained in a HUVEC frame is relatively low, the negative effects caused by the cells that exit and re-enter the ROI are more noticeable than in the case of MDCK data. Similarly to MDCK data, the HUVEC datasets exhibit substantial intra- and inter-frame intensity variations and is worth

noting that the sizeable changes in the morphology of the cells introduce an additional challenge for the cell segmentation process. These two cell lines, MDCK and HUVEC, are widely used to assess several biological mechanisms such as absorption, sensory reception and secretion, and since they are used as generic models for epithelial and endothelial cells, respectively, they are particularly popular in clinical research [87, 88]. As indicated above, the MDCK and HUVEC cell lines encompass a wide spectrum of challenges that include the improper image contrast, cellular agglomeration and high proliferation, and these issues provide a challenging scenario for all components of the proposed cell tracking and mitosis algorithm. These distinct characteristics proved particularly useful when employed to evaluate the impact of segmentation errors on the performance of the cellular tracking process. The strong clinical interest, in combination with the complexity of the cell migration and cell division processes, justify the use of these cell lines to assess the performance of the proposed framework. Figures 4.1.1 and 4.1.2 depicts four frames sampled from MDCK and HUVEC datasets to exemplify the challenges associated with the analysis of these cell lines.

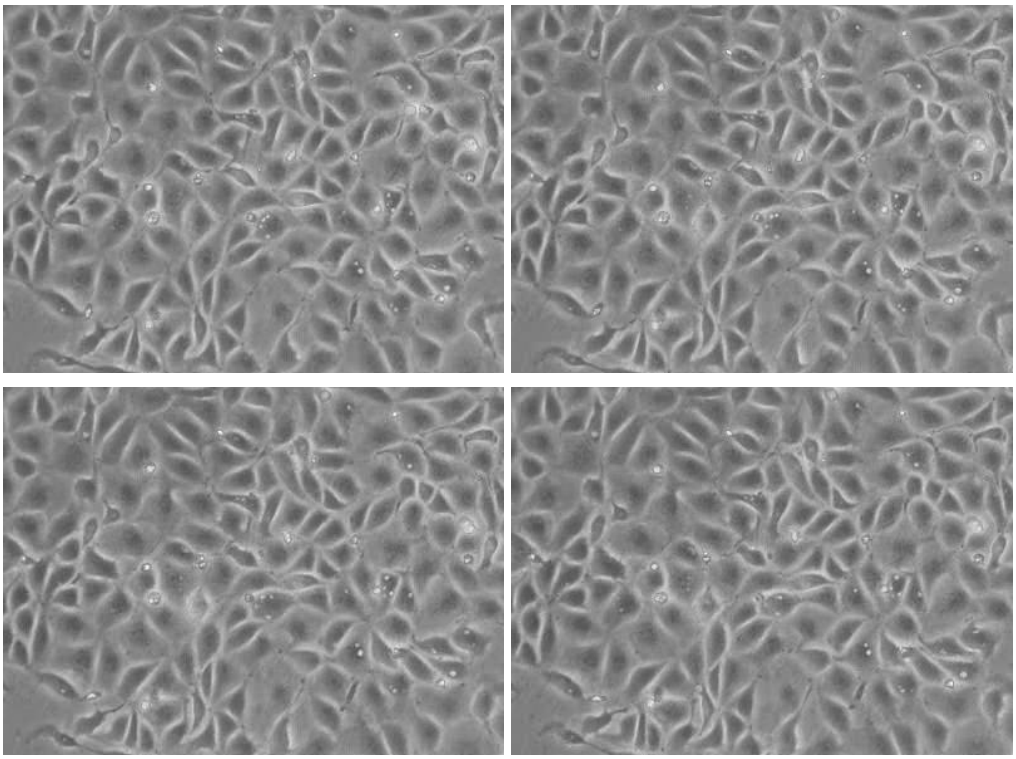

Figure 4.1.1. Phase-contrast cellular images. Four consecutive frames from a MDCK image sequence.

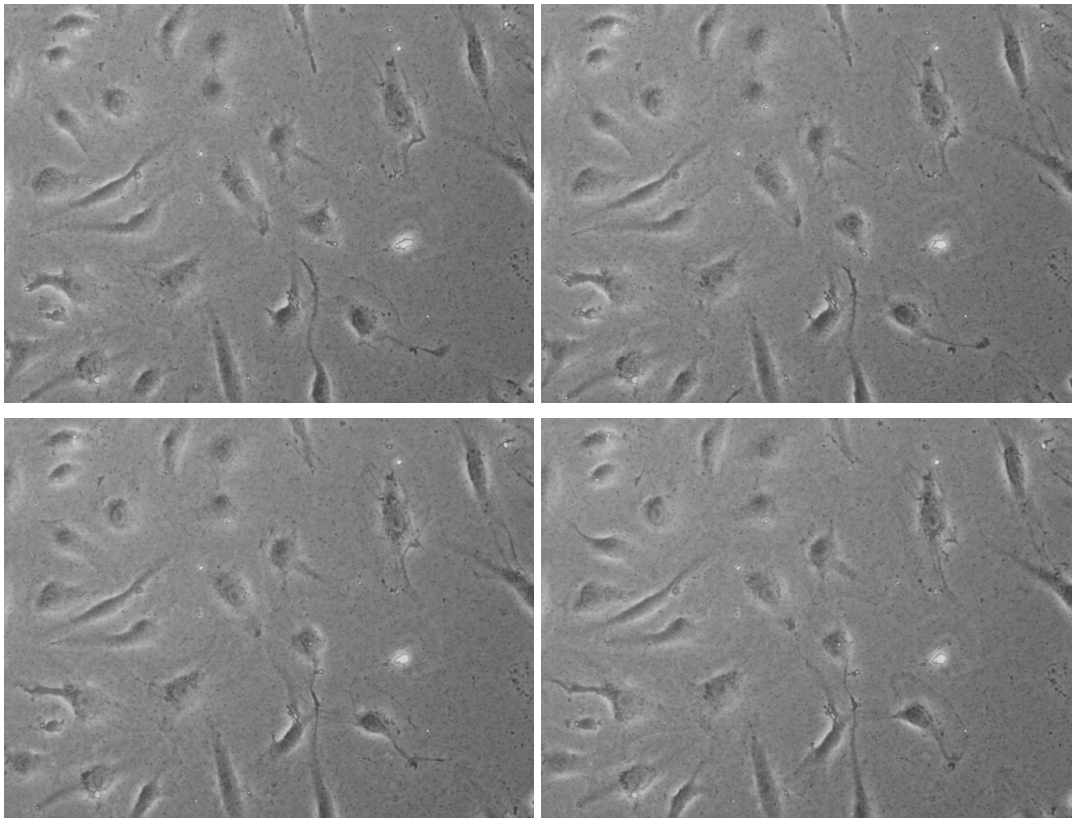

Figure 4.1.2. Phase-contrast cellular images. Four consecutive frames from a HUVEC image sequence.

To allow a direct comparison of the results obtained by the proposed algorithm with the results reported for state-of-the-art cell tracking methods, publicly available cellular datasets have also been included in the experimental study. In this regard, experimental results for two additional sequences of Murine Progenitor Neural (MNP) stem cells (phase-contrast data) and one image sequence of HeLa cells (fluorescence data) will complement the results obtained for MDCK and HUVEC cellular data. These publicly available datasets also raise a wide range of imaging and biology-related problems that need to be addressed by the cell tracking/mitosis detection algorithms and these challenges make these datasets particularly appropriate to be included in the experimental evaluation. Indeed, the MNP datasets exhibit low contrast, large changes in the cell morphology in consecutive frames of the sequence, and a high rate of cellular division, while the HeLa data is characterised by high cellular densities, a high rate of cellular divisions and large migration patterns. Figure 4.2 depicts two images sampled from the MNP

(1) MNP and (2) HeLa datasets were made available by Al-Kofahi *et al* [1] and Li *et al* [7] respectively. They were also used by other authors when they attempted to evaluate/compare the performance of their cell tracking algorithms. (1) http://www.landesbioscience.com/supplement/alkofahi.zip. (2) http://www.cbi-tmhs.org/Dcelliq/index.html

and HeLa datasets and it can be observed that the segmentation problem is substantially simplified when dealing with fluorescence (HeLa) image data.

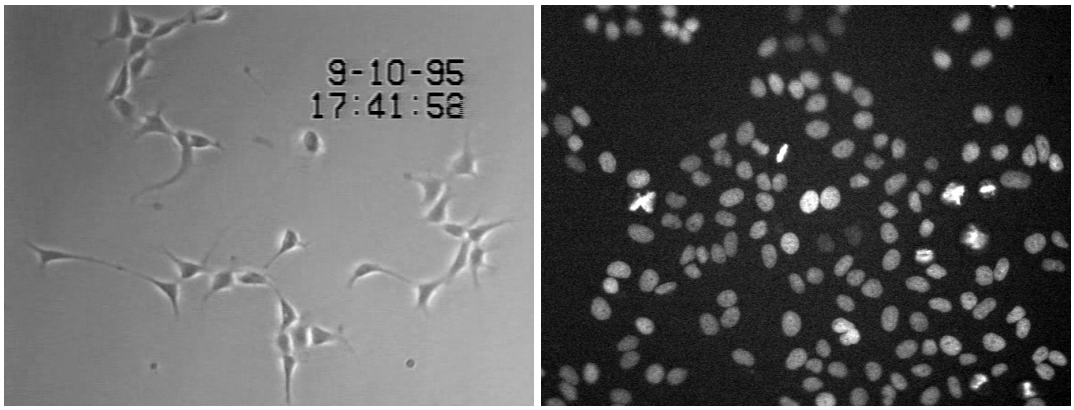

(a) (b)

Figure 4.2. Additional cellular datasets used in the experimental study. (a) MNP cellular data. (b) HeLa cellular data.

For clarity purposes, the performances achieved by cellular segmentation, tracking and mitosis detection components of the proposed framework are analysed in separate sections. This approach is also motivated by the fact that different metrics are used in the evaluation of the accuracy obtained by the different components of the proposed framework. In this sense, the proposed segmentation method is evaluated using a metric that samples the number of correctly segmented cells with respect to the total number of cells that are contained in the manually annotated data. On the other hand, the evaluation of the forward cell tracking algorithm is performed using metrics that sample the number of correct tracks (cell lineages) that are identified by the tracking algorithm when compared to those contained in the manually marked ground truth data. In a similar manner, the cell division accuracy is evaluated using quantitative indicators that assess the number of correctly identified parent-child links with respect to the manual annotated results. To facilitate an exhaustive performance analysis, the proposed cellular tracking framework was also evaluated on synthetic data. This approach is motivated by two reasons. Firstly, to isolate the undesired effects inserted by the segmentation errors, and secondly, to illustrate the theoretical and practical advantages associated with the proposed strategy when compared to traditional tracking strategies.

4.1 Generation of the ground truth data

To facilitate the numeric quantification of the proposed cellular tracking and mitosis detection framework, all datasets used in the experimental study were manually annotated. In this process the data has been annotated to allow the performance evaluation for each component of the developed framework: cell segmentation, cell tracking and mitosis detection.

The manual annotation process has been conducted by the Centre for Image Processing and Image Analysis (CIPA) researchers, and in this process, clinical collaborators provided additional input to validate the annotated data. The manual annotations include information regarding the location of the cells in each frame, i.e. the (x,y,t) coordinates of the cells' centroids, and this information is directly used to calculate performance indicators that quantify the accuracy of the developed segmentation technique (the metric employed to calculate the accuracy of the segmentation process involves the identification of the true positives (TP), false positive (FP) and false negatives (FN) and is introduced in the next section, equation 4.1.)

The next sets of annotations were conducted to generate ground truth data for the numerical quantification of the cell tracking algorithm. To achieve this goal, cell lineages (or cell tracks) were manually identified by analysing the migration patterns for each cell in consecutive frames of the sequence. During this process a unique index is generated for each identified track and this information is used in the calculation of tracking accuracy indicators (the tracking indicators that are employed to quantify the performance of the proposed cell tracking framework and state-of-the-art implementations introduced in Sections 4.4 and 4.7, equations 4.3 to 4.5).

The last sets of annotations were generated to facilitate the quantification of the mitosis detection process. In this sense, the manual tracking annotations were evaluated in a forward and backward manner and the mitosis events were visually validated by examining frames prior to and after the mitosis event. At the end of this manual annotation process, the locations of the parent and child cells were recorded, and this information was used to quantify the accuracy of the proposed mitosis

detection algorithm. The numerical evaluations carried out for each computational component of the proposed cellular tracking and mitosis detection framework are presented in detail in the following sections of this chapter.

4.2 Validation of the cellular segmentation algorithm

The proposed segmentation method has been evaluated on MDCK, HUVEC and MNP cellular sequences. Thus, the proposed segmentation method has been applied to nine different time-lapse phase-contrast sequences that consist of cellular data with different densities (for more details please refer to the discussion provided in the previous two sub-sections). As stated in Chapter 2, microscopy image analysis entails the application of specific protocols that are tuned for specific cellular applications. As a result, image data will have strong characteristics that are dictated by the type of cells that are under observation. Thus, the development of generic cell segmentation/detection methods that are able to accommodate the substantial differences between the datasets captured using different imaging protocols is extremely difficult. Therefore, in this work the main focus was on the development of a segmentation strategy for robust cell detection in phase-contrast data. To maximise the cell detection, the main idea associated with the proposed segmentation method consists in the identification of the intensity peaks in the image using the *h*-maxima transform. This approach proved efficient in increasing the detection rate and to reduce the level of false positives in the presence of non-uniform background and poor image contrast. The optimised values for the parameters *h, r* and α for each type of image sequence are illustrated in Table 4.1. It is useful to note that the parameter α does not have a direct role in the segmentation process, since its purpose is to restrict the maximum instantaneous cell displacement in two consecutive frames. This parameter has been included in Table 4.1 for clarity purposes, as this allows a targeted discussion in regard to the role of each parameter in the overall cellular tracking and mitosis detection framework.

Table 4.1. The values of the parameters *r*, *h* and α that are optimised for each type of cellular data.

			Parameters		
Dataset	Cell type	No. of sequence	*r*	*h*	α
	MDCK	3	15	19	12
	HUVEC	4	15	15	20
	MNP	2	11	10	15

The accuracy of the proposed cell segmentation method is evaluated based on the number of cells that are correctly segmented with respect to the number of cells that are manually identified in the ground truth data. In order to measure the segmentation accuracy, the number of true positive (TP), false negative (FN) and false positive (FP) are calculated. TP is the number correctly segmented cells, FN denotes the number of cells that are not segmented by the algorithm, while FP defines the number of incorrect segmentation decisions. The accuracy is calculated as follows,

$$Accuracy = \frac{TP}{TP + FN} \times 100\ \% \tag{4.1}$$

To illustrate the performance achieved by the proposed cell segmentation method when applied to phase-contrast image sequences, several visual examples are displayed in Figures 4.3 and 4.4. Figure 4.3 shows the results obtained by the proposed algorithm when applied to an image containing MNP cells. In Figure 4.3 the low contrast between the cells and the background, and the shallow intensity transitions between the borders of the cells that are clustered together can be clearly observed. (The areas covered by the clustered cells are marked with rectangles in the diagrams). In spite of these difficulties, the proposed segmentation algorithm is able to correctly identify the cells in the image (see Figure 4.3(b) where the contours of the identified cells and their corresponding centroids are overlaid on the original data).

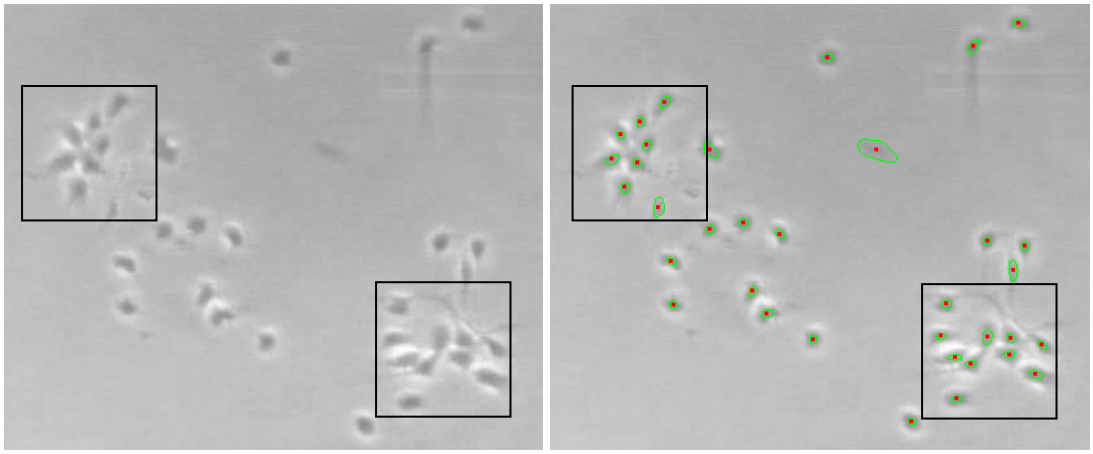

(a) (b)

Figure 4.3. Robustness of the segmentation in low contrast image. (a) A low contrast phase-contrast MNP image where the intensity transitions between the cells and the background are very shallow. Observe the faint intensity changes between the borders of the clustered cells. (b) Segmentation results that illustrate the robustness of the proposed segmentation method – note the precise identification of the individual cells in the presence of cellular agglomeration (clustering).

Figure 4.4 depicts additional results when the proposed algorithm has been applied to the MDCK, HUVEC and MNP images that are shown in Figures 4.1 and 4.2. These additional results further illustrate the accurate performance of the proposed cell segmentation algorithm when applied to different types of phase-contrast cellular data.

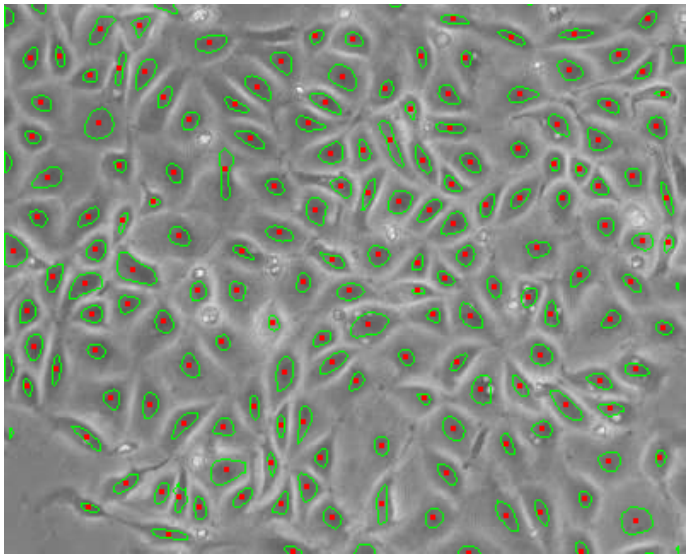

(a) MDCK

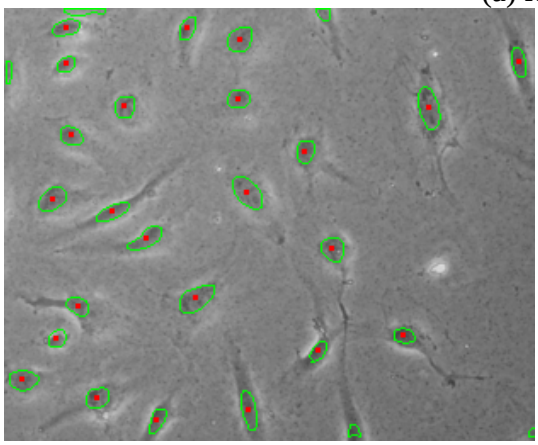

(b) HUVEC

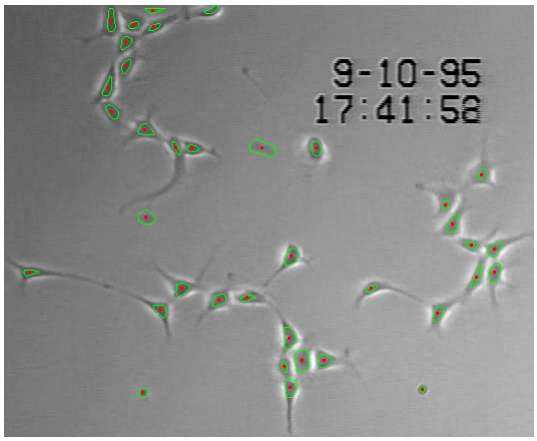

(c) MNP

Figure 4.4. Segmentation results when the proposed algorithm was applied to (a) MDCK, (b) HUVEC and (c) MNP images – the original MDCK and HUVEC images are shown in Figures 4.1.1 and 4.1.2

To numerically quantify the accuracy of the proposed cell segmentation algorithm, the TP, FP, FN and accuracy are calculated and the results are presented in Table 4.2. As indicated in Table 4.2, the numerical results are reported for nine image sequences where the number of frames for each dataset ranges from 100 to 320. The overall detection accuracy achieved by the developed cell segmentation technique is 90.08%, which is sufficiently high to obtain accurate cellular tracking results. More precisely, this segmentation accuracy permits the construction of local spatial cellular structures with sufficient precision that allows the association of the cells in consecutive frames of the image sequence. Also, as indicated in Section 3.2.2, the cell detection accuracy increases during forward and backward tracking by

employing the information in the intensity and temporal domains to redress the problems introduced by under-segmentation.

Table 4.2. Quantitative results when the segmentation method was applied to nine phase-contrast cell sequences.

Cell type	No. of Frames	Total no. cells	TP	FN	FP	Accuracy %
MDCK-1	100	16267	15845	422	346	97.41%
MDCK-2	100	11525	11211	314	389	97.28%
MDCK-3	100	16966	16450	516	599	96.96%
HUVEC-1	320	8936	7489	1447	123	83.81%
HUVEC-2	320	8377	7227	1150	567	86.27%
HUVEC-3	320	4588	3425	1163	176	74.65%
HUVEC-4	320	6342	5317	1025	847	83.84%
MNP-1	300	8919	8456	463	430	94.81%
MNP-2	300	9615	9199	416	1712	95.67%

4.3 Validation of the forward tracking algorithm

The main advantage associated with the proposed algorithm when compared to alternative tracking solutions is its resilience to segmentation errors. To provide a comprehensive performance evaluation of the proposed tracking algorithm, the experimental evaluation was conducted using synthetic and real cellular data. This evaluation approach has two main advantages. Firstly, it allows a controlled testing environment that illustrates the inabilities of standard tracking solutions to achieve appropriate results, and secondly, it allows one to quantify the negative impact of the segmentation errors in the tracking process. When the algorithm was applied to real cellular data, two distinct scenarios emerged. In the first scenario the proposed algorithm was evaluated on phase-contrast cellular data and the cells identified by the segmentation algorithm were directly passed to the forward tracking module. In the second scenario, the proposed tracking algorithm has been evaluated on fluorescent HeLa cellular data, a situation where the coordinates of the cells are *a priori* known (segmentation results are publicly available).

4.4 Experimental results using synthetic and manually annotated data

Synthetic and manually annotated datasets have been independently employed to evaluate the performance of the proposed cell association algorithm. The use of synthetic data to validate the proposed algorithm is justified since the cell tracking accuracy is not affected by errors that are introduced by other components of the frameworks such as the segmentation module.

The cell association method described in this thesis relies on the proximity and the local cellular structure and it is not dependent on other image features. To provide a detailed evaluation, the tracking accuracy achieved by the proposed method has been compared with the cell tracking accuracies obtained by two standard distance-based cell association techniques using both synthetic and manually annotated cellular data.

The synthetic data is generated using a set of random points that are distributed over a 195×165 image that represents the first frame of the sequence. The next frames are generated by applying a random motion to each cell in the previous frame, and this approach is sequentially applied until the desired number of frames is reached. The instantaneous (frame-to-frame) displacement S^t of a newly generated point X^t is calculated using the following equation,

$$\begin{aligned} S^t &= u * Q + 0.5 * f * Q^2 \\ X^t &= X^{t-1} + S^t \end{aligned} \tag{4.2}$$

where the u and f are the velocity and acceleration, respectively, and the value of the parameter Q is set to 2.0 in order to generate a small movement. The value of u is set within the range of [0,1] and the value of f is randomly selected from the normal distribution with zero mean and unit variance.

For evaluation purposes, two synthetic video sequences that contain 32 and 140 random points, respectively, were generated in agreement with equation (4.2). The application of the proposed cellular association method to this synthetically generated data indicates that the proposed tracking algorithm is able to achieve correct cellular association. To illustrate the limitations of the standard tracking solutions when applied to data that is characterised by random motion, a global distance minimisation method (please refer to Figure 2.2 in Chapter 2) has also been evaluated on the same data. In this method the nodes are associated based on the minimisation of a global cost function. The experimental results indicate that this minimisation process works reasonably well when the cells in the subsequent frames undergo small migration. However, it returns inappropriate results in the presence of significant cellular migration. To further illustrate the limitations of distance-based tracking solutions, additional results are reported when the nearest neighbour tracking algorithm is applied to the same data that was generated using (4.2).

To quantitatively assess the accuracy of the cellular tracking process, a metric that evaluates the level of correct tracking decisions has been introduced (please refer to Appendix A for additional qualitative results). In this regard, the tracking accuracy is given by the number of correct tracks that are identified by the algorithm with respect to the total number of tracks identified in the ground truth data (see equation 4.3). A track is deemed valid if all the cells that form it are correctly associated. Comparative results for all tracking methods evaluated in this study are reported in Tables 4.3a and 4.3b. From Table 4.3a, it can be observed that the proposed method returns 100% accuracy, while the tracking accuracies for the global distance matching and the nearest neighbour methods are only 93.75% and 81.25%, respectively when the algorithms were applied to the sequence that contains 32 points. Table 4.3b depicts the results when the analysed methods were applied to the sequence that contains 140 points and the results were as follows: 97.86% - proposed method, 82.86% - global minimum distance and 67.87% - nearest neighbour algorithm. The results reported in Tables 4.3a and 4.3b show that the proposed method substantially outperforms the standard tracking algorithms.

$$Accuracy = \frac{Number\ of\ valid\ track}{Total\ number\ of\ tracks} \times 100\% \qquad (4.3)$$

Table 4.3a. Comparative tracking results (for 32 points) when the proposed tracking method, global minimisation and nearest neighbour methods are applied to synthetic data generated using (4.2).

Method	No. of frames	Total no. of tracks	Successfully identified tracks	No. of incorrect tracks	Tracking accuracy
Proposed method	200	32	32	0	100%
Global minimum distance	200	32	30	2	93.75%
Nearest neighbour algorithm	200	32	26	6	81.25%

Table 4.3b. Comparative tracking results (for 140 points) when the proposed tracking method, global minimisation and nearest neighbour methods are applied to synthetic data generated using (4.2).

Method	No. of frames	Total no. of tracks	Successfully identified tracks	No. of incorrect tracks	Tracking accuracy
Proposed method	200	140	137	3	97.86%
Global minimum distance	200	140	116	24	82.86%
Nearest neighbour algorithm	200	140	95	45	67.86%

In the next set of tests, the proposed method will be evaluated on manually annotated cellular image sequences. In this performance evaluation scenario, the cells in each frame are manually marked, and the coordinates of the cells are passed to the forward tracking module to complete the cell association process. Similarly to the evaluation using synthetic data, the goal of these experiments is to evaluate the performance of the proposed cell association module independent of segmentation errors. The tracking accuracy is evaluated using equation (4.3) — as in the case of synthetic generated data — and the experimental results are reported in Table 4.4.

Table 4.4. Accuracy of the proposed tracking algorithm when applied to manually segmented cellular data.

Sequence	No. of frames	Total no. of track	Successfully identified tracks	No. of incorrect tracks	Tracking Accuracy
HUVEC-1	320	97	96	1	98.97%
MNP-1	320	38	38	0	100.00%
MDCK-1	100	190	190	0	100.00%

4.5 Experimental results for real cellular data - Automatic segmentation

In this section, the performance of the proposed tracking solution is evaluated on unmarked cellular data, where the algorithm attempts to redress the segmentation errors detailed in Chapter 3. To achieve this objective, the performance evaluation is conducted using ten time-lapse video sequences (3 MDCK, 4 HUVEC, 2 MNP and 1 HeLa) that present random migration and different levels of cellular proliferation. Since the validation of the proposed algorithm is conducted using different types of cellular data, the parameter α (that limits the maximum instantaneous cell displacement in two successive frames) is optimised for each video sequence as indicated in Table 4.1 (in the case of HeLa cells, $\alpha = 20$). When dealing with real cellular data, due to the low contrast present in the image, there are situations where cells are left undetected by the segmentation algorithm. As mentioned earlier, the tracking algorithm has been evaluated on ten challenging image sequences and experimental results are given in Table 4.5. From these ten image sequences, three are publicly available (HeLa and MNP) and they are also used to compare the tracking performances achieved by the proposed framework and state-of-the-art implementations. (This analysis is discussed in Section 4.7).

Table 4.5. Tracking results obtained when the proposed tracking framework was applied to MDCK, HUVEC, MNP and HeLa cellular datasets.

Sequence	Number of frames	Total tracks	Valid tracks	Tracking accuracy
MDCK-1	100	190	170	89.47%
MDCK-2	100	120	105	87.50%
MDCK-3	100	174	143	82.18%
HUVEC-1	320	54	44	81.48%
HUVEC-2	320	97	76	78.35%
HUVEC-3	320	98	81	82.65%
HUVEC-4	320	51	42	82.35%
MNP-1	1000	38	34	89.47%
MNP-2	1000	23	21	91.30%
HeLa	100	128	120	93.75%

The experimental results shown in Table 4.5 indicate that the tracking accuracy ranges from 78.35% to 93.75% depending on the type of data being examined. The lowest tracking accuracy is obtained for the HUVEC-2 dataset. This reduced performance is caused by the improper image contrast between cell regions and background, which in certain situations prevent the under-segmentation algorithm from identifying the correct location of the missing cells. In spite of these severe image acquisition issues, the proposed method is still able to produce tracking results that match or exceed the accuracy of the algorithms published in the literature. To visually sample the accuracy of the proposed tracking framework when applied to MDCK, HUVEC and publicly available datasets, a number of tracking examples are depicted in Figures 4.5.1 and 4.5.2. In these figures the cell tracks (lineages) are colour coded where with red and blue are marked the initial and the final positions of the tracked cells in the sequence.

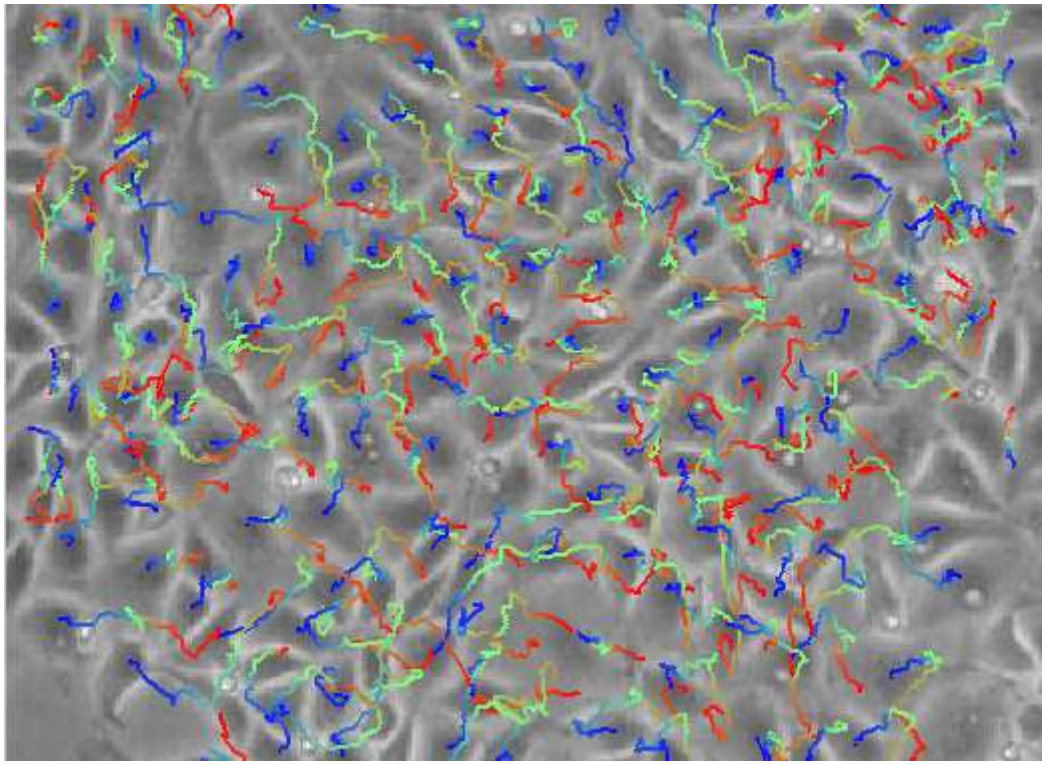

(a) MDCK

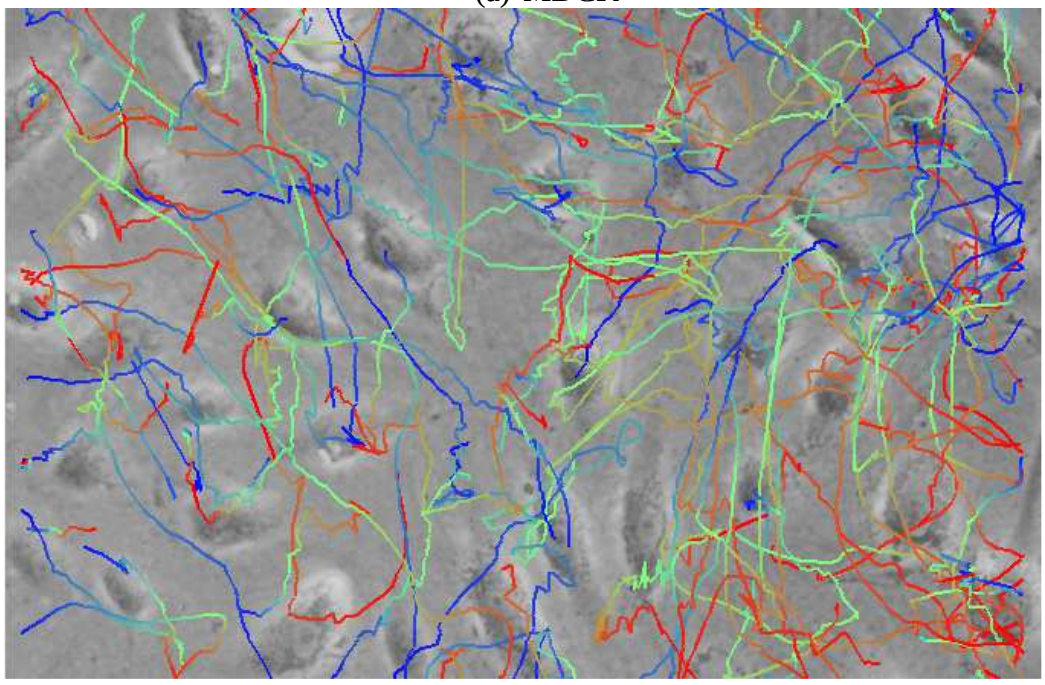

(b) HUVEC

Figure 4.5.1. Tracking results for (a) MDCK and (b) HUVEC data. The identified tracks illustrate the location (*x,y* coordinates) of the corresponding cells in the sequence – for visualisation reasons they are colour coded and overlaid on the original data. Red indicates the initial position of the cell, while blue indicates the last location of the cell in the cellular track.

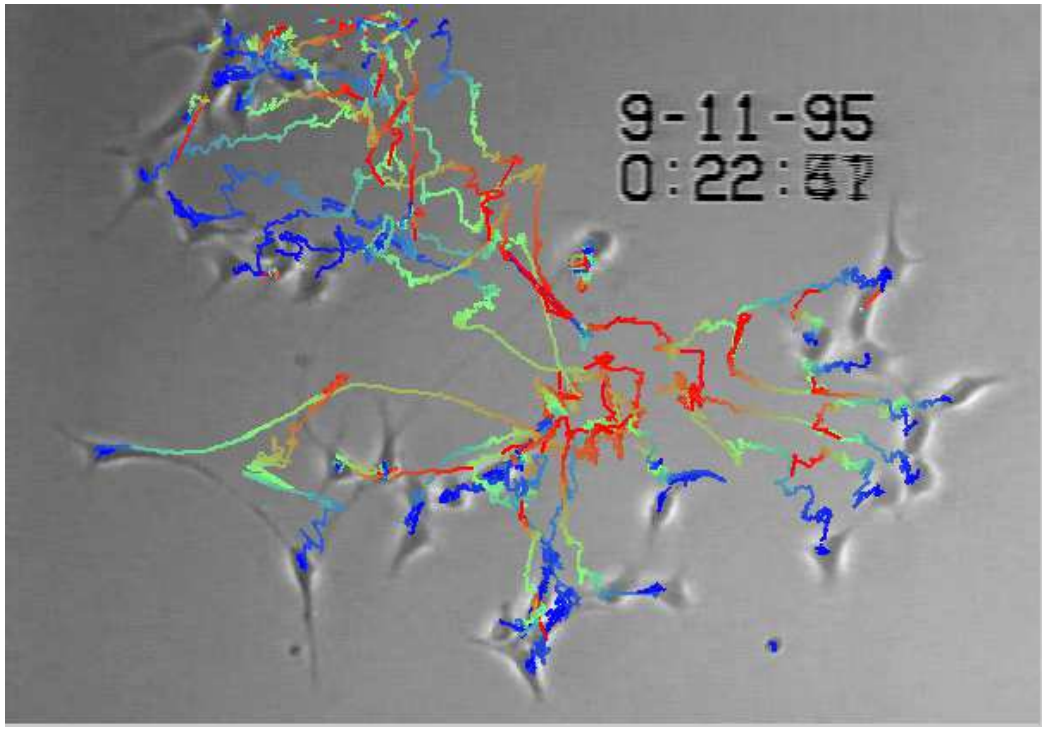

(a)MNP

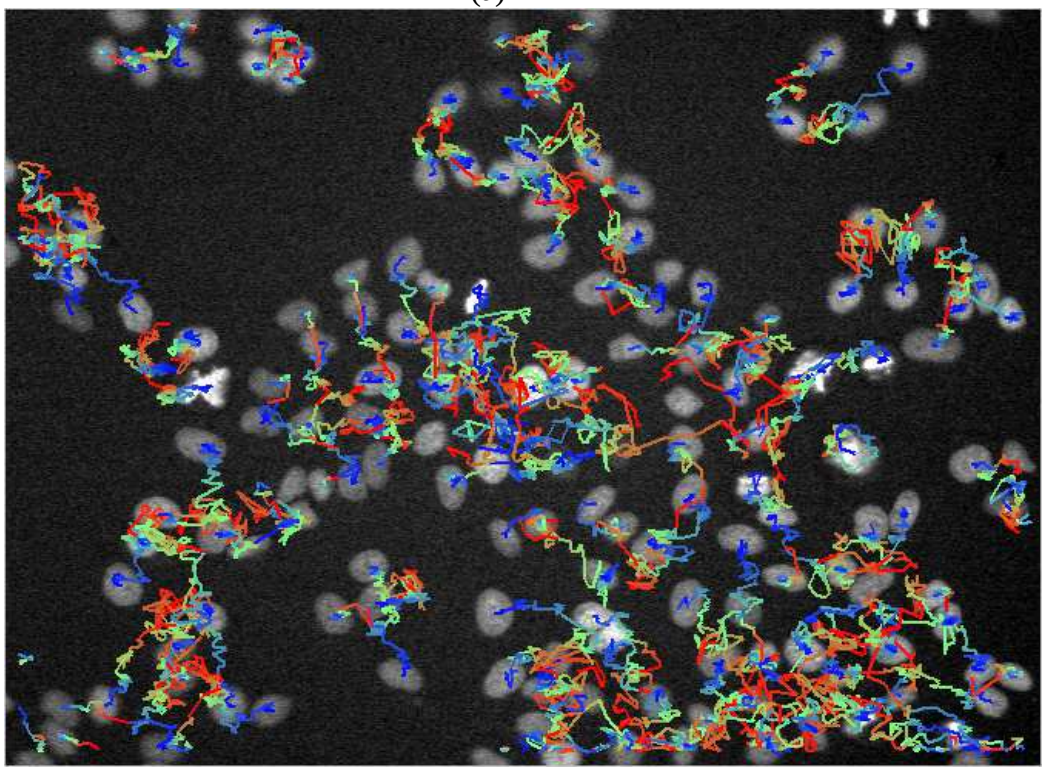

(b) HeLa

Figure 4.5.2. Tracking results for (a) MNP and (b) HeLa cellular data. The identified tracks illustrate the location (*x,y* coordinates) of the corresponding cells in the sequence – for visualisation reasons they are colour coded and overlaid on the original data. Red indicates the initial position of the cell, while blue indicates the last location of the cell in the cellular track.

4.6 Experimental results for cellular division (mitosis) detection

The aim of this section is to present quantitative indicators that illustrate the efficiency of the proposed mitosis detection algorithm. To numerically evaluate the accuracy of the mitosis detection, the parent-child cells links identified by the proposed backward tracking algorithm are compared with those identified in the manually annotated data. In other words, a mitosis event is deemed correctly identified if the locations (x,y,t coordinates) of the parent and child cells are the same as those found in the manually annotated data. Experimental results are reported in Table 4.6 where the mitosis detection accuracy is defined as the ratio between the sum of successfully identified parent-child links and the sum of actual cell division events that are identified in the manually marked data.

Table 4.6. Mitosis detection accuracy obtained by the proposed backward tracking strategy when applied to the MDCK and HUVEC, MNP and HeLa cellular data.

Sequence	No.of frames	Total mitosis events (manually annotated data)	Correctly detected mitosis events	Mitosis detection accuracy
MDCK-1	100	34	29	85.29%
MDCK-2	100	24	19	79.17%
MDCK-3	100	47	41	87.23%
HUVEC-1	320	15	13	86.67%
HUVEC-2	320	12	12	100%
HUVEC-3	320	24	23	95.83%
HUVEC-4	320	9	8	88.89%
MNP-1	1000	34	32	94.12%
MNP-2	1000	12	11	91.67%
HeLa	100	80	74	92.5%

The results shown in Table 4.6 indicate that the mitosis events are detected with 90.13% mean accuracy, where the worst results are obtained for MDCK data. This lower detection accuracy has been obtained for MDCK data and this is mainly caused by the large motilities of the new child cells during the cellular division process. The cellular division events are best visualised when the tracking results are

displayed in the form of 2D+time plots. Figures 4.6.1 and 4.6.2 illustrate a number of experimental results. In these diagrams, the forward tracking results are marked in black, the tracks identified by the under-segmentation module are marked in red and the mitosis event detection using backward tracking are marked in green.

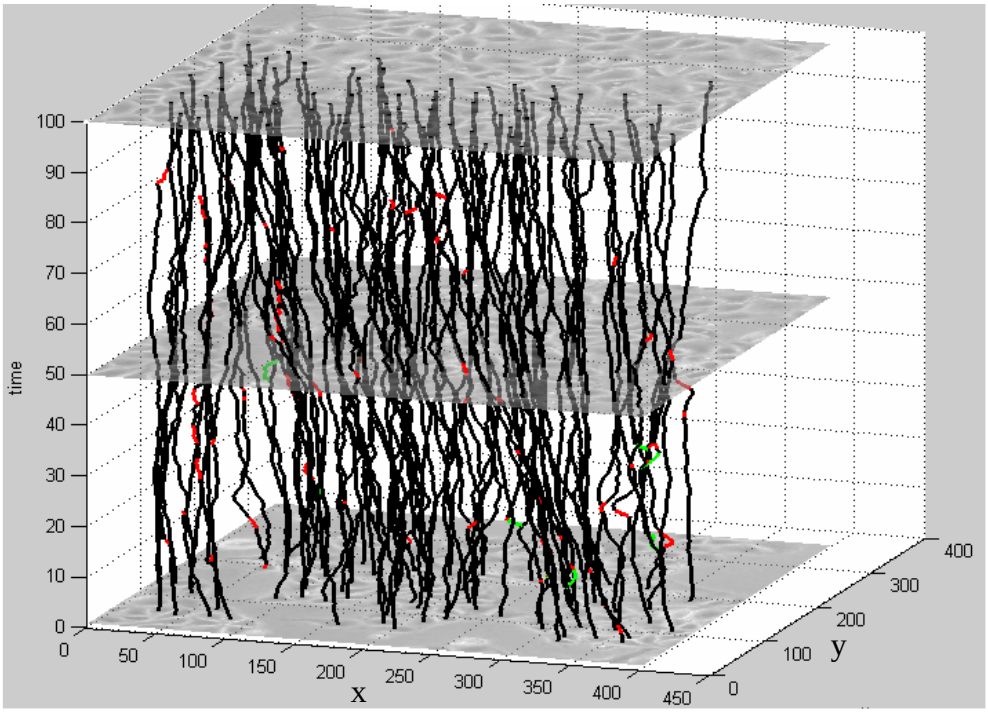

(a) MDCK

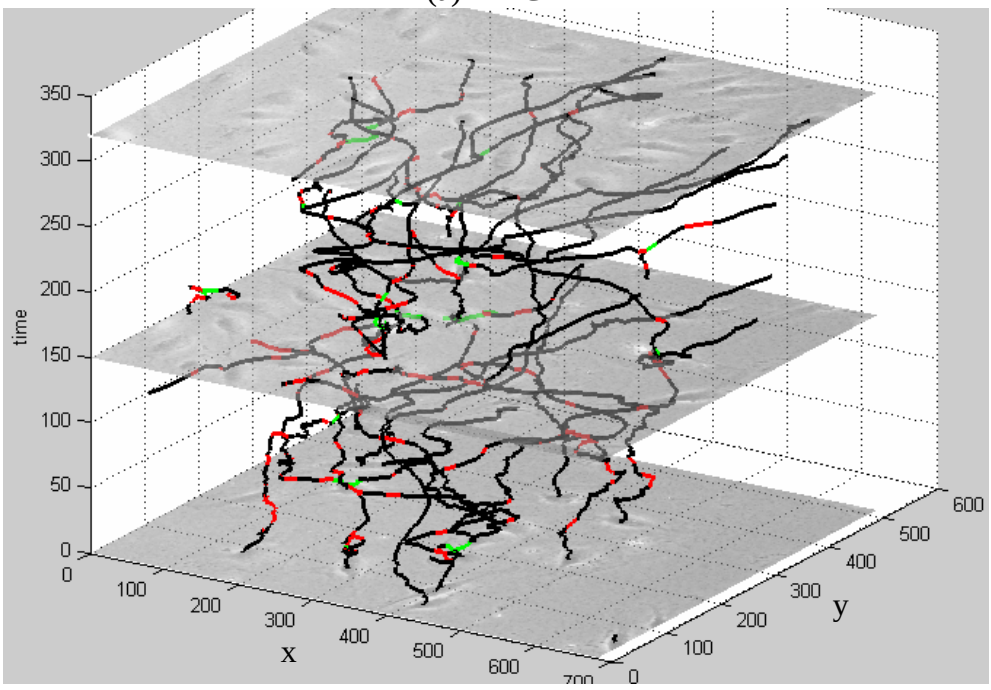

(b) HUVEC

Figure 4.6.1. 2D+time plots that illustrate the tracking and mitosis detection (in green) results. (a) MDCK data. (b) HUVEC data.

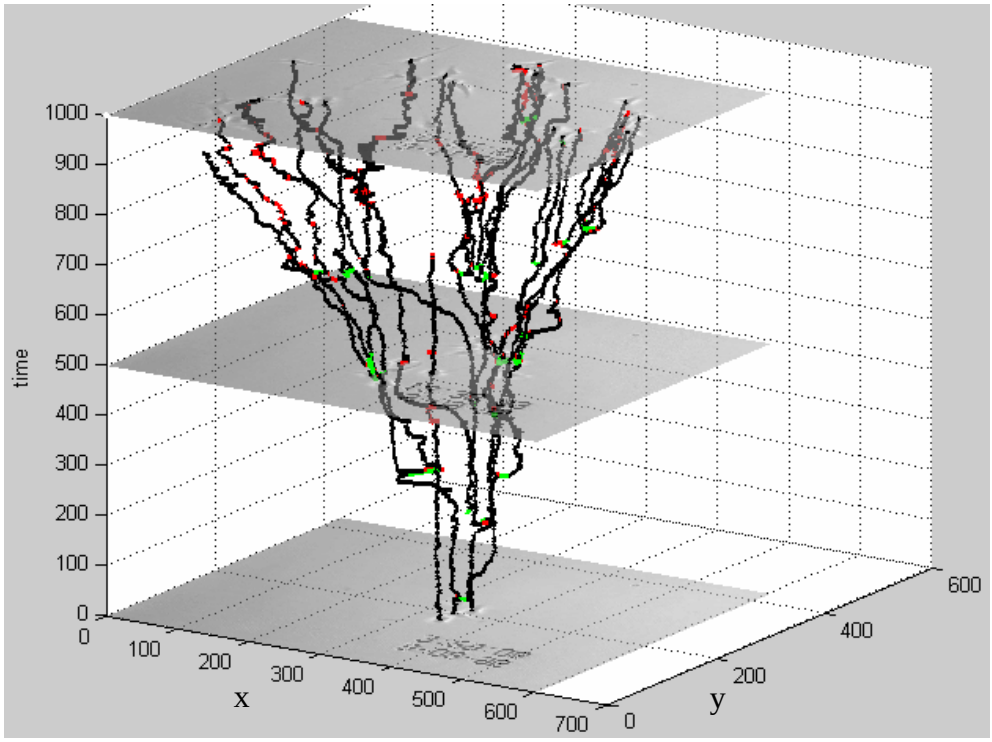

(a) MNP

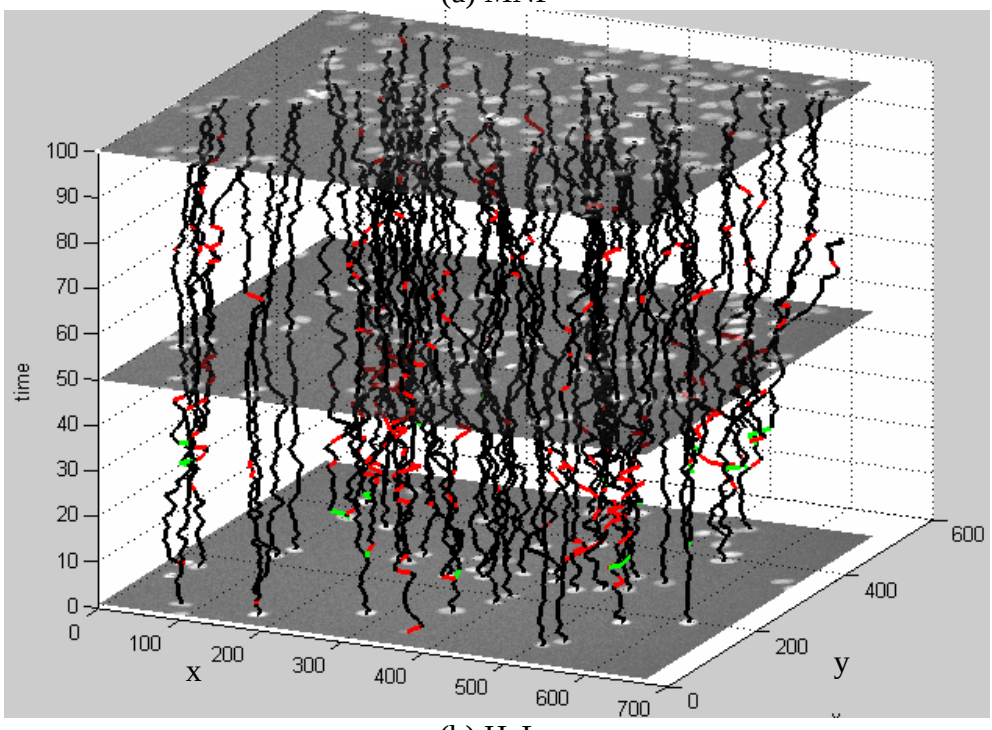

(b) HeLa

Figure 4.6.2. 2D+time plots that illustrate the tracking and mitosis detection results. (a) MNP data. (b) HeLa data. In these diagrams the mitosis events are marked in green. Full explanations in regard to the construction of these diagrams are provided in the main text.

4.7 Comparative results obtained by the proposed framework and state-of-the-art implementations

The aim of this section is to analyse the level of performance obtained by the proposed cellular tracking and mitosis detection framework against the state-of-the-art implementations that are published in the literature. In this regard, two state-of-the-art algorithms that were detailed in [12] and [7] are investigated in detail with respect to cellular tracking [7, 12] and mitosis detection [12] accuracy. To allow a direct comparison between the performances obtained by the proposed framework and the two state-of-the-art algorithms, the experimentation has been conducted using publicly available cellular data, namely two sequences of Murine Progenitor Neural (MNP) stem cells and one sequence of HeLa cells, data that was made available by Al-Kofahi *et al* [1] and Li *et al* [7], respectively.

In [7] the authors evaluated their tracking algorithm using four video sequences of HeLa cellular data, where each sequence contains 200 frames. Although they reported experimental results for all four sequences, only one sequence containing 100 frames was made publicly available. Thus, due to this restriction, the proposed framework has been evaluated only on this publicly available image sequence. To facilitate a fair comparison with the work detailed in [7], performance metrics such as Error Trace Rate (ETR in equation 4.4) and Error Matching Rate (EMR in equation 4.5) were calculated as indicated in the original paper [7]. These metrics are expressed in % and the smaller their value the better the performance of the algorithm. The comparative results obtained by the proposed method and the algorithm detailed in [7] are shown in Table 4.7.

$$ETR = \frac{number\ of\ \ track\ error}{total\ track} \times 100 \tag{4.4}$$

$$EMR = \frac{number\ of\ \ individual\ matching\ error}{total\ track} \times 100 \tag{4.5}$$

As illustrated in Table 4.7, the ETR and EMR obtained by [7] varies from 7.22% to 14.68% and 6.18% to 13.76%, respectively, while the ETR and EMR results obtained by the proposed method are 6.25% and 9%, respectively. The results reported in Table 4.7 indicate that the proposed method returns comparable ETR and EMR results with respect to [7] when applied to HeLa cell data. To provide more details about the experimental results, it is useful to note that the method proposed in [7] has been optimised for HeLa data and its tracking accuracy is highly dependent on the accuracy of segmentation. Contrary to this approach, the proposed method has not been optimised for any particular cell line and the errors caused by under-segmentation have been algorithmically redressed during the cell association process.

Table 4.7. ETR and EMR results obtained by the proposed method and the tracking technique detailed in [7].

	Proposed method	Method presented in [7]			
Error type	HeLa (100 frame)	HeLa-1 (200 frames)	HeLa-2 (200 frames)	HeLa-3 (200 frames)	HeLa-4 (200 frames)
ETR	6.25%	7.22%	14.68%	8.41%	9.16%
EMR	9.00%	6.18%	13.76%	8.41%	8.40%

The second state-of-the-art method analysed in this section has been detailed in [12] and it has been validated using both Hela [7] and MNP [1] cellular data. In this work the authors addressed both the cellular tracking and mitosis detection, a fact that allows a detailed comparison with the approach detailed in this thesis. Table 4.8 presents the experimental results returned by the proposed framework and the method detailed in [12]. These experimental results indicate that the method presented in this thesis outperforms the technique detailed in [12] with respect to both cellular tracking and mitosis detection. The cell tracking algorithm introduced in [12] is also able to address the issues caused by under-segmentation. However, the segmentation errors are only corrected for backward tracking and in many situations the normalised cross correlation process fails to identify the correct locations of the undetected cells in the presence of under-segmentation during cellular division. On the other hand, the proposed tracking framework redresses the segmentation errors during the forward and backward tracking and additional structural information has been incorporated to guide the tracking process and to identify the best locations for

undetected cells. These algorithmic procedures proved appropriate and the reported experimental results clearly indicate that the proposed approach returns higher cell tracking accuracy and mitosis detection than the method presented in [12].

Table 4.8. Cellular tracking and mitosis detection results obtained by the proposed method and the technique detailed in [12].

	Proposed method			Method presented in [12]		
Sequence	#of frames	Tracking	Division	#of frames	Tracking	Division
MNP-1	1000	89.47%	94.12%	1000	87.31%	83.76%
MNP-2	1000	91.30%	91.67%	1000	85.21%	84.62%
HeLa	100	93.75%	92.5%	500	85.01%	82.68%

Chapter 5:

Conclusions and Future Work

The major objective of this thesis was to detail the development of a novel computational framework that was designed to track multiple cells and detect cell division events in time-lapse image sequences. The automatic tracking of cells in large datasets has recently draw the attention of computer vision researchers, as the emergence of modern microscopy imaging rendered the manual annotation procedure unfeasible in many clinical studies. This fact has been emphasised in Chapter 2, where the most relevant algorithms on the topic of cell tracking and mitosis detection are analysed. Arising from the literature survey, it can be concluded that the most apparent characteristic of the published algorithms on the topic of automatic cell tracking is their strong application context. This conclusion is not unexpected since the imaging protocols are optimised for each type of cellular data. One objective of the research work detailed in this thesis is to advance a more flexible tracking and mitosis detection framework that can be successfully applied to a wider range of time-lapse cellular datasets. Thus, the major contributions that result from this thesis are located not only in the development of novel algorithms for segmentation, tracking and mitosis detection. Additional important contributions are associated with the exhaustive validation of the proposed framework on different types of cellular data and in the evaluation of its performance when compared to those offered by state-of-the-art cell tracking algorithms.

As indicated in Chapter 2, the robust identification of the corresponding cells in time-lapse image sequences is a challenging task that cannot be accomplished by applying standard feature-based tracking algorithms. This challenging scenario is primarily motivated by the constrained nature of the image acquisition process that prevents the acquisition of image data with good image contrast. Indeed, low image contrast is a distinct characteristic of the phase-contrast cellular data, and in this thesis several novel solutions have been advanced in order to achieve robust tracking

results. To this end, substantial research efforts were put into the development of a flexible tracking framework where the main goal was the optimisation of each computational step. In this sense, the cellular segmentation proved quite challenging, as the phase-contrast images exhibit shallow intensity transitions between the background and regions that define the cells' nuclei. In addition, this data presents noticeable intra- and inter- frame intensity variations. In the proposed approach, to reduce as much as possible the incidence of segmentation errors, a morphological algorithm based on the *h*-maxima has been developed. The experimental results indicate that the proposed solution is accurate, but in the presence of large changes in the cells' shape and substantial intensity variation there are situations when cells are not detected by the proposed algorithm. Thus, the lack of perfect segmentation results motivated the development of a flexible cellular association procedure that is able to identify the corresponding cells in the sequence in the presence of under-segmentation. In this regard, the proposed cell association framework is based on the evaluation of local structures that encode the neighbouring relationships between the cells in pairs of consecutive frames of the sequence, where the identification of the corresponding cells does not require any prior knowledge regarding the cell morphology or migration patterns. These characteristics associated with the proposed tracking methodology are particularly appropriate, as cell migration is often characterised by random motility patterns that cannot be accurately modelled by *a priori* motion estimators. As mentioned above, the occurrence of under-segmentation introduced a substantial problem that has to be addressed during the cell association process. A key issue was the embedding of a hybrid mechanism into the tracking procedure that is able to detect and correct the errors caused by the undetected cells.

Full details about the proposed multi-stage cell tracking algorithm are provided in Chapter 3. The availability of precise forward tracking results opened the opportunity to develop a backward tracking strategy whose goal is the robust identification of the mitosis events. During backward tracking, the cell tracks (or cell lineages) identified during forward tracking are evaluated in a reverse manner to link the child cells to the corresponding parent cells in all frames of the sequence. Nonetheless, the incidence of under-segmentation substantially complicates the mitosis detection, and again a pattern recognition driven mechanism has been applied to identify the undetected child cells that were generated by the cellular

division events. The proposed cellular tracking and mitosis detection framework has been tested on various types of cellular datasets and in-depth experimental results are reported in Chapter 4.

The experimental results demonstrate that the proposed cell tracking and mitosis detection framework has achieved the research objectives outlined in Chapter 1. In the next section, the major and minor contributions that are associated with this investigation are outlined.

5.1 Contributions

The development of the proposed cellular tracking and mitosis detection framework facilitated the investigation of a large spectrum of algorithms that generated the major and minor contributions associated with this research work. In this sense, the major contribution resulting from this investigation is the multi-stage computational framework that is able to adapt to the challenging image conditions that are associated with time-lapse phase-contrast data. Within this framework, the algorithm devised for cellular association represents the most visible contribution of this thesis. One particular novel element of this algorithm resides in the adaptive integration of the cellular topological information in the tracking process. This information proved particularly robust when tracking cellular structures in complex situations that are generated by random migration. The modular design of this computational component of the framework, and the optimal modality to encode and analyse the spatial relationships between the cells during the inter frame tracking process, opened the possibility of developing a flexible approach that was implemented to efficiently identify and redress the segmentation errors that are caused by improper image conditions. All these novel algorithmic solutions proved key in achieving accurate tracking results.

The second major contribution resulting from this investigation is associated with in the approach that has been developed to identify the cellular division events. The robust mitosis detection is critically important in the estimation of molecular indicators such as the cell cycle. In this thesis, a robust solution that entails a backward tracking procedure has been proposed. Similar to the forward tracking

algorithm, the incidence of under-segmentation has detrimental effects on the process that deals with the identification of the links between parent and child cells. To address this problem, a hybrid approach that entails the combination of a pattern recognition-based algorithm and the evaluation of the consistency of the local cellular structures in a sequential manner has been developed. One particular advantage of the proposed framework is the redressing of the segmentation errors for both forward and backward tracking processes and this approach has several theoretical and practical justifications. Firstly, it limits the possibility of incorrect tracking decisions, as the mitotic cells cannot be robustly identified during forward tracking, and secondly, it opened up the possibility of developing a multi-stage association process where the use of topological information is maximised.

The final major contribution resulting from this thesis can be identified in the comprehensive measurements of the performance of the proposed cellular tracking and mitosis detection framework using several types of time-lapse cellular data. In this regard, an enormous effort has been employed to generate the ground truth data with all of the datasets used in the experimental study being manually annotated. In this process, thousands of cells were manually annotated and their lineages (or cell tracks) were also manually identified by analysing the migration patterns for each cell in consecutive frames of the sequence. The ground truth data was used to quantify the accuracy of the proposed tracking framework. To further enhance the relevance of the experimental results, the proposed framework has been tested on publicly available datasets and its performance has been compared to those achieved by other relevant published algorithms. The comparative results indicate that the proposed technique outperforms the state-of-the-art implementation with respect to both cellular tracking and mitosis detection.

There are several minor contributions that are worth mentioning. The first is located in the development of the cell segmentation process. The cell segmentation proved a very challenging task and substantial efforts have been put into the development of a strategy that minimises the incidence of segmentation errors. In this research work several algorithms have been evaluated and the approach that involves the application of *h*-maxima proved the most reliable. Other minor contribution is associated with the identification of the most robust

features/methodology that can be applied in the identification of the segmentation errors. In this regard, the proposed solution applies an intensity-based normalised cross correlation process that aims to identify the location of the undetected cell that minimises the local disturbances in the cellular structures encoded by the Delaunay meshes.

5.2 Future directions of research

The main objective of this research work was to develop a robust cellular tracking and mitosis detection framework that shows a higher degree of flexibility and increased performance when compared to the most relevant state-of-the-art implementations. Based on technical content that was detailed in this thesis and the reported experimental results, it can be concluded that the overall outcome of this investigation was successful. However, there are future directions of research that can be investigated based on the main concepts that were studied in this thesis. One possible development will focus on the investigation of alternative solutions that can improve the accuracy of the cell association process in the presence of cell interaction and large cellular migration. This may involve the inclusion of specific features such as intensity information, cell overlap area and motility estimators to enhance the matching confidence when identifying the corresponding cells in the image sequence. Another interesting area of further research can include the identification of the mitosis events using *a priori* probabilistic models, as this information can be extremely useful when validating the parent-child cells links.

There is also a distinct future direction of research that may aim at the extension of the functionality of the proposed framework to allow its application to other biological studies such as the robust tracking of cells in in-vivo 3D data. This will require (at least a partial) redesign of the cellular association process, but the main theoretical developments detailed in this thesis can still be successfully applied to this new tracking scenario.

Another possible future development can address the application of the proposed tracking strategy to non-cellular application domains such as pedestrian tracking in crowded conditions, robust player tracking in sports events, feature

tracking in the context of gesture analysis, etc. All these application scenarios require the use of robust tracking solutions that can be potentially addressed by the proposed tracking strategy.

Appendix A:

Statistical Indicators that Quantify Cell Migration

Once the cellular tracking process is completed, the coordinates of the corresponding cells (x,y,t) are available for the entire image sequence and they can be used to calculate different statistics that describe the cell migration. Thus, the objective of this section is to introduce a number of statistical indicators such as the average speed, directional movement and distance travelled by the cells that can be used to quantify the cell migration [69, 74]. These statistics are increasingly used by the molecular scientists in the evaluation of biological processes related to cancer research or in the development of new drugs and treatments. For instance, the administration of various therapeutic agents/inhibitors has direct effects on the cellular migration and the frequency of mitosis events, and these indicators are particularly useful to assess the differences between the control and test specimens.

As indicated above three different measurements are usually calculated and analysed. The first is the average speed S_{avg} that is calculated for each cell using the following formula,

$$S_{avg} = \frac{1}{F-1} \sum_{t=2}^{F} \left| X_t - X_{t-1} \right| \qquad \text{(A.1)}$$

where F is the total number of frames and $X = \{x,y\}$ is the 2D spatial coordinate.
The second indicator is the active movement also known as directional/vectorial displacement that can be computed using the distance between the initial and the final position of a cell. Figure A1 provides an example that illustrates the calculation of the directional movement. The third indicator is the total cell displacement which is given by the summation of all inter-frame instantaneous displacements, i.e. the length of the path that was travelled by a cell as indicated in Figure A1.

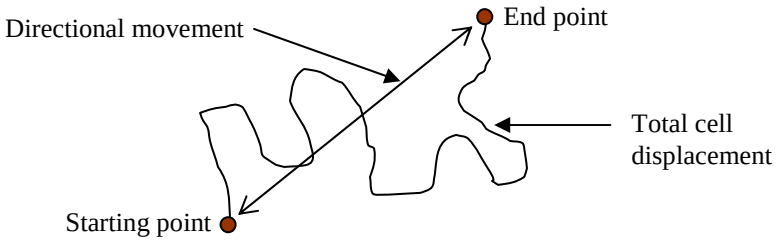

Figure A1. Diagram that illustrates the calculation of the directional movement and the total cell displacement.

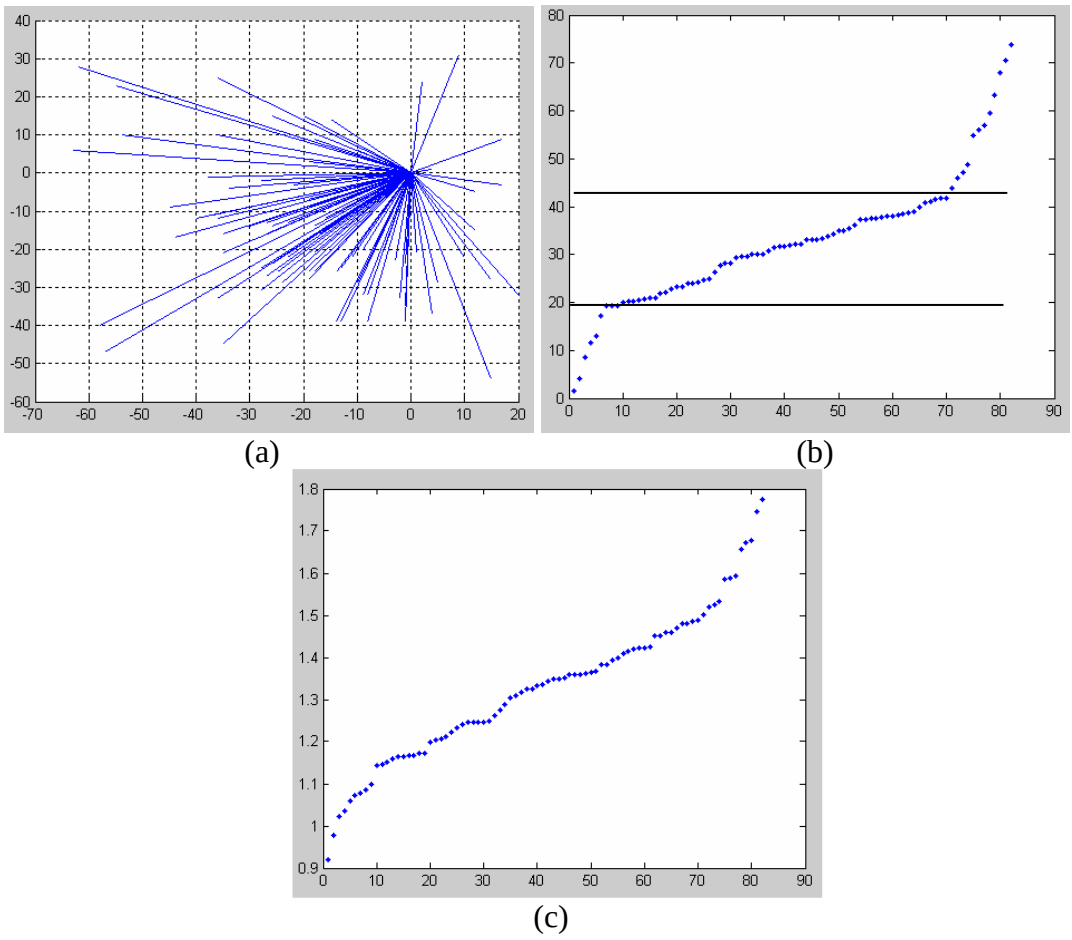

Figure A2. Cell migration indicators calculated for the MDCK-1 image sequence. (a) Directional movement. (b) Total cell displacement. (c) Average speed.

Figure A2 depicts the measurements calculated for a MDCK dataset where the active movement, total cell displacement and the average speed are shown in Figure A2(a), (b) and (c), respectively. The directional movement displayed in

Figure A2(a) indicates that most of the cells migrate in one dominant direction and the moving distance varies in the range 1 to 40 pixels. The total cell displacement is depicted in Figure A2(b) and it shows a variation between 1 to 80 pixels. The average speed indicator that is calculated for each cell is plotted in Figure A2(c) and it indicates a variation between 0.9 to 1.8 pixels per frame.

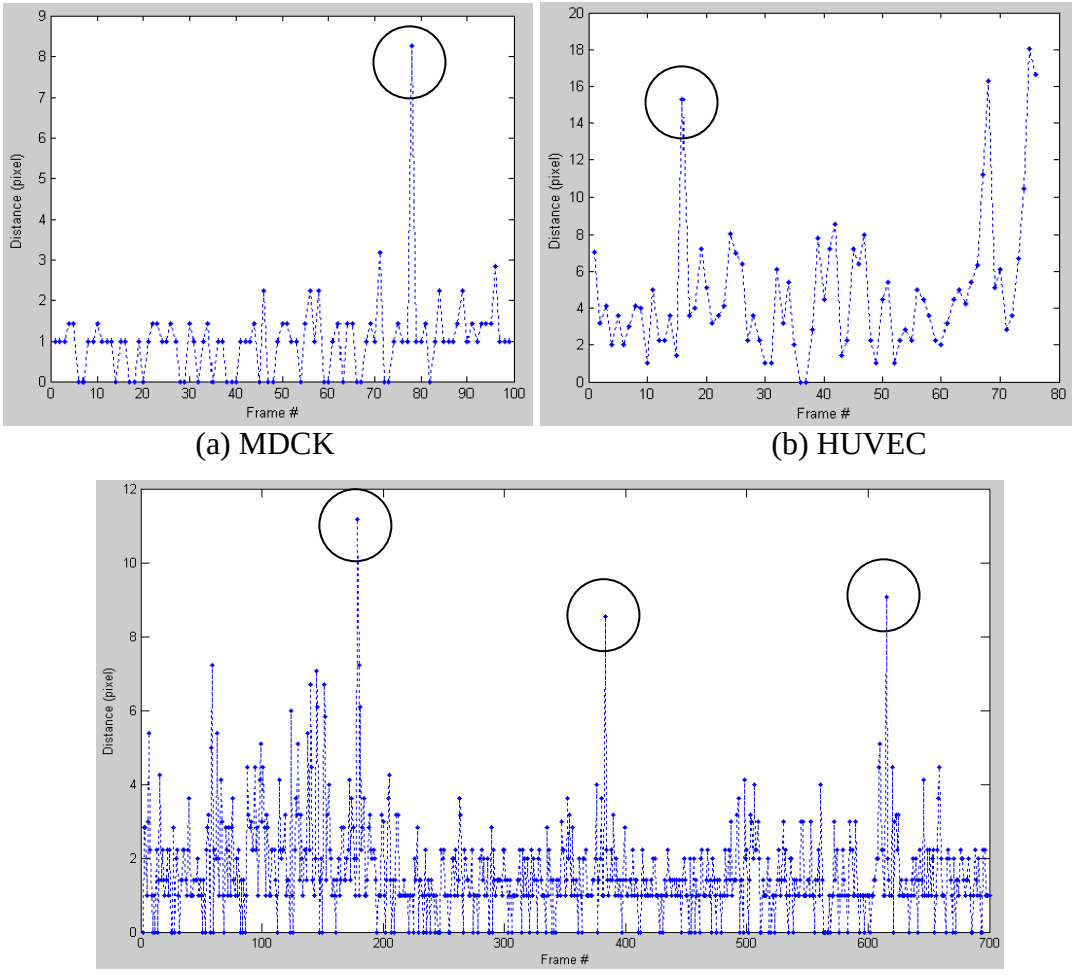

(a) MDCK (b) HUVEC

(c) MNP

Figure A3. The total cell displacement calculated for (a) MDCK, (b) HUVEC and (c) MNP datasets. The peaks in these diagrams are recorded for mitotic cells and for clarity reasons are marked with circles.

Figure A3 shows the total cell displacements that are calculated for all cells in the MDCK, HUVEC and MNP sequences. In this diagram it can be observed that the MDCK cells show the lowest motility while the HUVEC cells show the highest. In these diagrams the largest total cell displacements are recorded for mitotic cells

and this information is in particular useful in the assessment of the clinical effects that are induced by therapeutic agents.

Qualitative results

The statistics that quantify cellular migration are of great interests for molecular scientists. Thus, it is important that the statistics returned by the automated algorithm to be as accurate as possible. In order to evaluate the accuracy of the results obtained by the proposed framework, they are compared with the statistics obtained from manually marked up data. In this evaluation the active/directional movement of cells has been measured since it is an important indicator that quantifies the cell migration and its calculation is not affected by localization errors that may occur during the manual annotation process.

Comparative results are depicted in Figures A4.1 and A.4.2 where the directional movement returned by the proposed method and manually annotated data are indicated with blue and red dots, respectively. In these diagrams the *x* axis denotes the cell ID and *y* axis denotes the directional movement of a cell. For visualization purposes, the directional movement is calculated for a small number of cells in each sequence. From these graphs it can be observed that there is a good agreement between the directional movement obtained by the proposed method and that calculated from manually marked data. The overall deviation between these two sets of results is 10.5 percent. Thus, it can be concluded that the proposed method is suitable to extract the motility statistics that are able to accurately measure the cell migration patterns.

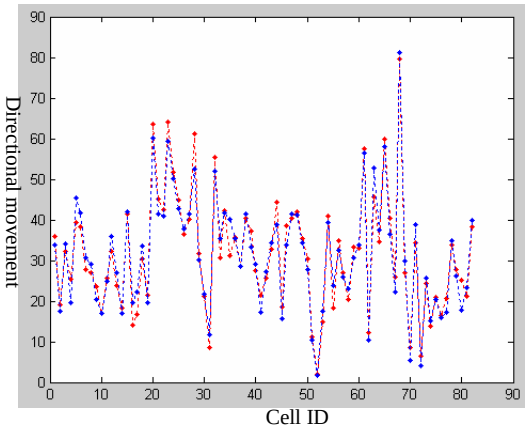

(a) MDCK-1

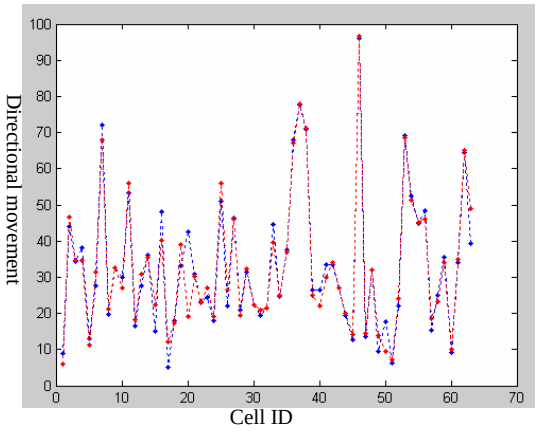

(b) MDCK-2

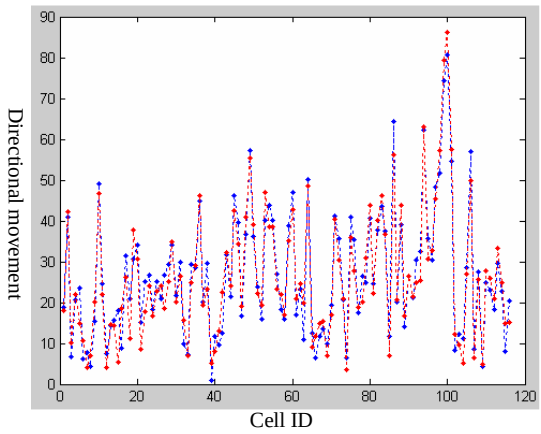

(c) MDCK-3

Figure A4.1. Directional movement extracted from MDCK data. Red dots - results extracted from manual marked-up data. Blue dots - results obtained by the proposed method.

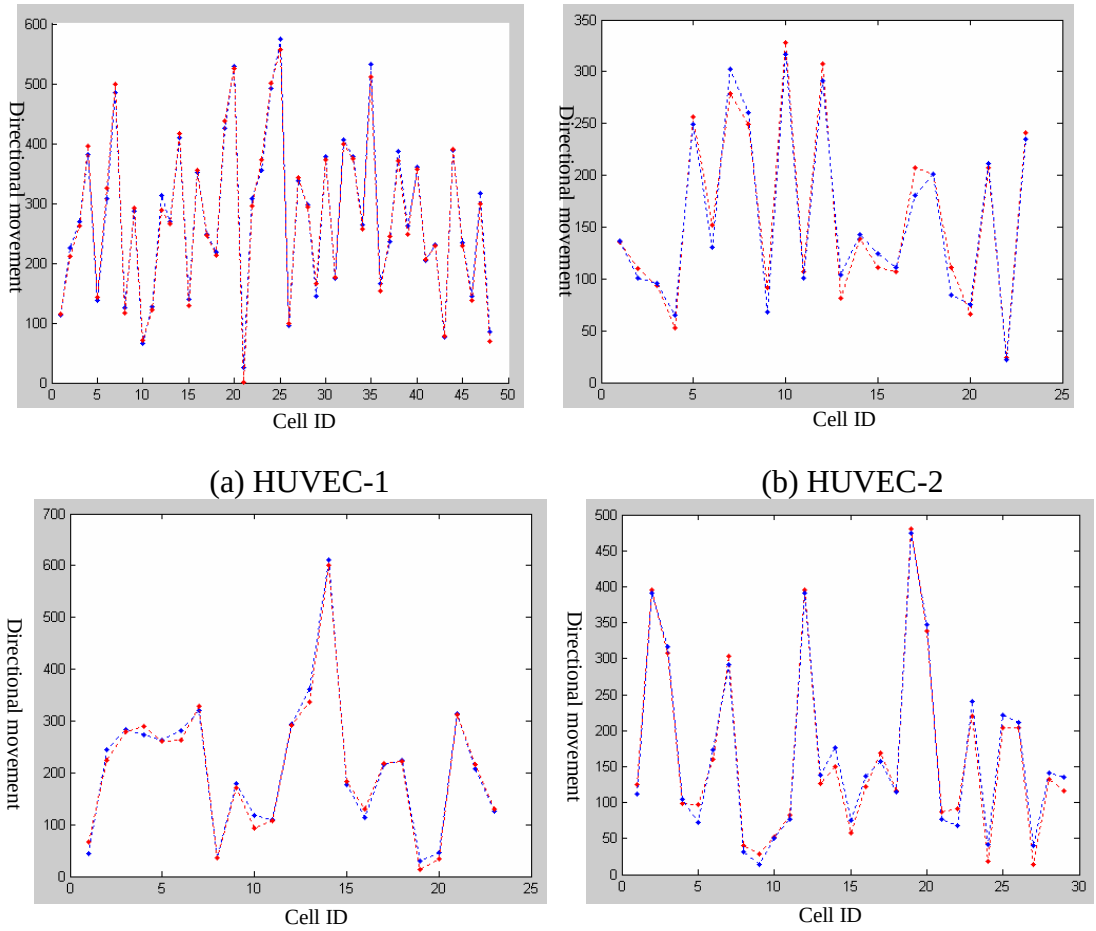

Figure A4.2. Directional movement extracted from HUVEC data. Red dots - results extracted from manual marked-up data. Blue dots - results obtained by the proposed method.

Appendix B:

Live Cell Image Acquisition

The objective of live cell imaging is to record key cellular events such as migration, division, cellular interaction, apoptosis etc. that help in the process of analyzing the biological mechanisms associated with various cellular events. Long term monitoring of cells is required to compute key indicators that are able to quantify the cell response to diverse stimuli. To facilitate this, live cells are grown in a chamber (incubator) that is designed to maintain the cell culture conditions in which cells remain in a healthy state for the duration of the experiments. To allow the extraction of statistical indicators relating to cellular activity, the cells are typically imaged by a microscope that is fitted with a computer-controlled digital camera. In this process it is critical that the interaction between the imaging system and cells to be maintained at minimal levels to avoid the insertion of undesired factors that may impact on the cell health. When cells are monitored for long periods of time, images are recorded at fixed intervals (normally few minutes) that are sufficiently large to sample the changes induced by cell migration and the frequency of cellular division and apoptosis with sufficient accuracy. This particular type of image acquisition is known as time-lapse imaging.

In general, time-lapse microscopy imaging system consists of three major components:

1) An incubator which is fitted to the stage of the microscope. The main role of this device is to maintain a constant environment for cells with respect to temperature, pressure and nutrition.

2) A microscope, which comprises optical components, an automated stage and a digital camera that records sequences of cellular images.

3) Computing devices that control the microscopy parameters during the time-lapse image acquisition process.

Since molecular biology scientist are interested in the analysis of a variety of cell lines, numerous imaging approaches have been developed to enhance the discrimination between the cells and the background (which is the culture medium where the cells are grown). These techniques include bright-field, dark-field, phase-contrast, confocal, fluorescence, etc. microscopy image modalities [109]. Each of these techniques has particular advantages and disadvantages when applied to specific cell lines [111]. Among these techniques, the phase-contrast and fluorescence imaging techniques proved the most common when applied to experiments that were concerned with the quantification of cell migration and cellular division [1, 7, 12].

Fluorescence microscopy uses artificial staining agents that illuminate the specimen with a specific band of wavelengths. This imaging process is extremely useful when applied to separate the cells from background, which has a much weaker response when the specimen is illuminated by the excitatory light. The fluorescence-stained cellular structures are associated with the high intensity pixels in the resulting image, as shown in Figure B.1, and due to high contrast this data is well suited for automated analysis. However, fluorescence illumination is too harmful when applied to many cell lines, as it has an undesired impact on the cell health. The combined toxicity effect caused by fluorescence staining and illumination is in particular detrimental when the specimen is monitored for long periods of time.

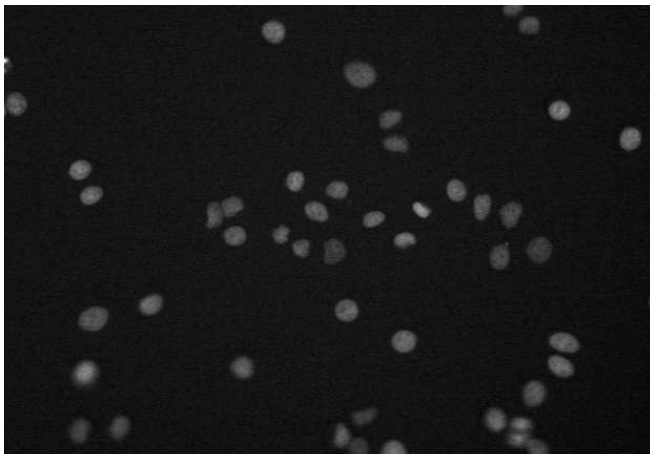

Figure B1. A sample image showing HeLa cells captured through fluorescence microscopy.

Phase-contrast techniques are based on an optical mechanism that translates the phase shift in the light passing through transparent materials into amplitude changes that result in an enhanced image contrast as shown in Figure B.2. Phase-contrast techniques are very common microscopy modalities since the contrast enhancement is obtained without loss of resolution. This imaging technique does not require staining that implies additional specimen preparation and does not causes detrimental effects on cell health. This property makes this technique suitable for live cell imaging since it is able to maintain the cells in a healthy state for long periods.

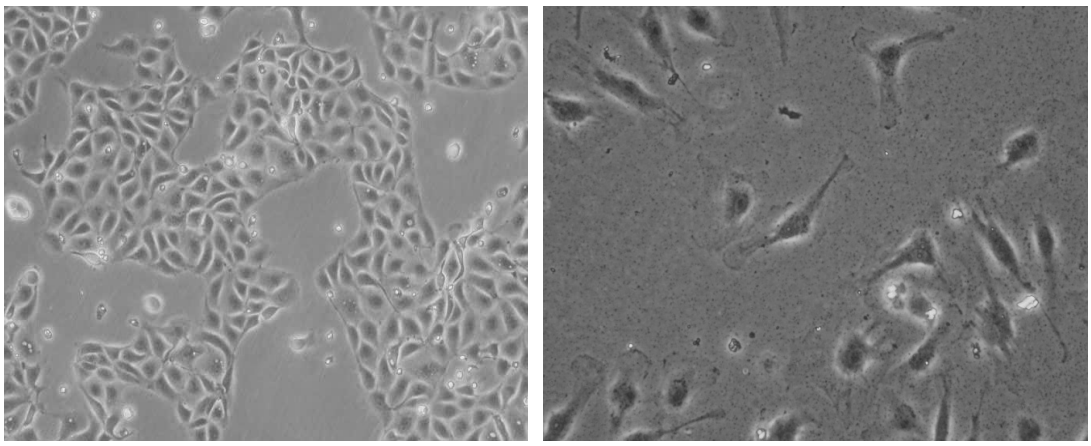

(a) (b)

Figure B2. Sample images showing (a) MDCK and (b) HUVEC cells captured using phase-contrast microscopy.

The proposed automated image analysis solution that has been reported in this thesis addresses the quantification of cell migration and cell division for phase-contrast MDCK and HUVEC cell lines. The MDCK and HUVEC cell images are captured at temporal resolutions that range from three to ten minutes depending on the objectives of each particular experiment. The spatial resolution varies between 1.3 to 0.87 μm depending on the imaged field of view.

References

[1] O. Al-Kofahi, R. J. Radke, S. K. Goderie, Q. Shen, S. Temple, and B. Roysam, “Automated cell lineage construction: A rapid method to analyze clonal development established with murine neural progenitor cells,” Cell Cycle, vol. 5, no. 3, pp. 327-335, February 2006.

[2] “Phase contrast microscope application in microscopy: Advantages and disadvantages,” http://www.microscopemaster.com/phase-contrast-microscope.html. (Last accessed Nov 2, 2011).

[3] Z. Yin, K. Li, T. Kanade, and M. Chen, “Understanding the optics to aid microscopy image segmentation,” in Proceedings of the International Conference on Medical Image Computing and Computer Assisted Intervention (MICCAI), LNCS, Beijing, September 2010, pp. 209-217.

[4] D. Padfield, J. Rittscher, and B. Roysam, “Coupled minimum-cost flow cell tracking for high-throughput quantitative analysis,” Medical Image Analysis, vol. 15, no. 4, pp. 650-668, August 2011.

[5] O. Debeir, P. van Ham, R. Kiss, and C. Decaestecker, “Tracking of migrating cells under phase-contrast video microscopy with combined mean-shift processes,” IEEE Transaction on Medical Imaging, vol. 24, no. 6, pp. 697–711, June 2005.

[6] O. Debeir, I. Camby, R. Kiss, P. van Ham, and C. Decaestecker, “A model-based approach for automated in vitro cell tracking and chemotaxis analyses,” Cytometry Part A, vol. 60, no. 1, pp. 29-40, July 2004.

[7] F. Li, X. Zhou, J. Ma, and S. T. C Wong, “Multiple nuclei tracking using integer programming for quantitative cancer cell cycle analysis,” IEEE Transaction on Medical Imaging, vol. 29, no. 1, pp. 96-105, January 2010.

[8] K. Li, E. D. Miller, M. Chen, T. Kanade, L. E. Weiss, and P. G. Campbell, “Cell population tracking and lineage construction with spatiotemporal context,” Medical Image Analysis, vol. 12, no. 5, pp. 546-566, October 2008.

[9] A. Mosig, S. Jäger, C. Wang, S. Nath, I. Ersoy, K. Palaniappan, and S. S. Chen, “Tracking cells in life cell imaging videos using topological alignments,” Algorithms for Molecular Biology, vol. 4, no. 10, pp. 1-9, July 2009.

[10] Q. Wang, J. Niemi, C. M. Tan, L. You, and M. West, “Image segmentation and dynamic lineage analysis in single-cell fluorescence microscopy,” Cytometry Part A, vol. 77A, no. 1, pp. 101-110, January 2010.

[11] N. Kharma, H. Moghnieh, J. Yao, Y.P. Guo, A. Abu-Baker, J. Laganiere, G. Rouleau, and M. Cheriet, “Automatic segmentation of cells from microscopic imagery using ellipse detection,” IET Image Processing, vol. 1, no. 1, pp. 39-47, March 2007.

[12] M. A. A. Dewan, M. O. Ahmad, and M. N. S. Swamy, “Tracking biological cells in time-lapse microscopy: An adaptive technique combining motion and topological features,” IEEE Transaction on Biomedical Engineering, vol. 58, no. 6, pp. 1637-1647, June 2011.

[13] K. Thirusittampalam, M. J. Hossain, O. Ghita, and P. F. Whelan, “A novel framework for tracking in-vitro cells in time-lapse phase contrast data,” in Proceedings of the British Machine Vision Conference, Aberystwyth, September 2010, pp.69.1–69.11.

[14] D. P. Mukherjee, N. Ray, and S. T. Acton, “Level set analysis for leukocyte detection and tracking,” IEEE Transaction on Image Processing, vol. 13, no. 4, pp. 562-572, April 2004.

[15] N. N. Kachouie, P. Fieguth, J. Ramunas and E. Jervis, “A model-based hematopoietic stem cell tracker,” in Proceedings of the International Conference on Image Analysis and Recognition, LNCS, Toronto, 2005, vol. 3656, pp. 861-868.

[16] K. Wu, D. Gauthier, and M. D. Levine, “Live cell image segmentation,” IEEE Transaction on Biomedical Engineering, vol. 42, no. 1, pp. 1–12, January 1995.

[17] C. Wählby, I. M. Sintorn, F. Erlandsson, G. Borgefors, and E. Bengtsson, “Combining intensity, edge, and shape information for 2D and 3D segmentation of cell nuclei in tissue sections,” Journal of Microscopy, vol. 215, no. 1, pp. 67–76, July 2004.

[18] A. Dufour, V. Shinin, S. Tajbakhsh, N. Guillén-Aghion, J. C. Olivo-Marin, and C. Zimmer, “Segmenting and tracking fluorescent cells in dynamic 3-D microscopy with coupled active surfaces,” IEEE Transaction on Image Processing, vol. 14, no. 9, pp. 1396-1410, September 2005.

[19] D. Comaniciu and P. Meer, “Cell image segmentation for diagnostic pathology,” Advanced Algorithmic Approaches to Medical Image Segmentation: State-of-the-Art Applications in Cardiology, Neurology, Mammography and Pathology, Springer-Verlag, vol. 0, pp. 541–558, 2002.

[20] J. C. Olivo-Marin, “Extraction of spots in biological images using multiscale products,” Pattern Recognition, vol. 35, no. 9, pp. 1989–1996, September 2002.

[21] A. Genovesio, T. Liedl, V. Emiliani, W. J. Parak, M. Coppey-Moisan, and J. C. Olivo-Marin, “Multiple particle tracking in 3-D+t microscopy: Method and application to the tracking of endocytosed quantum dots,” IEEE Transaction on Image Processing, vol. 25, no. 5, pp. 1062-1070, May 2006.

[22] N. Ray, S. T. Acton, and K. Ley, “Tracking leukocytes in vivo with shape and size constrained active contours,” IEEE Transaction on Medical Imaging, vol. 21, no. 10, pp. 1222-1235, October 2002.

[23] S. K. Nath, F. Bunyak, and K. Palaniappan, “Robust tracking of migrating cells using four-color level set segmentation,” in Proceedings of the International Conference on Advanced Concepts for Intelligent Vision System, LNCS, Antwerp, September 2006, vol. 4179, pp. 920-932.

[24] R. M. Jiang, D. Crookes, N. Luo, and M. W. Davidson, “Live-cell tracking using SIFT features in DIC microscopic videos,” IEEE Transaction on Biomedical Engineering, vol. 57, no. 9, pp. 2219-2228, August 2010.

[25] I. Smal, E. Meijering, K. Draegestein, N. Galjart, I. Grigoriev, A. Akhmanova, M. E. van Royen, A. B. Houtsmuller, and W. Niessen, "Multiple object tracking in molecular bioimaging by Rao-blackwellized marginal particle filtering," Medical Image Analysis, vol. 12, no. 6, pp. 764-777, December 2008.

[26] I. Smal, K. Draegestein, N. Galjart, W. Niessen, and E. Meijering, "Particle filtering for multiple object tracking in dynamic fluorescence microscopy images application to microtubule growth analysis," IEEE Transaction on Medical Imaging, vol. 27, no. 6, pp. 789-804, June 2008.

[27] L. Zhang, H. Xiong, K. Zhang, and X. Zhou, "Graph theory application in cell nuleus segmentation, tracking and identification," in Proceedings of the IEEE International Conference on Bioinformatics and Bioengineering, Boston, October 2007, pp. 226-232.

[28] J. Xie, S. Khan, and M. Shah, "Automatic tracking of escherichia coli in phase-contrast microscopy video," IEEE Transaction on Biomedical Engineering, vol. 56, no. 2, pp. 390-399, February 2009.

[29] J. Apgar, Y. Tseng, E. Fedorov, M. B. Herwig, S. C. Almo, and D. Wirtz, "Multiple-particle tracking measurements of heterogeneities in solutions of actin filaments and actin bundles," Biophysical Journal, vol. 79, no. 2, pp. 1095-1106, August 2000.

[30] S. Jaeger, Q. Song, and S. S. Chen, "DYNAMIK: A software environment for cell dynamics, motility and information tracking, with an application to Ras pathways," Bioinformtics, vol. 25, no. 18, pp. 2383-2388, July 2009.

[31] J. Yan, X. Zhou, Q. Yang, N. Liu, Q. Cheng, and S. T. C. Wong, "An effective system for optical microscopy cell image segmentation, tracking and cell phase identification," in Proceedings of the IEEE International Conference on Image Processing, Atlanta, October 2006, pp. 1917-1920.

[32] X. Chen, X. Zhou, and S. T. C. Wong, "Automated segmentation, classification, and tracking of cancer cell nuclei in time-lapse microscopy,"

IEEE Transaction on Biomedical Engineering, vol. 54, no. 4, pp. 762-766, April 2006.

[33] T. Kirubarajan, Y. Bar-Shalom, and K. R. Pattipati, “Multiassignment for tracking a large number of overlapping objects,” IEEE Transaction on Aerospace and Electronic Systems, vol. 37, no. 1, pp. 2-21, January 2001.

[34] T. Kanade, Z. Yin, R. Bise, S. Huh, S. Eom, M. F. Sandbothe, and M. Chen, “Cell image analysis: Algorithm, system and applications,” in Proceedings of the IEEE Workshop on Application of Computer Vision, Kona, January 2011, pp. 374-381.

[35] M. de Berg, O. Cheong, M. van Kreveld, and M. Overmars, “Computational geometry: Algorithms and applications,” Springer-3rd Ed, 2008, pp. 191-218.

[36] K. Thirusittampalam, M. J. Hossain, O. Ghita, and P. F. Whelan, “Cellular tracking in time-lapse phase contrast images,” in Proceedings of the Irish Machine Vision and Image Processing, Dublin, September 2009, pp. 77-82.

[37] M. Liu, R. K. Yadav, A. R. Chowdhury, and G. V. Reddy, “Automated tracking of stem cell lineages of arabidopsis shoot apex using local graph matching,” Plant Journal, vol. 62, no. 1, pp. 135-147, April 2010.

[38] M. Kass, A. Witkin, and D. Terzopoulos, “Snakes: Active contour models,” International Journal of Computer Vision, vol. 1, no. 4, pp. 321-331, 1988.

[39] S. Osher and J. Sethian, “Fronts propagating with curvature-dependent speed: Algorithms based on Hamilton–Jacobi formulations,” Journal of Computational Physics, vol. 79, no. 1, pp. 12–49, November 1988.

[40] D. M. Tsai and C. T. Lin, “Fast normalized cross correlation for defect detection,” Pattern Recognition Letters, vol. 24, no. 15, pp. 2625-2631, November 2003.

[41] D. Comaniciu, V. Ramesh, and P. Meer, “Kernel-based object tracking,” IEEE Transaction on Pattern Analysis and Machine Intelligence, vol. 25, no. 5, pp. 564-577, May 2003.

[42] F. Leymarie and M. D. Levine, “Tracking deformable objects in the plane using an active contour model,” IEEE Transaction on Pattern Analysis and Machine Intelligence, vol. 15, no. 6, pp. 617-634, June 1993.

[43] A. P. Goobic, M. E. Welser, S. T. Acton, and K. Ley, “Biomedical application of target tracking in clutter,” in Proceedings of the 35th Asilomar Conference on Signals, Systems and Computers, Pacific Grove, November 2001, vol. 1, pp. 88–92.

[44] C. Zimmer, E. Labruyère, V. Meas-Yedid, N. Guillén, and J. C. Olivo-Marin, “Segmentation and tracking of migrating cells in videomicroscopy with parametric active contours: A tool for cell-based drug testing,” IEEE Transaction on Medical Imaging, vol. 21, no. 10, pp. 1212-1221, October 2002.

[45] X. Wang, W. He, D. Metaxas, R. Mathew, and E. White, “Cell segmentation and tracking using texture-adaptive snakes,” in Proceedings of the IEEE International Symposium on Biomedical Imaging: from Nano to Macro, Arlington, April 2007, pp. 101-104.

[46] H. Delingette and J. Montagnat, “Shape and topology constraints on parametric active contours,” Computer Vision and Image Understanding, vol. 83, no. 2, pp. 140–171, August 2001.

[47] N. Ray and S. T. Acton, “Motion gradient vector flow: An external force for tracking rolling leukocytes with shape and size constrained active contours,” IEEE Transaction on Medical Imaging, vol. 23, no. 12, pp. 1466-1478, December 2004.

[48] D. Padfield, J. Rittscher, N. Thomas, and B. Roysam, “Spatio-temporal cell cycle phase analysis using level sets and fast marching methods,” Medical Image Analysis, vol. 13, no. 1, pp. 143-155, February 2009.

[49] B. Zhang, C. Zimmer, and J. C. Olivo-Marin, “Tracking fluorescent cells with coupled geometric active contours,” in Proceedings of the IEEE International Symposium on Biomedical Imaging: Nano to Macro, Arlington, April 2004, vol. 1, pp. 476-479.

[50] L. Miroslaw, A. Chorazyczewski, F. Buchholz, and R. Kittler, “Correlation-based method for automatic mitotic cell detection in phase contrast microscopy,” in Proceedings of the International Conference on Computer Recognition Systems, 2005, vol. 30, pp. 627-634.

[51] E. P. Careta, M. T. Cisneros, O. Debeir, J. S. Mondragón, J. G. A. Cervantes, O. G. I. Manzano, D. M. Arrioja, E. P. Pantoja, and G. N. Romero, “Cell tracking by normalized cross-correlation with image processing,” in Proceedings of the IEEE Summer Topical Meetings, Acapulco, July 2008, pp. 43-44.

[52] X. Yang, H. Li, and X. Zhou “Nuclei segmentation using marker-controlled watershed, tracking using mean-shift, and Kalman filter in time-lapse microscopy,” IEEE Transactions on Circuits and Systems I, vol. 53, no. 11, pp. 2405-2414, November 2006.

[53] J. Cui, S. T. Acton, and Z. Lin, “A Monte Carlo approach to rolling leukocyte tracking in vivo,” Medical Image Analysis, vol. 10, no. 4, pp. 598-610, August 2006.

[54] W.J. Godinez, M. Lampe, S. Wörz, B. Müller, R. Eils, and K. Rohr, “Deterministic and probabilistic approaches for tracking virus particles in time-lapse fluorescence microscopy image sequences,” Medical Image Analysis, vol. 13, no. 2, pp. 325-342, April 2009.

[55] R. E. Kalman, “A new approach to linear filtering and prediction problems,” ASME Transaction on Basic Engineering, vol. 82, no. D, pp. 35-45, 1960.

[56] M. S. Arulampalam, S. Maskell, N. Gordon, and T. Clapp, “A tutorial on particle filters for online nonlinear/non-Gaussian Bayesian tracking,” IEEE Transaction on Signal Processing, vol. 50, no. 2, pp. 174-188, February 2002.

[57] N. H. Nguyen, S. Keller, E. Norris, T. T. Huynh, M. G. Clemens, and M. C. Shin, “Tracking colliding cells in vivo microscopy,” IEEE Transaction on Biomedical Engineering, vol. 58, no. 8, pp. 2391-2400, August 2011.

[58] N. N. Kachouie and P. W. Fieguth, “Extended-Hungarian-JPDA: Exact single-frame stem cell tracking,” IEEE Transaction on Biomedical Engineering, vol. 54, no. 11, pp. 2011-2019, November 2007.

[59] J. Cheng, E. G. L. Koh, S. Ahmed and J. C. Rajapakse, “Joint tracking of cell morphology and motion,” in Proceedings of the IAPR International Conference on Pattern Recognition in Bioinformatics, LNCS, Sheffield, September 2009, vol. 5780, pp. 36-45.

[60] J. Degerman, T. Thorlin, J. Faijerson, K. Althoff, P. S. Eriksson, R. V. Put, and T. Gustavsson, “An automatic system for in vitro cell migration studies,” Journal of Microscopy, vol. 233, no. 1, pp. 178-191, January 2009.

[61] D. Padfield, J. Rittscher, and B. Roysam, “Spatio-temporal cell segmentation and tracking for automated screening,” in Proceedings of the IEEE International Symposium on Biomedical Imaging: from Nano to Macro, Paris, May 2008, pp. 376 - 379.

[62] O. Debeir, V. Mégalizzi, N. Warzée, R. Kiss, and C. Decaestecker, “Videomicroscopic extraction of specific information on cell proliferation and migration in vitro,” Experimental Cell Research, vol. 314, no. 16, pp. 2985-2998, October 2008.

[63] S. Huh and M. Chen, “Detection of mitosis within a stem cell population of high cell confluence in phase-contrast microscopy images,” in Proceedings of the IEEE Conference on Computer Vision and Pattern Recognition, Providence, June 2011, pp. 1033 - 1040.

[64] S. Huh, D. F. E. Ker, R. Bise, M. Chen, and T. Kanade “Automated mitosis detection of stem cell populations in phase-contrast microscopy images,” IEEE Transaction on Medical Imaging, vol. 30, no. 3, pp. 586-596, March 2011.

[65] A. A. Liu, K. Li, and T. Kanade, “Mitosis sequence detection using hidden conditional random fields,” in Proceedings of the IEEE International Symposium on Biomedical Imaging: Nano to Macro, Rotterdam, April 2010, pp. 580-583.

[66] A. Quattoni, S. Wang, L. Morency, M. Collins, and T. Darrell, “Hidden conditional random fields,” IEEE Transaction on Pattern Analysis and Machine Intelligence, vol. 29, no. 10, pp. 1848–1852, October 2007.

[67] H. Geerts, M. D. Brabander, R. Nuydens, S. Geuens, M. Moeremans, J. D. Mey, and P. Hollenbeck, “Nanovid tracking: A new automatic method for the study of mobility in living cells based on colloidal gold and video microscopy,” vol. 52, no. 5, pp. 775-782, November 1987.

[68] I. Adanja, O. Debeir, V. Megalizzi, R. Kiss, N. Warzee, and C. Decaestecker, “Automated tracking of unmarked cells migrating in three-dimensional matrices applied to anti-cancer drug screening,” Experimental Cell Research, vol. 316, no. 2, pp. 181-193, January 2010.

[69] Y. Sato, G. Poynter, D. Huss, M. B. Filla, A. Czirok, B. J. Rongish, C. D. Little, S. E. Fraser, and R. Lansford, “Dynamic analysis of vascular morphogenesis using transgenic quail embryos,” PLOS ONE, vol. 5, no. 9, September 2010.

[70] V. Sethuraman, A. French, D. Wells, K. Kenobi, and T. Pridmore, “Tissue-level segmentation and tracking of cells in growing plant roots,” Machine Vision and Applications, doi 10.1007/s00138-011-0329-9, March 2011.

[71] J. W. Mao, L. W. Wang, T. Jacob, X. R. Sun, H. Li, L. Y. Zhu, P. Li, P. Zhong, S. H. Nie, and L. X. Chen, “Involvement of regulatory volume decrease in the migration of nasopharyngeal carcinoma cells,” Cell Research, vol. 15, pp. 371–378, 2005.

[72] M. Butenuth and C. Heipke, “Network snakes: Graph-based object delineation with active contour models,” Machine Vision and Application, doi: 10.1007/s00138-010-0294-8, August 2010.

[73] K. Thirusittampalam, M. J. Hossain, O. Ghita, and P. F. Whelan, “Cell segmentation in time-lapse phase contrast data,” in Proceedings of the Irish Machine Vision and Image Processing Conference (IMVIP), Dublin, September 2011, pp. 120-121.

[74] M. J. Hossain, P. F. Whelan, A. Czirok, and O. Ghita, “An active particle-based tracking framework for 2D and 3D time-lapse microscopy images,” in Proceedings of the 33rd Annual International Conference of the IEEE Engineering in Medicine and Biology Society (EMBC), Boston, August 2011, pp. 6613-6618.

[75] Z. Khan, T. Balch, and F. Dellaert, “MCMC-based particle filtering for tracking a variable number of interacting targets,” IEEE Transaction on Pattern Analysis and Machine Intelligence. vol. 27, no. 11, pp. 1805–1819, November 2005.

[76] R. Fabbri, L. D. F. Costa, J. C. Torelli, and O. M. Bruno, “2D Euclidean distance transform algorithms: A comparative survey,” ACM Computing Surveys, vol. 40, no. 1, 2008.

[77] N. Otsu, “A threshold selection method from gray level histograms,” IEEE Transactions on System, Man, and Cybernetics, vol. smc-9, no. 1, pp. 62–66, 1979.

[78] Y. Al-Kofahi, W. Lassoued, W. Lee, and B. Roysam, “Improved automatic detection and segmentation of cell nuclei in histopathology images,” IEEE Transaction on Biomedical Engineering, vol. 57, no. 4, pp. 841-852, April 2010.

[79] A. Dufour, R. Thibeaux, E. Labruyère, N. Guillén, and J. C. Olivo-Marin, “3-D Active meshes: Fast discrete deformable models for cell tracking in 3-D time-lapse microscopy,” IEEE Transaction on Image Processing, vol. 20, no. 7, pp. 1925-1937, July 2011.

[80] J. Cui, N. Ray, S. T. Acton, and Z. Lin, “An affine transformation invariance approach to cell tracking,” Computerized Medical Imaging and Graphics, vol.32, no. 7, pp. 554-565, July 2008.

[81] Y. Chen, P. Quelhas, and A. Campilho, “Low frame rate cell tracking: A Delaunay graph matching approach,” in Proceedings of the IEEE International Symposium on Biomedical Imaging: From Nano to Macro, Chicago, March-April 2011, pp. 1015 – 1018.

[82] F. Li, X. Zhou, and S. T.C. Wong, “Optimal live cell tracking for cell cycle study using time-lapse fluorescent microscopy images,” in Proceedings of the International Workshop on Machine Learning in Medical Imaging, LNCS, Beijing, September 2010, vol. 6357, pp. 124-131.

[83] R. Bise, Z. Yin, and T. Kanade “Reliable cell tracking by global data association,” in Proceedings of the IEEE International Symposium on Biomedical Imaging: From Nano to Macro, Chicago, March-April 2011, pp. 1004 - 1010.

[84] X. Zhou and Y. Lu, “Efficient mean shift particle filter for sperm cells tracking,” in Proceedings of the International Conference on Computational Intelligence and Security, Beijing, December 2009, pp. 335 – 339.

[85] T. Otaki, “Artifact halo reduction in phase contrast microscopy using apodization,” Optical Review, vol. 7, no. 2, pp. 119-122, 2000.

[86] I. Ersoy, F. Bunyak, V. Chagin, M. C. Cardoso, and K. Palaniappan, “Segmentation and classification of cell cycle phases in fluorescence imaging,” in Proceedings of the Medical Image Computing and Computer-Assisted Intervention (MICCAI), LNCS, London, 2009, vol. 5762, pp. 617-624.

[87] “Madin-Darby Canine Kidney Epithelial Cells (MDCK Line),” http://learn.hamamatsu.com/galleries/digitalimages/mdck/mdckcells.html, (Last accessed Nov 7, 2011)

[88] E. T. Jordan, M. Collins, J. Terefe, L. Ugozzoli, and T. Rubio “Optimizing electroporation conditions in primary and other difficult-to-transfect cells,” Journal of Biomolecular Techniques, vol. 19, no. 5, pp. 328-334, December 2008.

[89] D. J. Stephens and V. J. Allan, “Light microscopy techniques for live cell imaging,” Science Biological Imaging, vol. 300, no. 5616, pp. 82-86, April 2003.

[90] B. Isherwood, P. Timpson, E. J. McGhee, K. I. Anderson, M. Canel, A. Serrels, V. G. Brunton, and N. O. Carragher, “Live cell in vitro and in vivo imaging applications: Accelerating drug discovery,” Pharmaceutics, vol. 3, no. 2, pp. 141-170, April 2011.

[91] S. Landry and P. L. McGhee, “Monitoring live cell viability: Comparative study of fluorescence, oblique incidence reflection and phase contrast microscopy imaging techniques,” Optics Express, vol. 12, no. 23, pp. 5754-5759, November 2004.

[92] J. Cheng and J. C. Rajapase, “Segmentation of clustered nuclei with shape markers and marking function,” IEEE Transactions on Biomedical Engineering, vol. 56, no. 3, pp. 741-748, March 2009.

[93] U. Adiga, R. Malladi, R. Fernandez-Gonzalez, and C. O. D. Solorzano, “High-throughput analysis of multispectral images of breast cancer tissue,” IEEE Transactions on Image Processing, vol. 15, no. 8, pp. 2259-2268, August 2006.

[94] K. Palaniappan, I. Ersoy, and K. Nath, “Moving object segmentation using the flux tensor for biological video microscopy,” LNCS, no. 4810, pp. 483-493, 2007.

[95] F. Li, X. Zhou, H. Zhao, and S. T. C. Wong, “Cell segmentation using front vector flow guided active contours,” International Conference on Medical Image Computing and Computer-Assisted Intervention, vol. 12, no. 2, pp. 609-616, 2009.

[96] X. Zhou, F. Li, J. Yan, and S. T. C. Wong, “A novel cell segmentation method and cell phase identification using Markov model,” IEEE Transactions on Information Technology in Biomedicine, vol. 13, no. 2, pp. 152-157, March 2009.

[97] F. Li, X. Zhou, J. Zhu, J. Ma, X. Huang, and S. T. C. Wong, “High content image analysis for human H4 neuroglioma cells exposed to CuO nanoparticles,” BMC Biotechnology, vol. 7, no. 66, October 2007.

[98] K. Shafique and M. Shah, “A noniterative greedy algorithm for multiframe point correspondence,” IEEE Transaction on Pattern Analysis and Machine Intelligence, vol. 27, no. 1, pp. 51-65, January 2005.

[99] A. Bouchemha, A. Nait-Ali, N. Doghmane, “A robust technique to characterize the palmprint using radon transform and Delaunay triangulation,” International Journal of Computer Applications, vol. 10, no. 10, pp. 35-42, November 2010.

[100] F. Hoffmann, K. Kriegel, and C. Wenk, “Matching 2D patterns of protein spots,” in Proceedings of the 14th Annual Symposium on Computational Geometry, 1998, pp.231-239.

[101] J. Dai, W. Luo, M. Jin, W. Zeng, Y. He, S. T Yau, and X. Gu, “Geometric accuracy analysis for discrete surface approximation,” in Proceedings of the 4th International Conference on Geometric Modeling and Processing, vol. 24, no. 6, August 2007, pp. 323-338.

[102] D. Shin and T. Tjahjadi, “Similarity invariant Delaunay graph matching,” in Proceedings of the Joint IAPR International Workshop, SSPR & SPR, Orlando, December 2008, vol. 5342, pp. 25-34.

[103] D. P. Huttenlocher, G. A. Klanderman, and W. J. Ruklidge, “Comparing images using the Hausdorff distance,” IEEE Transactions on Pattern Analysis and Machine Intelligence, vol. 15, no. 9, pp. 850-863, September 1993.

[104] B. Gunsel, A. M. Tekalp, and P. J. L.Van Beek, “Content-based access to video objects: Temporal segmentation, visual summarization, and feature extraction,” vol. 66, no. 2, pp. 261-280, April 1998.

[105] V. A. Sujan and M. P. Mulqueen, “Fingerprint identification using space invariant transforms,” Pattern Recognition Letters, vol. 23, no. 5, pp. 609-619, March 2002.

[106] A. M. Finch, R. C. Wilson, and E. R. Hancock, “Matching Delaunay graphs,” Pattern Recognition, vol. 30, no. 1, pp. 123-140, January 1997.

[107] J. W. Jaromczyk and G. T. Toussaint, “Relative neighborhood graphs and their relatives,” Proceedings of the IEEE, vol. 80, no. 9, pp. 1502-1517, September 1992.

[108] P. Bose, L. Devroye, W. Evans, and D. Kirkpatrick “On the spanning ratio of Gabriel graphs and β-skeletons,” in Proceedings of the 5th Latin American Symposium on Theoretical Informatics, Cancun, April 2002, vol. 2286, pp. 479-493.

[109] D. B. Murphy, “Fundamentals of light microscopy and electronic imaging,” John Wiley and Sons, October 2001.

[110] M. M. Frigault, J. Lacoste, J. L. Swift and C. M. Brown, “Live-cell microscopy – tips and tools,” Journal of Cell Science, vol. 122, pp. 753-767, 2009.

[111] “Introduction to live-cell imaging techniques,” http://www.microscopyu.com/articles/livecellimaging/index.html (Last accessed Jan 26, 2012).